

AD-A035 275

AIR FORCE INST OF TECH WRIGHT-PATTERSON AFB OHIO SCH--ETC F/G 20/5
LASER POINTING AND TRACKING USING AN ADAPTIVE EXTENDED KALMAN F--ETC(U)
DEC 76 Z H LEWANTOWICZ

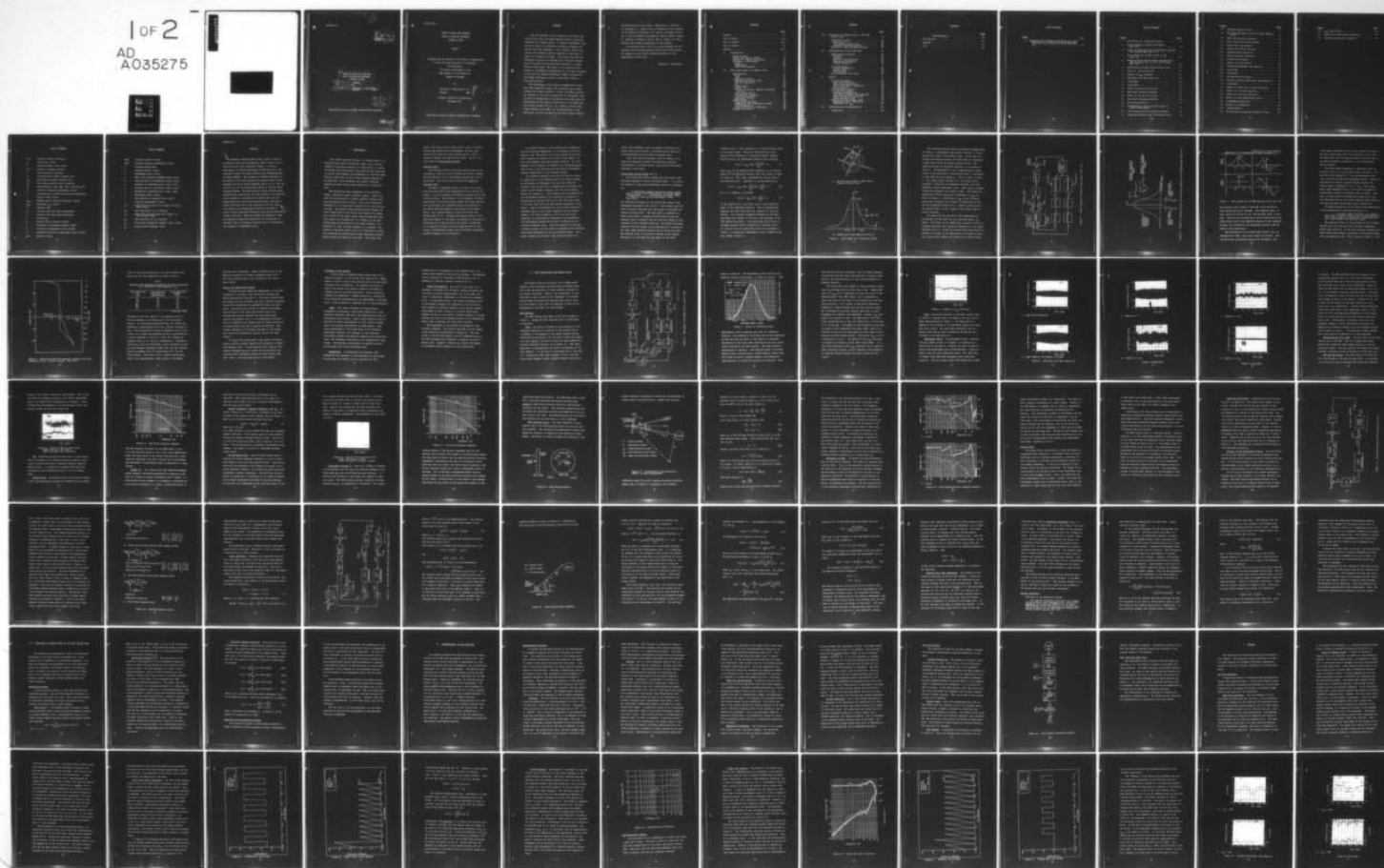
UNCLASSIFIED

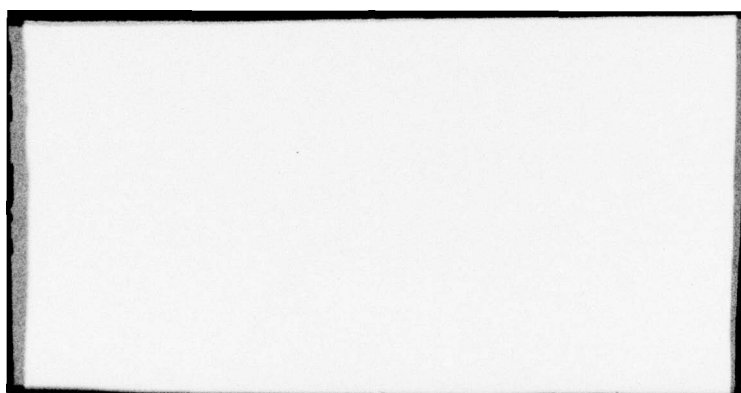
06/EE/76-29

NL

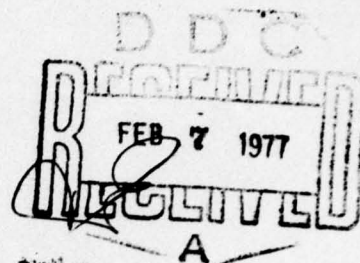
1 OF 2

AD
A035275





GE/EE/76-29



6
LASER POINTING AND TRACKING
USING AN ADAPTIVE EXTENDED
KALMAN FILTER

9 MASTER'S THESIS

14 GE/EE/76-29

10
Zdzislaw H. Lewantowicz
Captain USAF

11 Dec 76

12 153p.

Approved for public release; distribution unlimited.

012 225
498

LASER POINTING AND TRACKING USING AN ADAPTIVE EXTENDED KALMAN FILTER

THESIS

Presented to the Faculty of the School of Engineering
of the Air Force Institute of Technology
Air University
in Partial Fulfillment of the
Requirements for the Degree of
Master of Science

by

Zdzislaw H. Lewantowicz, B.S.
Captain USAF

Graduate Electrical Engineering
December 1976

Approved for public release; distribution unlimited.

A

Preface

With the explosive rate of growth of the laser technology since 1960, the laser beam has become a potential candidate as a weapon system. In another development since the early 1960's the theories on optimal estimation and control have been developed. Still another concept--the conical scan tracking--has been applied in the world of radar for a number of decades. The conical scan and the estimation theories are combined with a digital minicomputer to achieve fine pointing and tracking of a target with the laser beam. The result of the labors of this thesis is a breadboard implementation of the above concepts at the Air Force Weapons Laboratory (AFWL), Kirtland Air Force Base, New Mexico, where a laser beam "tracks" a large ball bearing.

The achievement of the results presented here would have been impossible without the assistance and guidance rendered me by Major Richard M. Potter, my thesis advisor. His devotion to the duty of keeping me on the proper track can best be exemplified by the patient hours upon hours of discussions and the piles of chalk-dust in the chalk tray. Very sincere thanks go to Lt. Col. James D. Dillow, this thesis sponsor at the AFWL, for his hospitality at the laboratory, and for the material and moral support that he

provided during my stay there. Additionally, gratitude is expressed to: Captain Peter A. Maybeck for his guidance in the theory of estimation, Dr. Alan B. Callendar for his aid in the minicomputer programming, Captain James E. Negro, Lt. Stanley R. Robinson, and Dr. Gary B. Lamont for their interest and valuable assistance in this problem.

The greatest debt I owe is to my wife Maryann for her enormous love and understanding during this trying period. Her support was the single greatest motivator in the preparation of this work.

Zdzislaw H. Lewantowicz

Contents

	<u>Page</u>
Preface	ii
List of Tables	vii
List of Figures	viii
List of Symbols	xi
Abstract	xiii
I. Introduction	1
Research Goals	2
Analog ALOT Control Scheme	4
Digital vs. Analog ALOT Control	14
Statement of the Problem	15
Scope	15
Assumptions	15
Goals and Standards	16
II. ALOT System Model and Kalman Filter	17
ALOT Modeling	17
Glint	17
Bias	21
Measurement Noise	21
Photomultiplier Tube (PMT)	25
PMT Low Pass Filter	25
A/D	26
Kalman Filter	26
Dither "d"	27
Digital Integrator, Optimal Controller, and D/A	28
D/A Low Pass Filter	28
Disturbance Process Θ_T	29
Fine Pointing Mirror	31
Decoupling of Axes	34
Kalman Filter	36
Simplified ALOT Model	38
Modeling of the Disturbance Process	38
Filter Equations	42
Pointing Error Sign Estimation	49
Optimal Controller	50

Contents

	<u>Page</u>
III. Simulation of Kalman Filter in the ALOT Control Loop	54
Simulation Concepts	54
White Noise v	54
Disturbance Process $\theta_T(k)$	55
Frequency Response Algorithm	56
Operation of the Simulation Program	56
IV. Implementation of the Algorithm	58
Implementation Problems	59
Precision	59
Scaling	60
Round-off and Truncation	61
Exponential Evaluation	61
Program Modularity	62
Two Axis Program	63
Program Flexibility	63
Monitor Table	63
Flow Diagram	63
Error Rejection Bode Plots	65
V. Results	66
CDC 6600 Simulation	66
Open Loop Simulation	66
Choice of Shaping Filter	67
First Order Filter Simulation	69
Error Rejection	73
ALOT Laboratory Results	74
Single Axis Results	75
Two-Axes Implementation	85
ALOT Model Parameter Perturbations	91
Target Search and Acquisition	95
Algorithm Sensitivity	95
Adaptive Extended Kalman Filter	97
Measurement Noise Adaptation	97
Adaptation for I_{\max}	100
VI. Conclusions and Recommendations	108
Conclusions	108

Contents

	<u>Page</u>
Recommendations	110
Bibliography	112
Appendix	113
Vita	136

List of Tables

<u>Table</u>		<u>Page</u>
I	TABULATED JUMP RESONANCE FREQUENCIES AND ERROR AMPLITUDES AS A FUNCTION OF INPUT AMPLITUDE $ \theta_T $	13

List of Figures

<u>Figure</u>		<u>Page</u>
1	Glint Model for a Spherical Target	6
2	Block Diagram of Conical Scan System (Ref 2:55)	8
3	Effect of Pointing Error on Reflected Intensity for Dithered Beam (Ref 2:53)	9
4	Error Signal Out of PMT and Out of AGC (Ref 2:67)	10
5	Measured Closed Loop Frequency Response with Jump Resonance for $\theta_T = 100 \sin \omega t (\mu\text{rad})$ (Ref 2:91)	12
6	ALOT Model and Kalman Filter Control Loop . .	18
7	Glint vs. x-Pointing Error	19
8	Example of I_{\max} Variation	21
9	PMT Noise--All Room Lights Off	22
9	(continued)	23
9	(continued)	24
10	Effect of PMT Low Pass Filter	26
11	PMT Filter Frequency Response	27
12	Effect of D/A Low Pass Filter	29
13	D/A Filter Frequency Response	30
14	Fine Pointing Mirror	31
15	Transformation from Electrical Signal to Linear Displacement	32
16	Fine Pointing Mirror Frequency Response . . .	35
17	Simplified Digital ALOT with Kalman Filter . .	39

<u>Figure</u>		<u>Page</u>
18	Possible Shaping Filters	41
19	Two Axes ALOT Model with First Order Shaping Filters	43
20	Beam Pointing Angle Geometry	45
21	Main Program Functional Diagram	64
22	Kalman Gain Time History	70
23	Single State Filter Variance	71
24	Simulated Error Rejection	74
25	Single Axis Error Rejection	76
26	Variance Time History	77
27	Kalman Gain Time History	78
28	Tracking Photographs (Non-Adaptive)	80
28	(continued)	81
28	(continued)	82
29	Two Axis Error Rejection	87
30	Two Axes Tracking Photographs (Non-Adaptive) .	89
30	(continued)	90
31	Effect of Dither Size on Error Rejection . . .	92
32	Effect on R on Error Rejection	93
33	Effect of Q on Error Rejection	94
34	Effect of Strong Measurement Noise v	97
35	R Adaptation Algorithm	99
36	Effect of R Adaptation	99
37	R Time History	101
38	Two Axis Error Rejection--Adaptive Filter . .	103

<u>Figure</u>		<u>Page</u>
39	I_{\max} Time History	104
40	Kalman Gain Time History (Adaptive)	106
41	Variance Time History (Adaptive)	107


List of Symbols

A/D	Analog to digital converter
b	Glint bias (volts)
d	Discrete dither (μrad , volts)
D/A	Digital to analog converter
F	State transition constant
f_B	Low pass filter break frequency (Hz)
f_{θ_T}	Disturbance process frequency (Hz)
G_m	Fine pointing mirror gain ($\mu\text{rad}/\text{volt}$)
G_P	Photomultiplier tube (PMT) gain ($\text{volt}/\text{watt}/\text{cm}^2$)
h	Predicted intensity measurement (volts)
H	Linearization of predicted intensity measurement
I	Output of PMT (volts)
I_{\max}	Maximum target reflected intensity (volts)
\hat{I}_{\max}	Estimated I_{\max} (volts)
k	Discrete time
k^-	Discrete time just before measurement
k^+	Discrete time just after measurement
K	Kalman gain
P	Kalman filter variance (volts^2)
Q	Strength of disturbance process (μrad^2)
R	Strength of measurement noise (volts^2)
\hat{R}	Estimated strength of measurement noise (volts^2)
RES	Residual (volts)


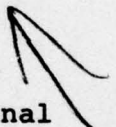
List of Symbols

SRES	Filtered residual (volts)
SZET	Filtered intensity measurement (volts)
T	Sampling period (sec)
u	Feedback control (volts)
v	Measurement noise (volts)
w	White noise driving a shaping filter (μrad)
x	Pointing error in x-direction (μrad , volts)
\hat{x}	Estimate of x-pointing error (μrad , volts)
y	Pointing error in y-direction (μrad , volts)
\hat{y}	Estimate of y-pointing error (μrad , volts)
z	Measurement model (volts)
α	Time constant of shaping filter (sec^{-1})
ζ	Intensity measurement (volts)
θ_T	Target pointing angle with respect to mirror base (μrad)
$\dot{\theta}_T$	Time derivative of θ_T ($\mu\text{rad}/\text{sec}$)
θ_m	Laser beam pointing angle with respect to mirror base (μrad)
$\dot{\theta}_m$	Time derivative of θ_m ($\mu\text{rad}/\text{sec}$)
σ_G	Glint model dispersion (spread) (μrad , volts)
ω_d	Analog dither frequency (rad)

ABSTRACT



An adaptive extended Kalman filter (EKF) is used in an Adaptive Laser Optics Techniques (ALOT) control loop to track the glint from a spherical target. A fourfold improvement in tracking bandwidth is obtained over a conventional conical scan ALOT tracking loop implemented with the same hardware. The increase in tracking bandwidth is manifested in the ratio between the (conical scan) dither frequency and the tracking bandwidth which is 2.5:1 for the EKF and 10:1 for the conventional analog or digital glint tracking schemes. The EKF provides correct pointing error estimates over essentially the entire range of the pointing error, whereas in a conventional conical scan loop the demodulated error versus true pointing error function is highly non-linear due to the nonlinearity of the glint. This results in a demonstrated ability of the EKF to track a larger amplitude disturbance than the conventional conical scan loop. Adaptive schemes are employed to make the estimation algorithm insensitive to fluctuations in the mean level of reflected intensity and to variations in the strength of measurement noise.



I. Introduction

This report presents the use of a Kalman filter in an Adaptive Laser Optical Techniques (ALOT) glint tracking scheme for precision pointing of a laser beam at a target. The Kalman filter and control algorithm has been simulated on the CDC 6600 computer and implemented in the ALOT demonstration laboratory at the Air Force Weapons Laboratory, Kirtland AFB. This estimation and control algorithm improved the ALOT control loop bandwidth by a factor of four.

The high-energy laser potentially is an effective weapon, especially against airborne targets. Before the laser can be realized as a weapon, however, several engineering problems must be solved. One of the significant problems is in the precision pointing of the laser beam at a target. Any relative high frequency motion between the laser output beam and the target will disperse the energy over an area of the target larger than the beam spot size. Since target kill probability is a function of the time average peak energy density on the target surface, it is essential to limit the beam dispersal to a minimum. The purpose of the ALOT control loop is to eliminate or reduce this dispersal by controlling the small amplitude relative motion between the beam and the target. This motion can

result from target motion, beam jitter, mirror vibration, optical path bending by the atmosphere, and any other device jitter that can cause relative motion, real or apparent, between the beam and the target. We will call this motion the disturbance process.

Research Goals

The tracking ability of the ALOT control loop can be discussed in terms of a ratio between the dither frequency and the bandwidth of the disturbance process that can be controlled. This ratio will be called the dither-to-response ratio.

Although as expressed earlier, the goal is to minimize the laser beam energy dispersion over an area of the target, it is not possible to eliminate entirely all of the relative motion. Additionally, it is necessary to induce a known amount of relative motion between the laser beam and the target before any information about the position of the laser beam with respect to the target can be determined. This induced motion is called the dither and denoted here as "d". Although any induced motion of the beam with respect to the target is contrary to the goal of minimizing the relative motion, the dither is essential. It is generally of small relative amplitude and its frequency is considerably higher than the highest disturbance process frequency to be controlled.

An accepted measure of the tracking loop bandwidth is the error-rejection-bandwidth. It is defined as the frequency at the -3dB point on the error rejection Bode plot. Error rejection is defined as $20 \log [1/(1+G)]$, where G is the unity-feedback open-loop transfer function. For this problem, error rejection is defined as $20 \log |X(j\omega)/\theta_T(j\omega)|$ where X and θ_T are the pointing error and the disturbance process respectively in the frequency domain.

The dither-to-response ratio will be used as a basis of comparison for the different ALOT loop control schemes. We can present two arguments for using the dither-to-response ratio as the basis, assuming that the dither frequency is the highest frequency that the fine pointing system can respond to. First, assume that the bandwidth at the disturbance process to be controlled is stated as a specification, and that the cost of the tilt mirror used in the ALOT loop rises with the required bandwidth of the mirror. Then it is economical to use a mirror which has a bandwidth equal to the dither frequency and not greater. However, the dither frequency, and in turn the mirror bandwidth, is determined by multiplying the bandwidth of the disturbance process that we want to control by the dither-to-response ratio. Thus the bandwidth of the disturbance process and the dither-to-response ratio determine the minimum bandwidth of the fine pointing mirror. Secondly, assume that we have a fine pointing mirror of a

given fixed bandwidth, then the highest disturbance frequency that we can control is determined by dividing the mirror bandwidth by the dither-to-response ratio.

Thus, the dither-to-response ratio is chosen as the basis for comparison between the previously achieved performances in the ALOT control loop and the performance realized in this study.

Analog ALOT Control Scheme (Ref 2)

The analog ALOT control scheme uses the conical scan principle employed in search and track radars. It is not a new concept in laser beam directional control as evidenced by:

A multidither tracking and focus control system has at various times been referred to by many names: 'Conical Scan' . . . , 'Beam Active Tracking' (BAT), or 'Adaptive Laser Optical Techniques' (ALOT) (Ref 6:12).

The following discussion of the analog ALOT control loop paraphrases portions of Ref 2:52-57. This concept uses the laser radiation reflected from the target to determine the angular pointing error. The laser beam is dithered in a small circle about a nominal pointing direction and the pointing error is deduced from the resulting changes in the intensity of the reflected radiation. The sensed reflected radiation from the target can be described as a function of the laser beam pointing direction and is called the glint. The pointing error in one axis is defined as the angular deviation x at the beam from the center of the glint,

boresight error. This translates to a linear pointing error in the target plane. The glint reflected from a ball bearing can be modeled as a bivariate Gaussian (Normal) function with a two dimensional pointing error argument.

$$I(x,y) = I_{\max} \exp\left(-\frac{x^2 + y^2}{2\sigma_G^2}\right) + b \quad (1)$$

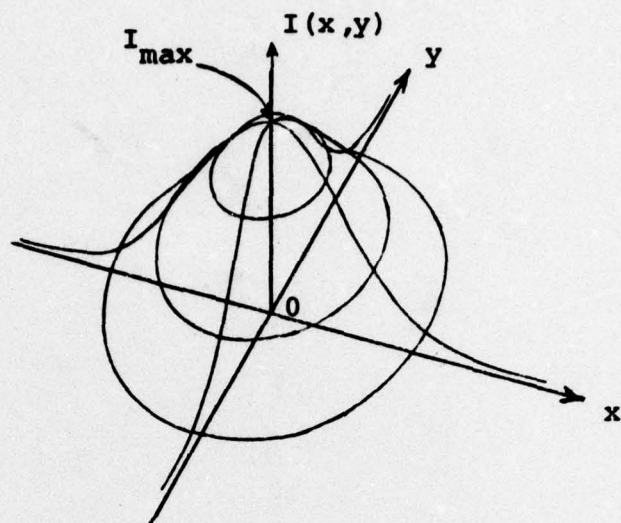
where I_{\max} is the maximum return intensity, σ_G is the dispersion of the Gaussian function, and b is a bias, as shown in Figure 1a. The x and y arguments are the two axes of the pointing mirror. Equation (1) can be rewritten as:

$$I(x,y) = I_{\max} \exp\left(-\frac{x^2}{2\sigma_G^2}\right) \exp\left(-\frac{y^2}{2\sigma_G^2}\right) + b \quad (1a)$$

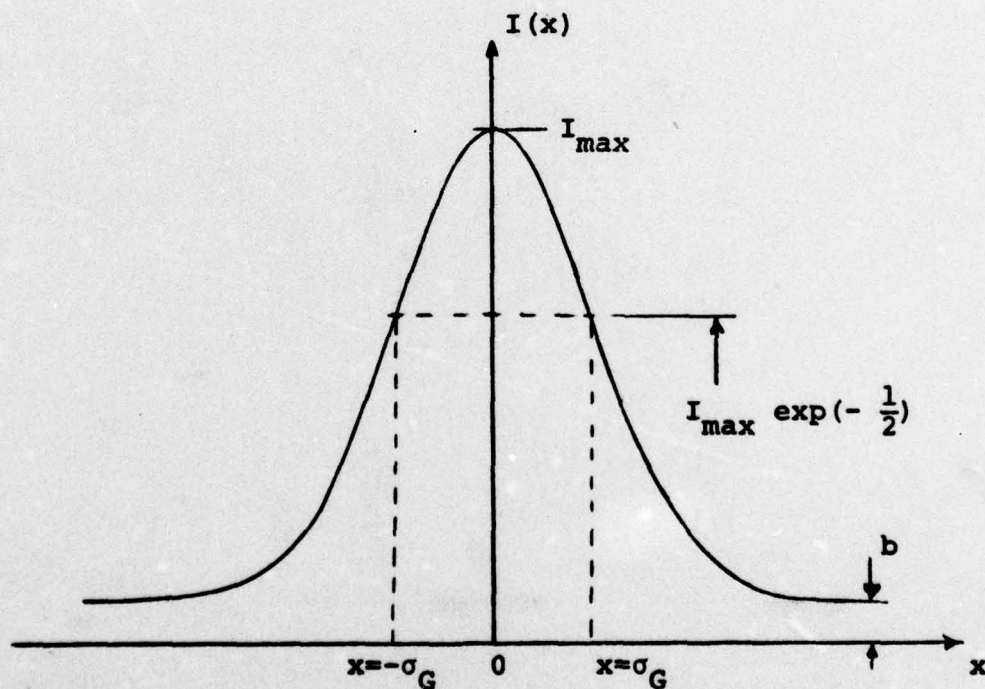
For $y = 0$, Equation (1) becomes

$$I(x,0) = I_{\max} \exp\left(-\frac{x^2}{2\sigma_G^2}\right) + b \quad (2)$$

In the single axis x , the glint $I(x,0)$ is the resulting model of the reflected intensity. This is generated by sweeping the laser beam along the "equator" of the ball bearing. The reflected intensity increases as the beam approaches the "center" of the ball, and decreases as the beam departs the center. The single-axis glint then is a unimodal function which is modeled by a Gaussian curve. The two-axis and the single-axis glints are presented in Figure 1; a single-axis experimental glint is shown in the next chapter (Figure 7).



a. Two Axis Glint Model without Bias b
(Traced from Ref 8:52)



b. Single Axis Glint Model with Bias b

Figure 1. Glint Model for a Spherical Target

The two-axis pointing system is presented schematically in Figure 2. Disregarding the y-axis in Figure 2, we can discuss the single x-axis control loop. In the case of a single-axis pointing system, the laser beam is dithered by a small angle about the nominal pointing angle. The resulting change in reflected intensity $\epsilon(t)$ is shown in Figure 3. The magnitude of $\epsilon(t)$ is approximately proportional to the amplitude of the pointing error x , provided x is less than the glint spread σ_G . This is shown in Figure 4. The tested signal includes $\epsilon(t)$, the nominal glint intensity, a bias due to background radiation, and wide bandwidth (white) measurement noise. This signal is passed through the automatic gain control (AGC). This makes the demodulation scheme essentially independent of I_{\max} as shown in Figure 4. Variations in I_{\max} can be caused by laser power variation, by a change in composition of the optical transmission medium (e.g., smoke or haze passing the optical path), or by a change in the target range or target curvature.

The signal exiting the AGC is then demodulated by multiplying the AGC output by the reference dither (ω_d) signal. The output of the demodulator consists of the low frequency pointing error signal and harmonics of the dither frequency (Ref 2). Since only the pointing error signal is desired, the output of the demodulator is filtered to pass the pointing error signal and attenuate all other signals.

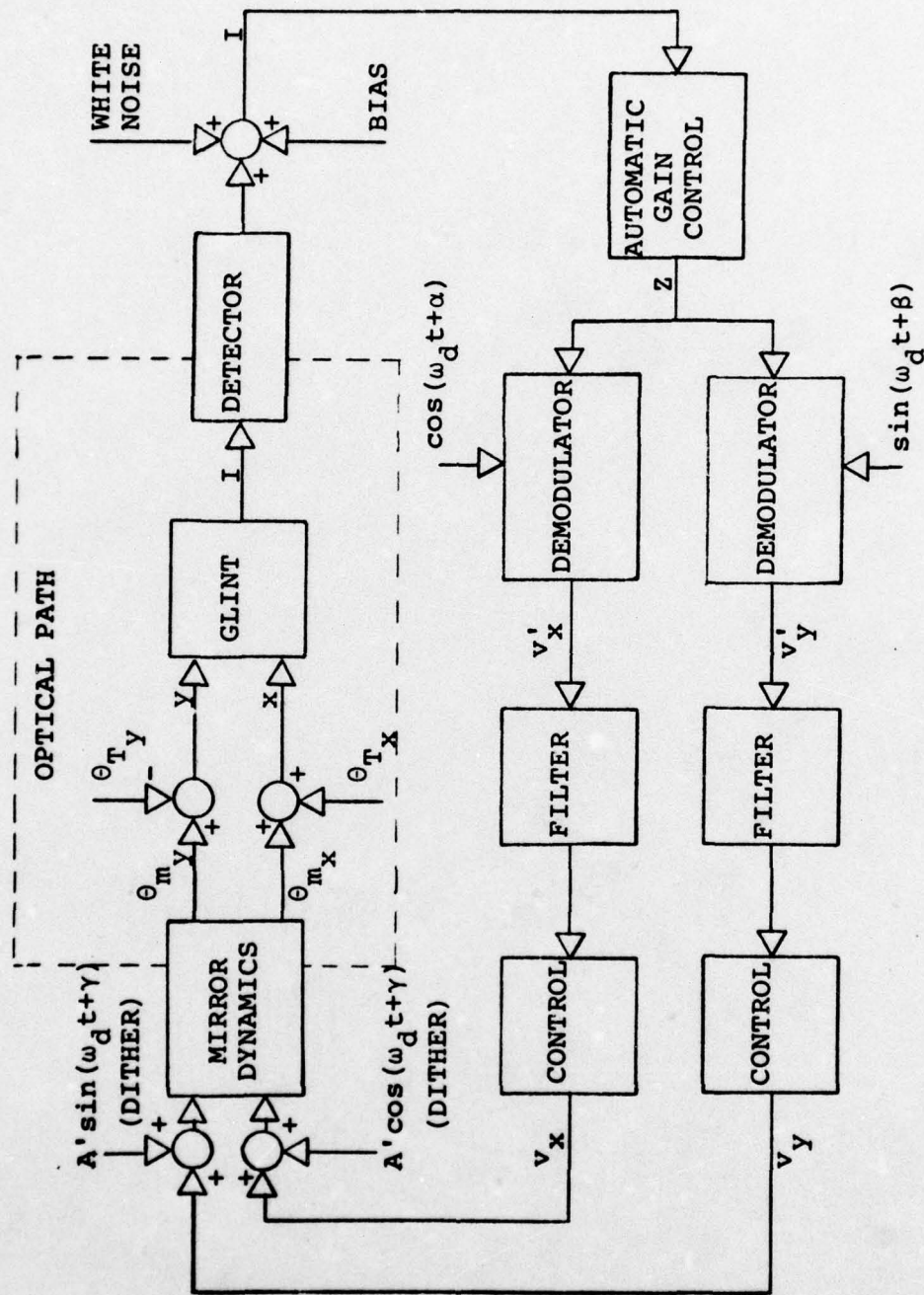


Figure 2. Block Diagram of Conical Scan System (Ref 2:55)

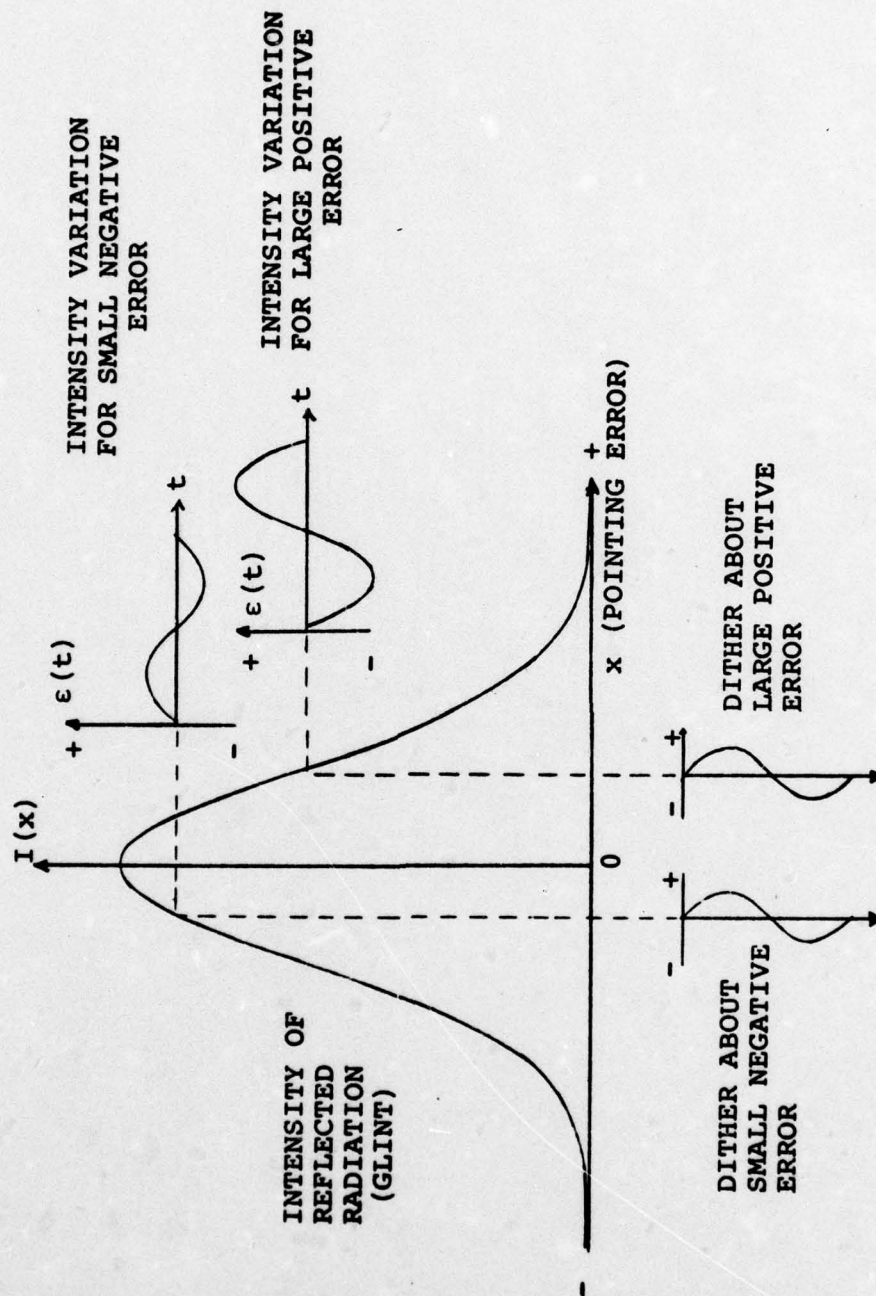


Figure 3. Effect of Pointing Error on Reflected Intensity for Dithered Beam (Ref 2:53)

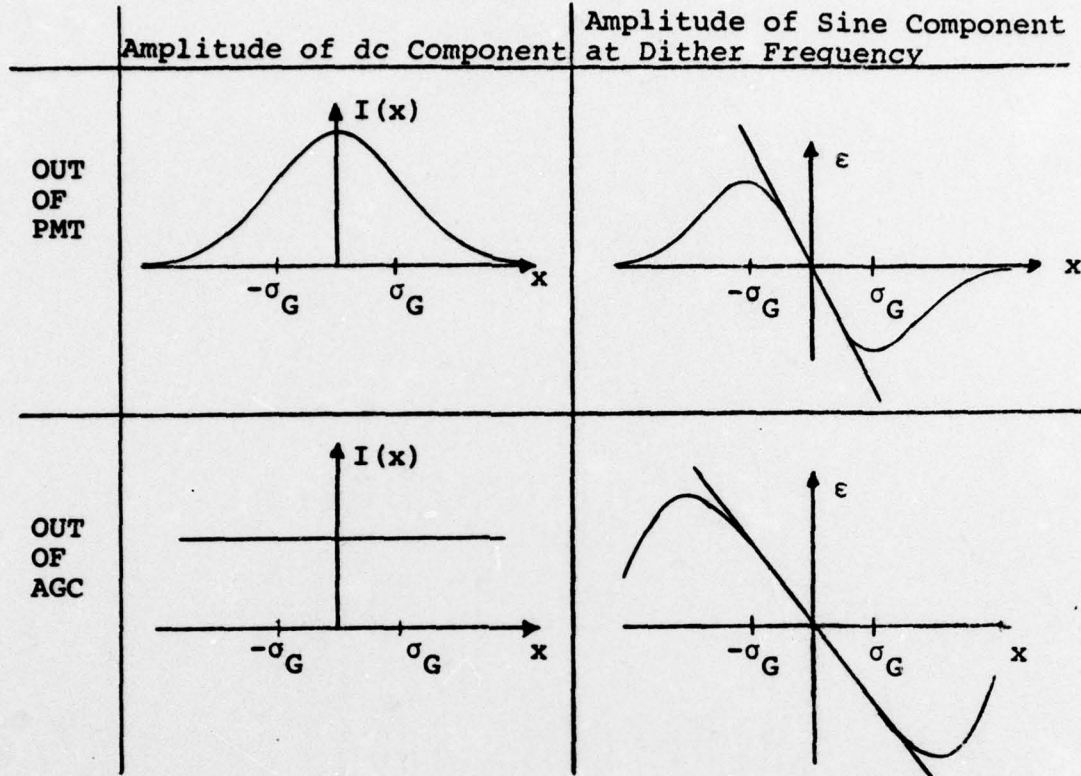


Figure 4. Error Signal Out of PMT and Out of AGC (Ref 2:67)

The pointing error signal is then fed to the controller, which generates mirror commands. This command signal, in turn, drives the mirror to null the pointing error in that axis. How well the pointing error can be eliminated by the analog ALOT control loop depends primarily on the frequency content, the strength of the disturbance process, and the control loop limitations.

The limitations of the analog ALOT control loop, as implemented at AFWL, come from a number of sources. Here the three most significant sources are discussed: the

linear model assumption has a limited region of validity, the small phase margin due to the low-pass filter after the demodulator and the inherent design limitation due to the lack of modeling flexibility in this conventional analog approach.

The linear model assumption is reasonably good for pointing error $|x| \approx .5\sigma_G$ as can be seen in Figure 4. For pointing errors beyond $|x| \approx .5\sigma_G$ the deviation of the curve from the straight line increases greatly. When this pointing error signal is passed through the AGC, the linear region is expanded to $|x| \approx 1.5\sigma_G$. This linear model works reasonably well in the closed loop ALOT for target-mirror angular disturbances that are small. However, if these angular perturbations exceed $|x| \approx 1.5\sigma_G$ the large deviation of the derived pointing error from the true pointing error causes ALOT loop to break lock.

The phase problem due to the filter after demodulation is best described by a quotation from Ref 2:73:

. . . the higher order the filter, the sharper the cutoff. However, higher order filters cause additional phase losses and reduce the system phase margin. This reduces the stability margin.

The combined effect of the nonlinearity and the phase problem due to the low-pass filter causes a phenomenon called jump resonance. At the jump resonance frequency the ALOT control loop suddenly introduces a catastrophic phase shift and amplitude loss. This is shown in Figure 5. The

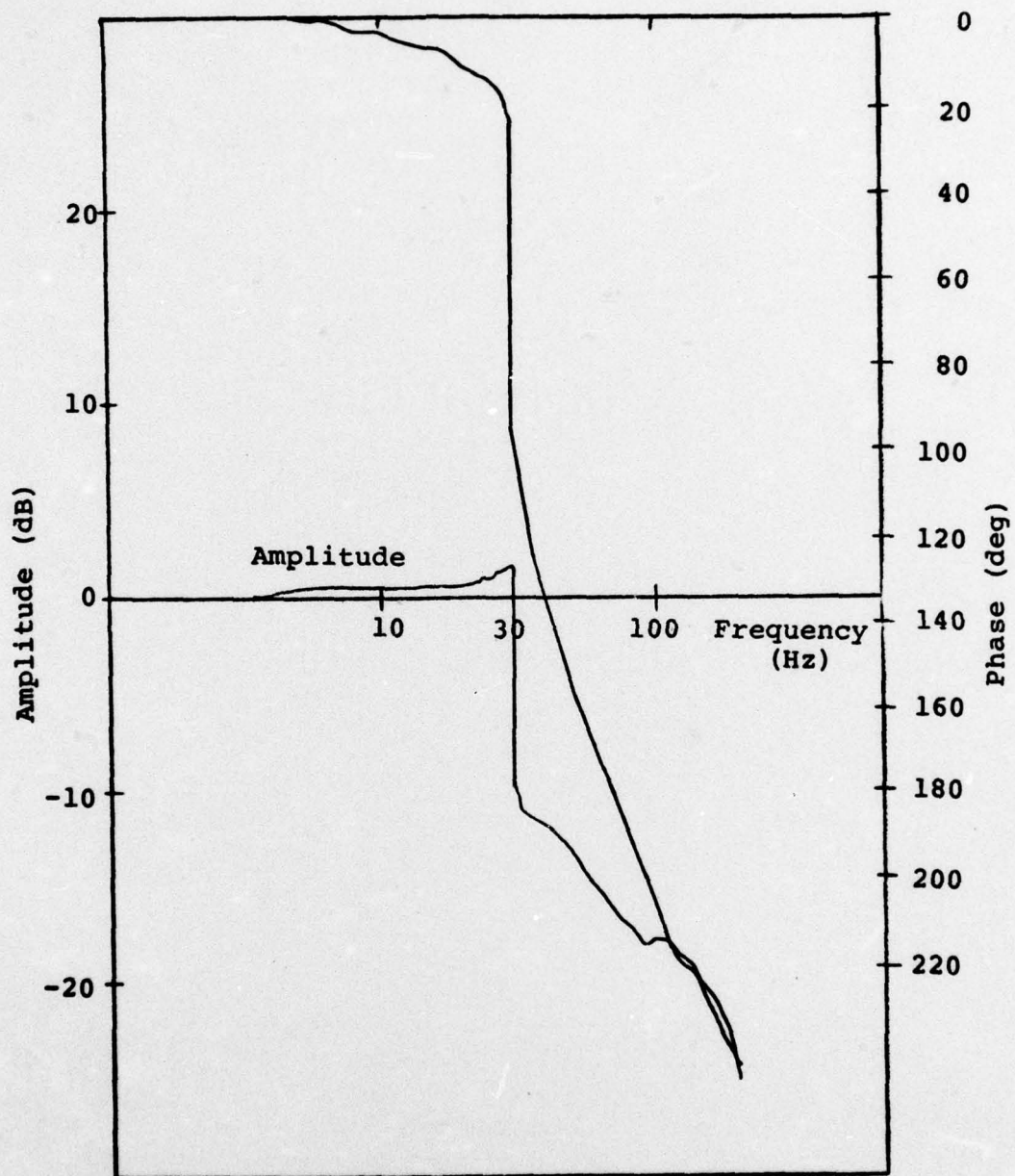


Figure 5. Measured Closed Loop Frequency Response with Jump Resonance for $\theta_T = 100 \sin \omega t (\mu\text{rad})$ (Ref 2:91)

effect of the input amplitude on the jump-resonance frequency and the error amplitude are shown in Table I.

Table I
TABULATED JUMP RESONANCE FREQUENCIES AND ERROR AMPLITUDES
AS A FUNCTION OF INPUT AMPLITUDE $|\theta_T|$

Input Amplitude $ \theta_T $ μrad	Jump Resonance Frequency, Hz (experimental)	Error Amplitude $\sqrt{x^2+y^2}$ μrad
30	52	79
40	48	85
60	36	45
100	33	56
150	24	32
200	21	30

(From Ref 2:92)

According to Ref 2:92 (Table I), the response ratio is heavily dependent on the amplitude of the disturbance process. For disturbance amplitudes $A \leq \sigma_G$ the closed loop bandwidth is approximately 50 Hz for a dither frequency of 1KHz. This translates to dither-to-response ratio of 20:1. In Ref 6:12 an open loop bandwidth of 50 Hz was obtained at a dither frequency of 750 Hz or 1 KHz, for a dither-to-response ratio of 15:1 and 20:1 respectively. Although no theoretical limit was calculated, control engineers at the Air Force Weapons Laboratory (AFWL) feel that the limiting dither-to-response ratio is approximately 10:1 for the analog system. This limit is for a control system operating in the approximately linear region of the highly

nonlinear error processor. Recent laboratory work at the AFWL has resulted in a dither-to-response ratio of 6:1. The control method used is not available at the time of this writing.

Digital vs. Analog ALOT Control

A digital control scheme was implemented, at the ALOT breadboard of the AFWL, which essentially mimicked the analog ALOT control loop (Ref 7). The glint tracking idea was viewed as a hill-climbing task and a gradient algorithm using first differences was implemented using a minicomputer. The result was a dither-to-response ratio comparable to that of the analog ALOT control loop, 10:1. Although the digital technique did not significantly improve the response ratio, it did demonstrate the feasibility of replacing the complex array of analog devices in the ALOT control loop with a digital minicomputer. The biggest advantage of the digital approach is the tremendous flexibility afforded by digital devices and techniques.

In view of the limitations in the analog and digital control schemes, another approach was necessary to improve the response ratio. It was suggested that a digital stochastic estimator may do a better job of extracting the pointing error information within the ALOT control loop. This, then, is the beginning point of this thesis.

Statement of the Problem

In this study an extended Kalman filter which is an optimal estimator, in the minimum mean squared error (MMSE) sense, is used to extract the pointing error from the highly nonlinear glint information. An "optimal" controller is used in the closed loop system to improve the dither-to-response ratio of the ALOT controller. Three engineering problems are emphasized: modeling simplicity, feasibility of the algorithm implementation, and improvement of response ratio. These problems are expanded upon in later paragraphs.

Scope. This study considers the target motion, atmospheric disturbances, laser beam instabilities, laser platform vibrations, PMT noise, and computational errors as disturbance noise sources. Simple noise models are used to describe the above disturbances, as other current studies strive for accurate descriptions of these models. This study concentrates on the proper model of the nonlinear measurement function, the treatment of this nonlinear relationship between the measured intensity and the pointing error, and reasonable efficiency of the computational techniques. The nonlinear relationship is treated by relinearizing about the current operating point.

Assumptions. In approaching this problem, some assumptions are necessary in the definition of the problem. The detailed noise models are not necessary for the

demonstration of improvement of the response ratio, and simple noise models are used for this purpose. The measured return intensity as a function of the pointing error is modeled by a Gaussian (Normal) function, Eq (1).

Goals and Standards. The goal of this study is to implement in hardware and software a digital estimator and controller utilizing simple models, but at the same time attain a significant improvement in the dither-to-response ratio. As mentioned earlier, the dither-to-response ratio is the primary standard for comparison of the results of this research to previous results in this control problem. Achievement of useful results in a control application depends not only on the control technique applied to a given problem, but also on the adequate choice of the mathematical models used to describe the "real-world" problem.

The development of the problem is discussed in the following sequence. The control loop model and the Kalman filter equations are presented in Chapter II. The simulation on the CDC 6600 computer and the implementation on the ALOT breadboard are discussed in Chapters III and IV respectively. Chapter V contains the results and Chapter VI recommends future research in this problem area.

II. ALOT System Model and Kalman Filter

The Kalman filter is an optimal (in the MMSE sense) recursive data processing algorithm which processes observation data and arrives at a "best" possible estimate of the unknown variables. However, the "optimality" of this algorithm is only as good as the "goodness" of the mathematical model describing the physical ALOT control loop. For this reason a great deal of attention is given to the development of the model for this problem.

ALOT Modeling

The ALOT control loop model in one axis is shown in Figure 6. Perhaps the most important part of that model is the glint.

Glint. The glint is defined as the intensity of the reflected radiation as a function of the pointing error. It depends on the geometry of the target surface and the laser beam cross-section. For the case in which the target is a ball bearing, the glint is very well approximated by a bivariate Gaussian function, as in Figure 1a. (The laser beam waist is approximately one fourth the diameter of the ball bearing.) If the glint is considered only in one axis, i.e., holding the other axis argument at zero, then the glint model becomes a single argument Gaussian function as

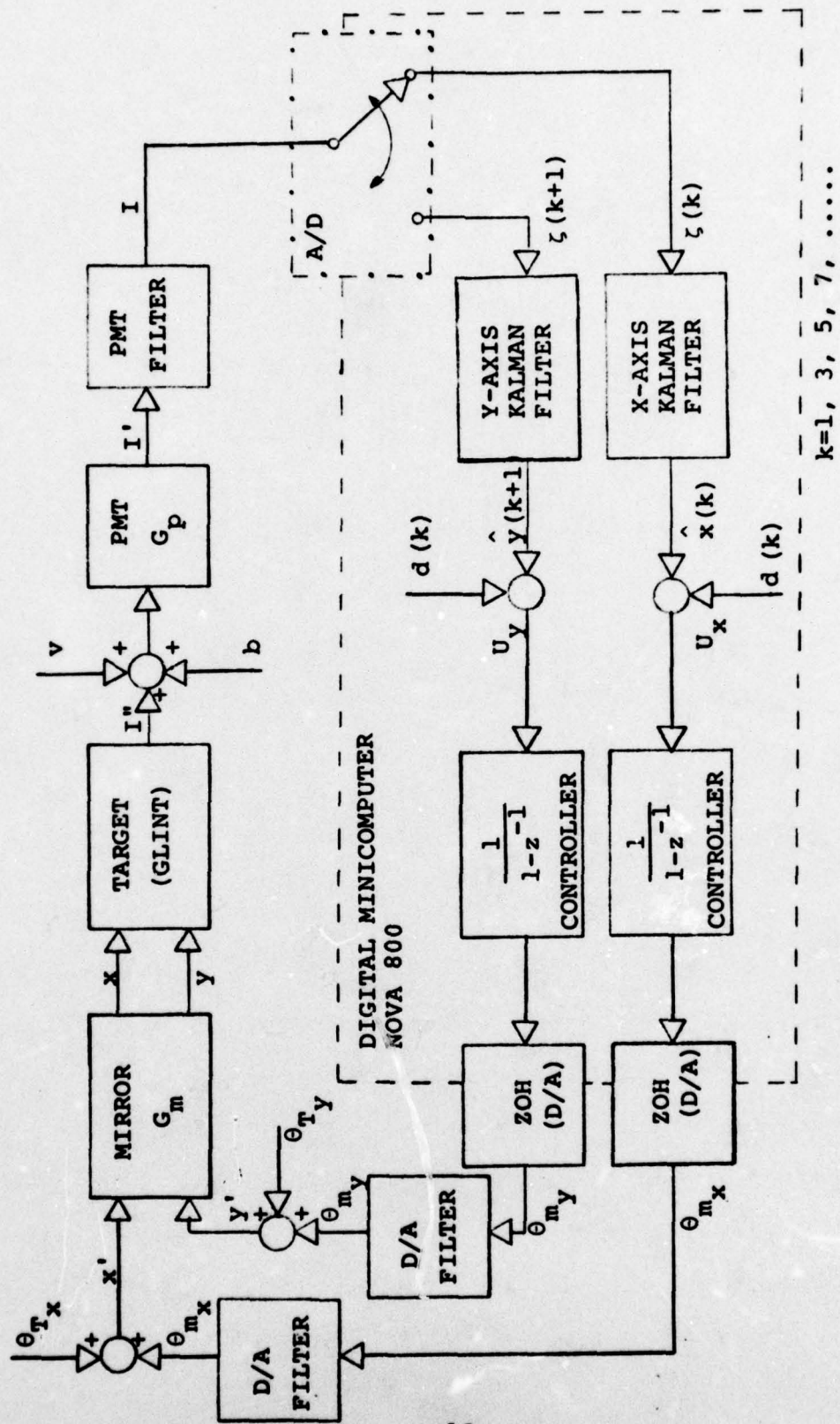


Figure 6. ALOT Model and Kalman Filter Control Loop

shown in Figure 1b. The experimental glint with the true Gaussian function superimposed, is shown in Figure 7. This

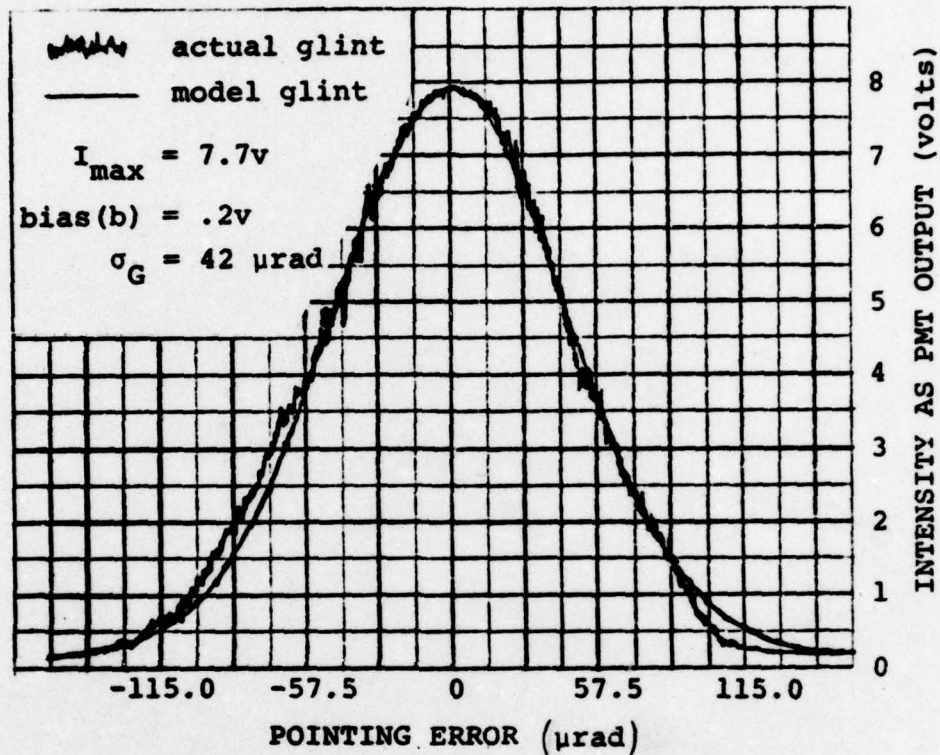


Figure 7. Glint vs. x-Pointing Error

experimental glint is modeled very well by a Gaussian function. The goodness of this model can be best explained by the fact that the glint is the result of a physical convolution of the laser beam cross-section and the reflectivity function of the ball bearing. The beam intensity distribution is Gaussian. The spherical shape of the ball bearing target reflects even a uniform density (small diameter) beam in quite a Gaussian manner; this reflection characteristic is called the reflectivity function. Then

when the ball bearing reflection, that is closely Gaussian, is convolved with the laser beam that has a Gaussian cross-section, the resulting glint is very closely modeled by a Gaussian function.

The glint model also depends on three parameters other than the pointing errors in the x and y axis. These parameters are I_{\max} and b, expressed in volts--the units of the photomultiplier tube (PMT) sensor, and σ_G expressed in volts--the units of the input to the actuators of the fine pointing mirror. For a target of nonvarying dimensions located at a fixed distance from the fine pointing mirror and illuminated by non-time varying laser beam, σ_G and b parameters are constant and measurable. However, I_{\max} was found to be varying in time. The amplitude of this variation varied from day to day, but ranged from .2 volts peak to 1.0 volts peak. One sample of this variation can be seen in Figure 8 which represents the sensor (PMT) output as a function of time for the case where the laser beam is illuminating the ball bearing center. The average I_{\max} is 3.75 v and bias b is 0.25 v. The source of this I_{\max} variation is caused by a variation in the laser output power. In a real world application this I_{\max} variation can be caused by other additional sources, such as changing target geometry, or changing distance between the laser tracker and the target.

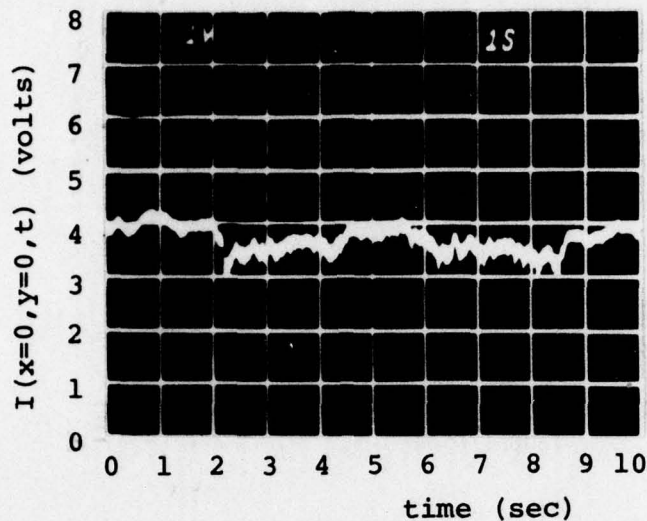
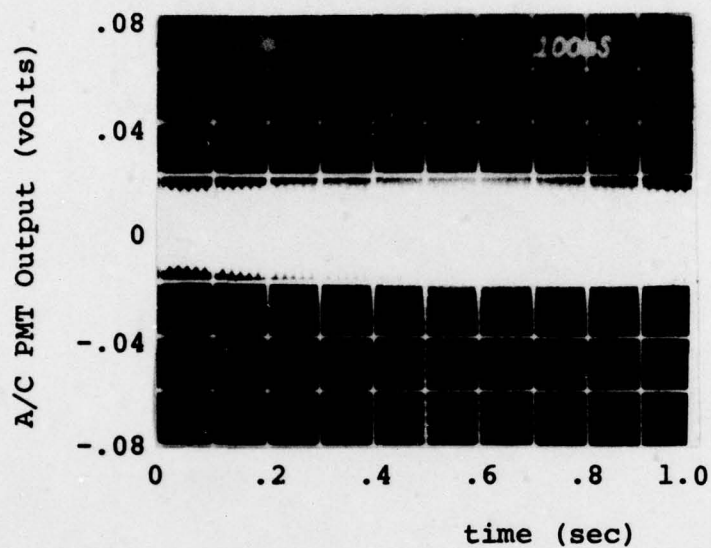


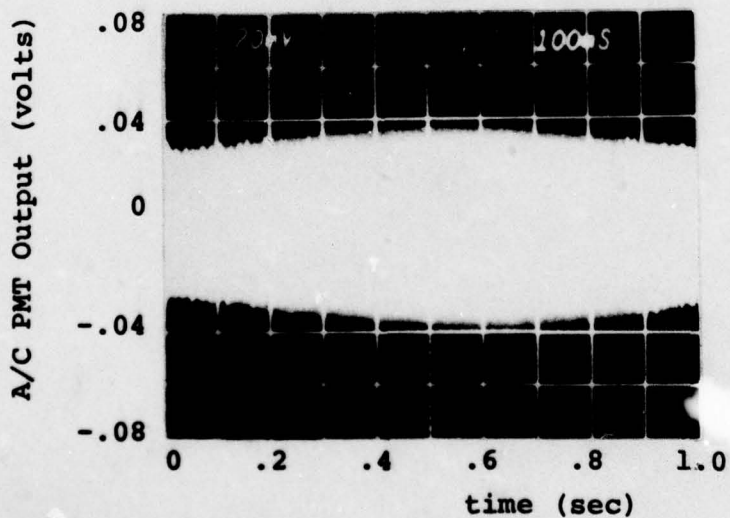
Figure 8. Example of I_{\max} Variation

Bias. Continuing clockwise on the ALOT control loop in Figure 6, constant bias b is added to the glint and is shown experimentally in Figure 7. The magnitude of b depends on the strength of the background lights and equipment pilot lights. The laser beam scattering from the optical bench optics also is sensed by the PMT and contributes to the magnitude of b .

Measurement Noise. The measurement noise v entering the same summer as bias b in Figure 6, is modeled as a white noise of strength R . Consider the data in Figure 9 showing the measurement noise characteristics. Figure 9a shows a very low level background noise. The laser beam is capped, only electronic equipment pilot lights are turned on. The 60 Hz power coming from these pilot lights

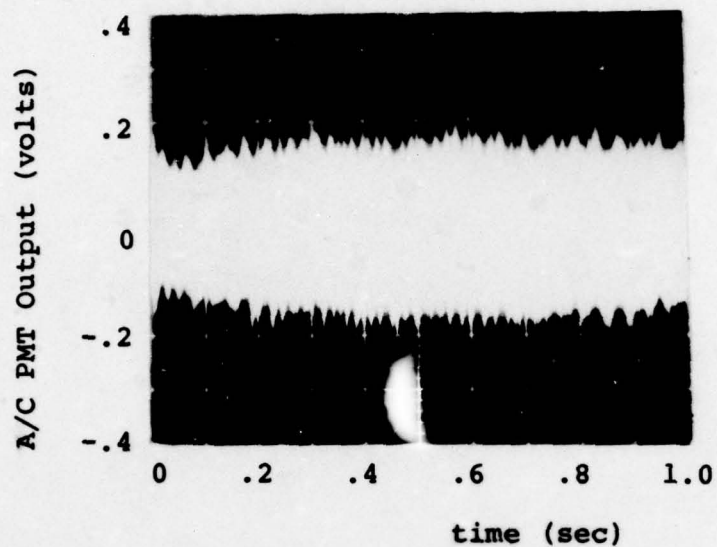


a. Laser Beam Covered Up

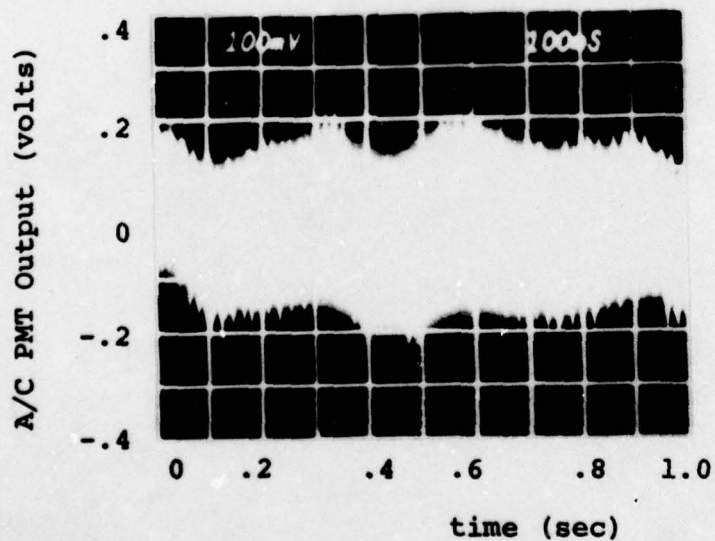


b. Laser Beam on, Off Target, on Velvet

Figure 9. PMT Noise--All Room Lights Off

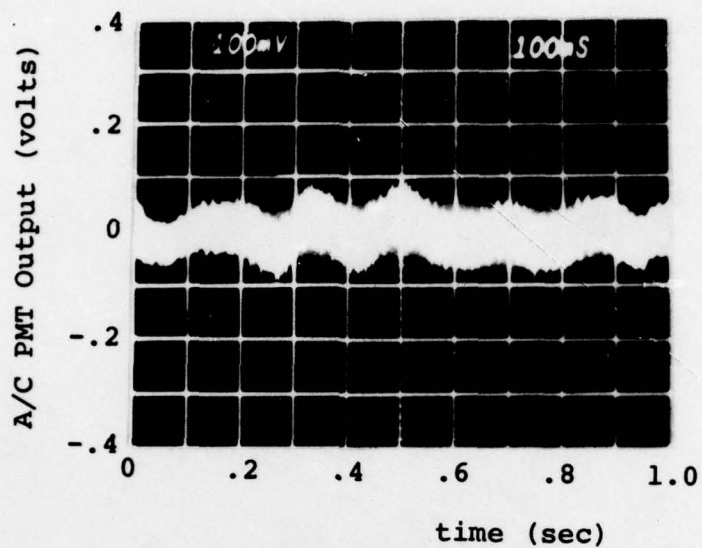


c. Beam at $x = 0$

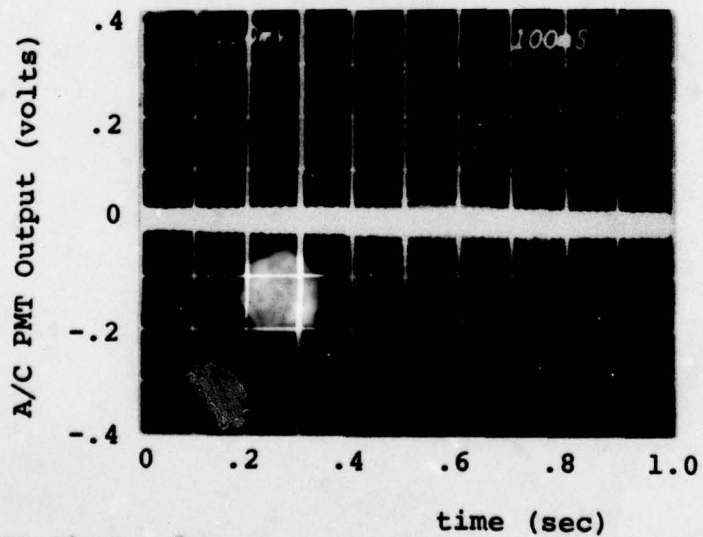


d. Beam at $x = 1\sigma_G$

Figure 9 (continued)



e. Beam at $x = 2\sigma_G$



f. Beam at $x = 3\sigma_G$

Figure 9 (continued)

is evident. The PMT generated white noise appears to be considerably smaller than .02 v and will be neglected. Figure 9b shows PMT output with the laser beam off target and reflecting from a black velvet background. Figure 9c shows the PMT output with the beam positioned at $x=0$, $y=0$, i.e., at the center of the ball bearing target. The noise level increased by a factor of five over that in Figure 9b. (Note change of scale in the photos.) Figures 9d, 9e, and 9f show the PMT output for the beam pointing at $x=1\sigma_G$, $x=2\sigma_G$, and $x=3\sigma_G$ respectively. Although these photographs confirm the wide band of this measurement noise, it also points out the noise magnitude dependence on the pointing error, or on the position of the laser beam on the steel ball target. Additionally, in Figures 9d and 9e a low frequency (approx. 0-10 Hz) fluctuation is evident and appears to be strongly related to the low frequency fluctuation evident in Figure 7. The modeling of these measurement noise sources is deferred to a later paragraph.

Photomultiplier Tube (PMT). The next block in the ALOT control loop is the PMT. This is a complex non-linear device that transforms light energy entering it into an electrical signal. The non-linearity was shown to be insignificant, therefore the PMT is modeled as a pure gain-- G_p .

PMT Low Pass Filter. The next block in the ALOT control loop diagram is the PMT low pass filter. Its purpose is to filter out high frequencies well above the frequency

content of the dither and control loop signals. This filter cuts down the frequency content of the "white" measurement noise, and significantly decreasing its variance. Figure 10 shows the effectiveness of the PMT low pass filter, and Figure 11 shows the PMT filter Bode plot.

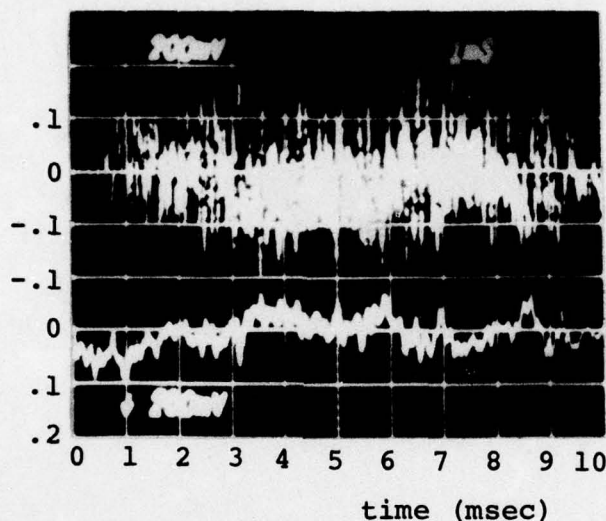


Figure 10. Effect of PMT Low Pass Filter
Upper--Raw (A/C) PMT Output
Lower--Filtered (A/C) PMT Output

A/D. Following the PMT low pass filter in the control loop is a sampler, or an analog-to-digital converter (A/D). It is a 12-bit device with a conversion speed of approximately 40 μ sec. It requires an external clock pulse for initiation of the conversion and has a 0-10 volt sample range.

Kalman Filter. Following the A/D is the digital Kalman filter algorithm which processes the sampled data to provide

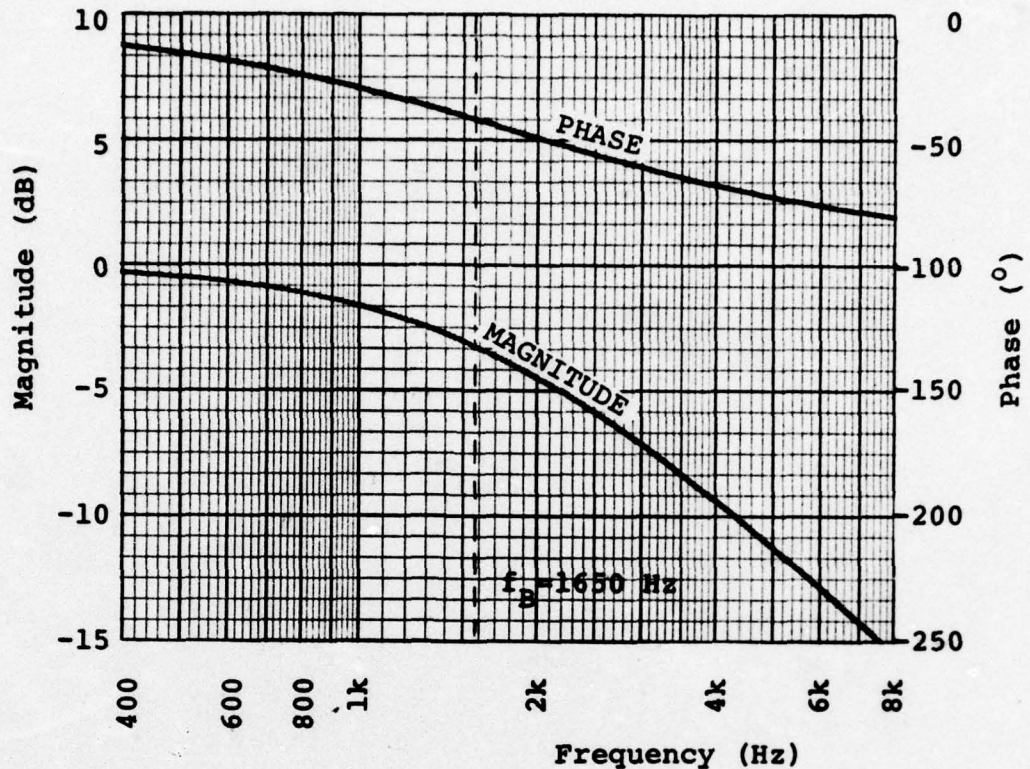


Figure 11. PMT Filter Frequency Response

the best possible estimates (in the MMSE sense), \hat{x} and \hat{y} , of the pointing errors in the x and y axes respectively. Since from this point in the control loop both the x and y loops are identical, only the x channel will be discussed. The development of the Kalman filter is deferred to a later section.

Dither "d". In a conical-scan type modulation-demodulation scheme a controlled perturbation is applied in the form of a dither to extract information from a system. In this digital control scheme it is necessary, as pointed out in an earlier discussion, to induce a controlled motion in

each axis so that pointing error information can be extracted. This controlled motion is in the form of a discrete (step) dither (d) that is applied simultaneously with the loop control input.

Digital Integrator, Optimal Controller, and D/A. The control signal $u(k) = -\hat{x}(k^+) + d(k)$, consisting of the best estimate of the pointing error together with the dither, is added to the previous mirror pointing direction.

$$\theta_m(k+1) = \phi_m \theta_m(k) + B_m u(k) \quad (3)$$

where $\phi_m = 1$, and $B_m = 1$

In a later section it will be shown that this is a deadbeat optimal controller. This digital signal is then converted through the digital-to-analog converter (D/A). The D/A is a 12-bit zero order hold (ZOH), with a range of -10 to +10 volts. The D/A conversion is considered instantaneous upon command. The output of the D/A is a piecewise constant (step) signal.

D/A Low Pass Filter. Since the step signal ideally contains the entire frequency spectrum, it is not a desirable signal to drive the fine pointing mirror. This mirror, which will be discussed in the following paragraph, has a finite bandwidth, however, this finite bandwidth mirror has resonances at higher frequencies. Thus the fine pointing mirror is susceptible to excitation in its higher harmonics by the higher frequencies contained in the step function. To eliminate this undesirable effect the step output of the

D/A is passed through the D/A low pass filter. The effect of the D/A low pass filter on the D/A step output can be seen in Figure 12. Figure 13 shows the D/A filter Bode plot. Thus it can be seen that the high frequency excitation of the mirror is eliminated without attenuating any dither or control information. The bandwidth of this filter is 350 Hz.

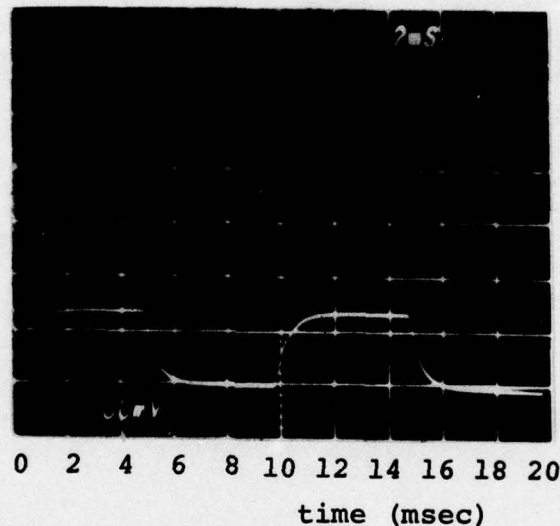


Figure 12. Effect of D/A Low Pass Filter
 Upper--D/A Output (.5v/cm)
 Lower--Filtered D/A Output (.2v/cm)

Disturbance Process θ_T . There are a number of sources of disturbances that may cause the unwanted movement of the laser beam away from the desired pointing direction. It could be the vibration of the target with respect to inertial space. The laser optics platform, primarily the fine pointing mirror, is susceptible to vibrations. The induced

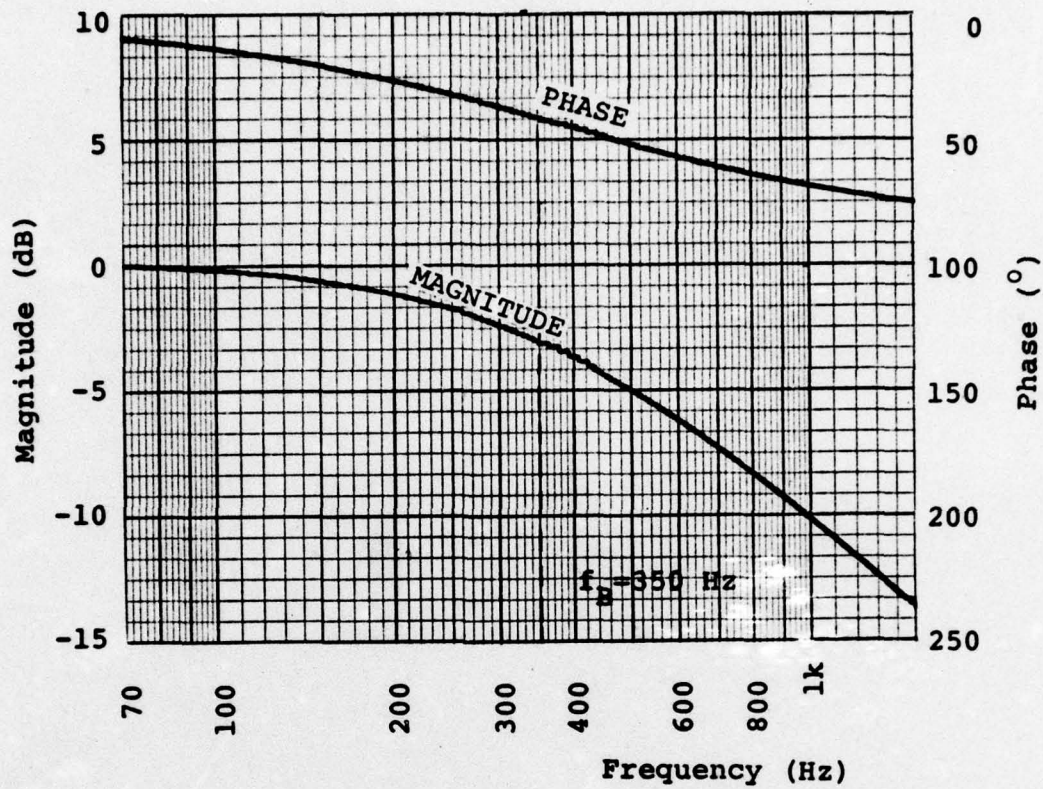


Figure 13. D/A Filter Frequency Response

relative motion of the optical components and the fine pointing mirror motion with respect to inertial space causes the laser beam to depart from the desired pointing direction. Atmospheric disturbances can cause the refraction of the beam away from the target, and stray electric signals in the mirror actuation system will cause an undesirable motion of the beam. All of the above disturbances cause relative angular motion of the mirror pointing direction with respect to the target. Alternatively, we can think of this disturbance motion as the motion of the target with respect to the

laser beam pointing direction. The important point is that all of the above mentioned disturbance sources cause relative random motion between the mirror beam pointing direction and the target. This relative random motion will be called the disturbance process and symbolized by θ_T for the x mirror tilt axis. The characteristics of the disturbance process will be discussed in a later paragraph.

Fine Pointing Mirror. The final component in this control loop is the fine pointing mirror and the two actuator assembly. The actuators are piezoelectric stacks that expand and contract in response to the electrical signal inputs. The mirror in Figure 14 shows the locations of the

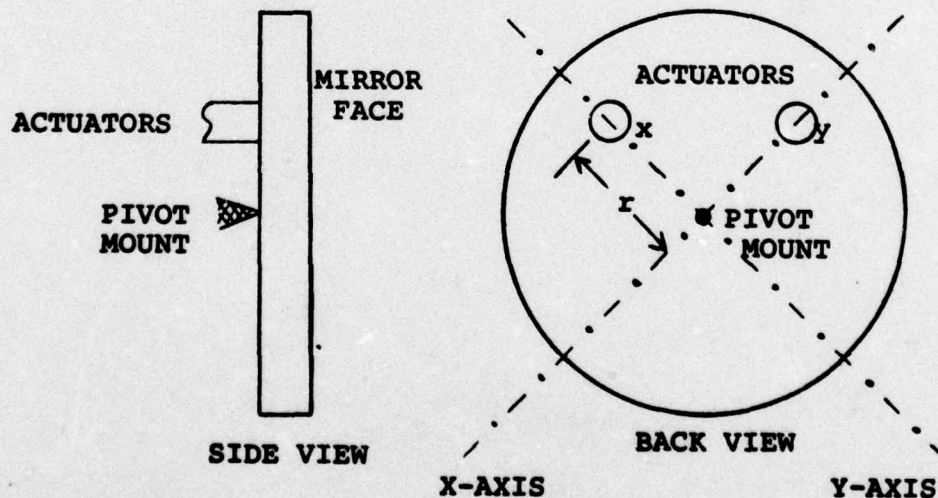


Figure 14. Fine Pointing Mirror

linear actuators, and Figure 15 shows the transformation of linear motion to angular motion. Assume that the beam

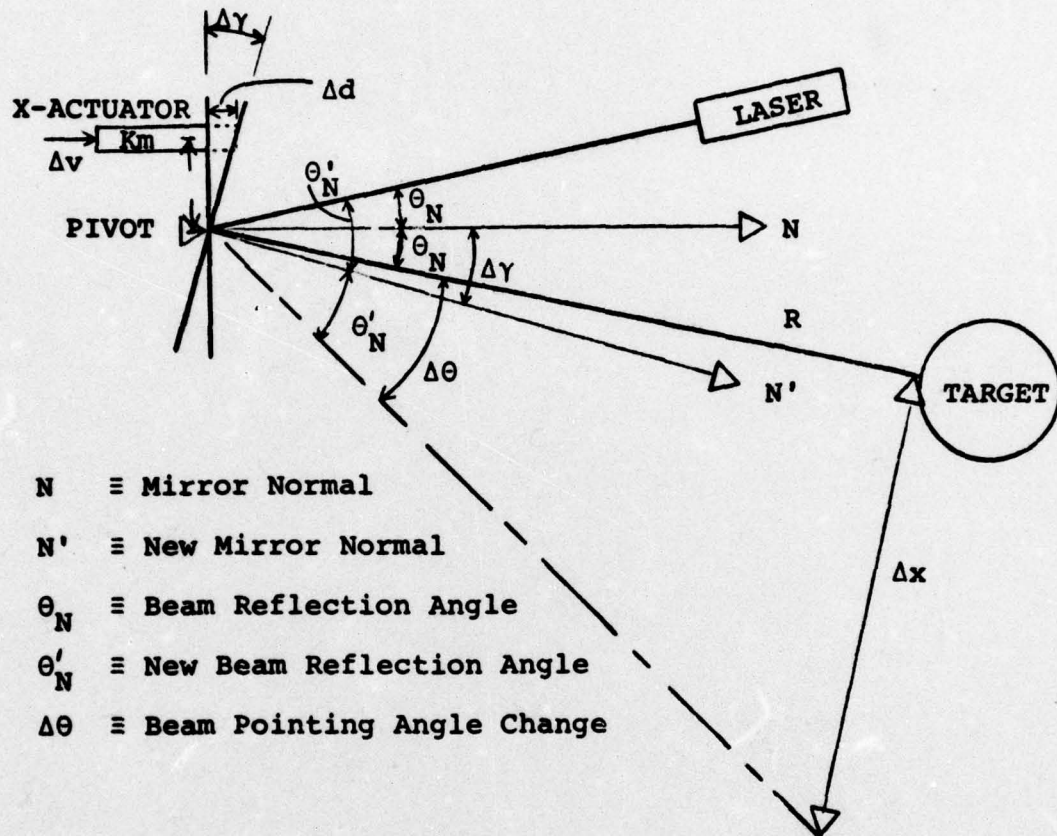


Figure 15. Transformation from Electrical Signal to Linear Displacement

reflection angle is θ_N for a neutral x-actuator position. Assume that a voltage Δv is applied to the actuator.

Assuming that the actuator response is linear the displacement $K_m \Delta d$ is produced where K_m is the actuator gain. Then the mirror tilt $\Delta \gamma$ for small angles is

$$\Delta \gamma = \tan^{-1} \frac{\Delta d}{r} \approx \frac{\Delta d}{r} = \frac{\Delta v K_m}{r} \quad (4)$$

where r is the actuator moment arm.

Also, from Figure 12 we have (Snell's law)

$$2\theta_{N'} = 2\theta_N + \Delta \theta \quad (5a)$$

$$\theta_{N'} = \theta_N + \Delta \gamma \quad (5b)$$

where $\theta_{N'}$ is the new beam reflection angle, and $\Delta \theta$ is the beam pointing angle change. Then substituting (5b) into (5a) we get

$$\Delta \theta = 2\Delta \gamma \quad (5c)$$

However, we desire the output Δx in terms of Δv .

$$\Delta x = \sqrt{R^2 + \Delta x^2} \sin \Delta \theta \quad (5d)$$

where R is the distance from the fine pointing mirror to the target. For small angles $\Delta \theta$, Δx is small with respect to R and $\Delta \gamma$ can be approximated by

$$\Delta x = R \Delta \theta = 2R \Delta \gamma = \frac{2R}{r} \Delta v K_m \quad (5e)$$

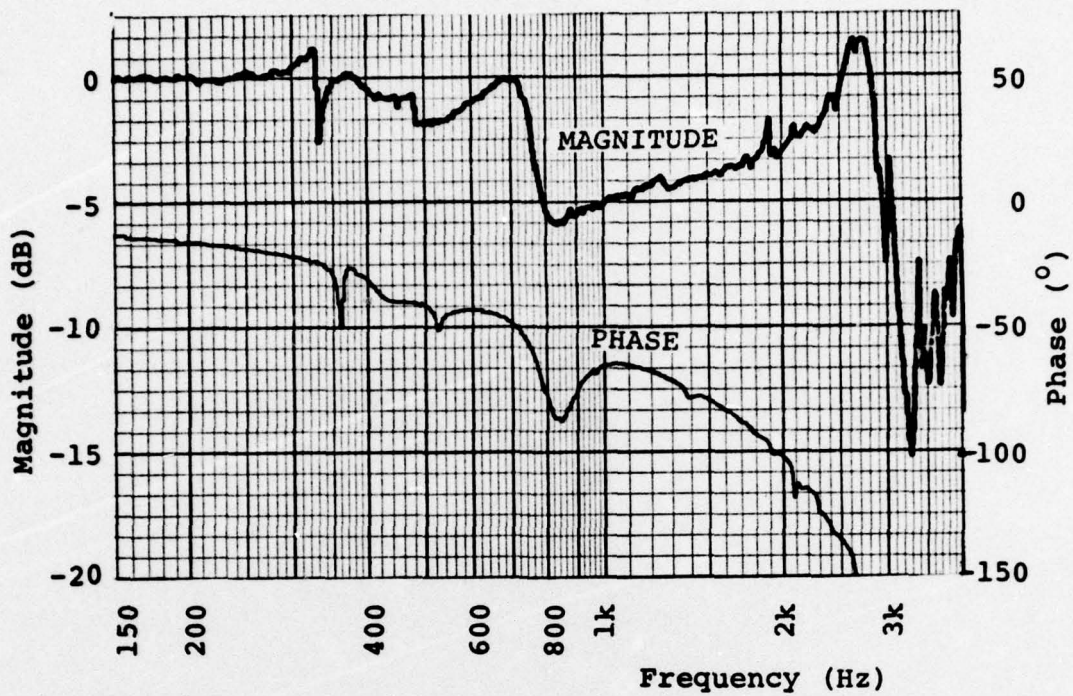
The final relation is

$$\frac{\Delta x}{\Delta v} = \frac{2RK_m}{r} \quad (5f)$$

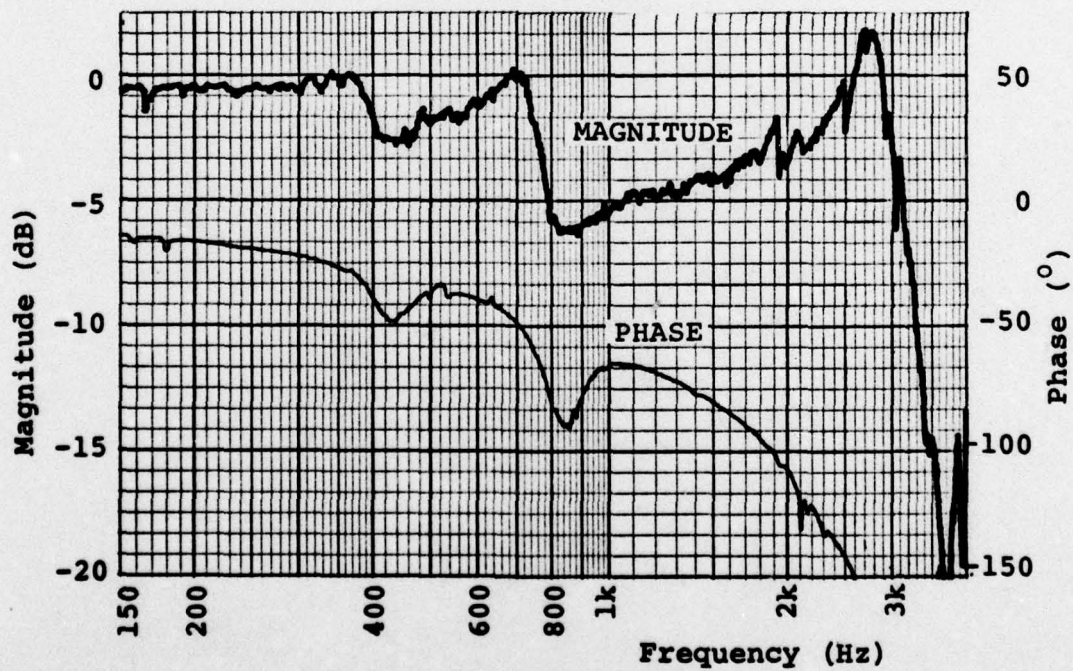
where $\Delta x/\Delta v$ is the fine pointing mirror transfer function.

The bandwidth of the fine pointing mirror is high. Bode plots in Figures 16a and 16b show the x-axis and y-axis frequency response of the tilt mirror. The frequency responses in the two axes are reasonably close as expected from a mirror that is mounted symmetrically on the actuators and the pivot point. The significant resonances appearing above 400 Hz may be the interaction between the flexible mirror attachment points and the masses of the mirror and actuators. Whatever the cause of these resonances, it is not desirable to operate the mirror at a frequency above 400 Hz. To preclude the necessity for modeling of these resonances, the highest frequency of the control loop, i.e., the dither rate, was set at or below 400 pulses per second. This corresponds to a basic dither frequency of 200 Hz. Up to 300 Hz the mirror frequency response is essentially flat and can be modeled by a transfer function consisting of a simple gain-- G_m .

Decoupling of Axes. In general the coupling between the two axes can be expected. Two sources of possible axes coupling exist: first is the mechanical cross-coupling of the axes due to the imperfect mirror and actuator assembly, and the second is due to the coupling of the axes in the estimation algorithm. The mechanical cross-coupling is weak at frequencies below 500 Hz as observed in the laboratory, and therefore not modeled. The axes coupling due to the estimation algorithm is significant, especially at



a. x-axis



b. y-axis

Figure 16. Fine Pointing Mirror Frequency Response

higher disturbance process (θ_T) frequencies. The effect of this coupling is presented in a later chapter. However in the ALOT model it is assumed that at lower θ_T frequencies the cross-coupling is negligible and modeled as non-existent. This decoupling is based on the premise that the dither and control in each axis is independent from the other axis. This is possible by alternating the dither and control between the two channels, that is the dither and control in one axis are independent in time from the dither and control in the other axis. Because of this assumed lack of axes correlation, the pointing error estimation and control can be accomplished by two parallel and independent algorithms, alternating in time.

Kalman Filter

The Kalman filter introduction in these paragraphs is paraphrased from Reference 3. The Kalman filter recursive algorithm uses all available measurements, regardless of their precision, to provide the best possible estimate of the unknown parameters. It does so in presence of measurement noises and system disturbances. The Kalman filter can be shown to be the best filter of any conceivable form if three restrictions are met. First, the system and the state measurements must be linear. Second, the system and measurement noises must be effectively white, that is, the bandwidth of these noises must be wider than the bandwidth

of the system to be controlled. Third, these noises must be Gaussian, that is the distribution of the noise amplitudes takes on the shape of a normal (Gaussian) bell-shaped curve.

Statistically the state variable can be described by a conditional probability density function conditioned on the measurement history. Since the Gaussian assumption is made, this conditional probability density function can be completely described by the first and second moments, or by its conditional mean and variance.

The ALOT control loop is a nonlinear system. The nonlinearity is in the relationship between the pointing error of the laser beam and the intensity of the reflected energy from the target as shown in Eq (1). The dynamic model of the ALOT control loop is linear. The nonlinearity of the measurement can be relinearized about the operating point. Because of the necessity to relinearize, the estimator takes on the form of an extended Kalman filter (EKF). The other two restrictions are fulfilled as the measurement noise and the ALOT system driving disturbance process are assumed to be both Gaussian and white. The disturbance process is narrow band, however, it can be modeled as the output of a shaping filter driven by white Gaussian noise.

Simplified ALOT Model. Considering only the x-axis, Figure 6 is simplified. The y-axis is an "image" of the x-axis. The PMT and the D/A low pass filters are simplified to a gain, as the bandwidths of these filters exceed the bandwidth of interest in the ALOT control loop. The fine pointing mirror and the PMT are operated within respective regions that can be modeled by simple gains. The ZOH will also be simplified to a pure gain, at the discrete times k , to keep the modeling simple. However, it must be remembered that for control system frequencies approaching the Nyquist rate limit a significant phase lag is introduced. Combining all of the gains into the fine pointing mirror gain G_m , the simplified ALOT loop is presented in Figure 17. The parameter that remains to be discussed is the disturbance process θ_T .

Modeling of the Disturbance Process. The disturbance process θ_T was described in an earlier paragraph as the random relative motion between the mirror platform and target. It is not the purpose of this study to prepare an accurate model of the random disturbance process, but to develop a working model for the laboratory implementation.

If it is to be controlled, this random disturbance process must be band limited, it is already assumed to be random. This band limited disturbance process can be modeled as the output of a shaping filter driven by white noise. Only three questions then remain to be answered.

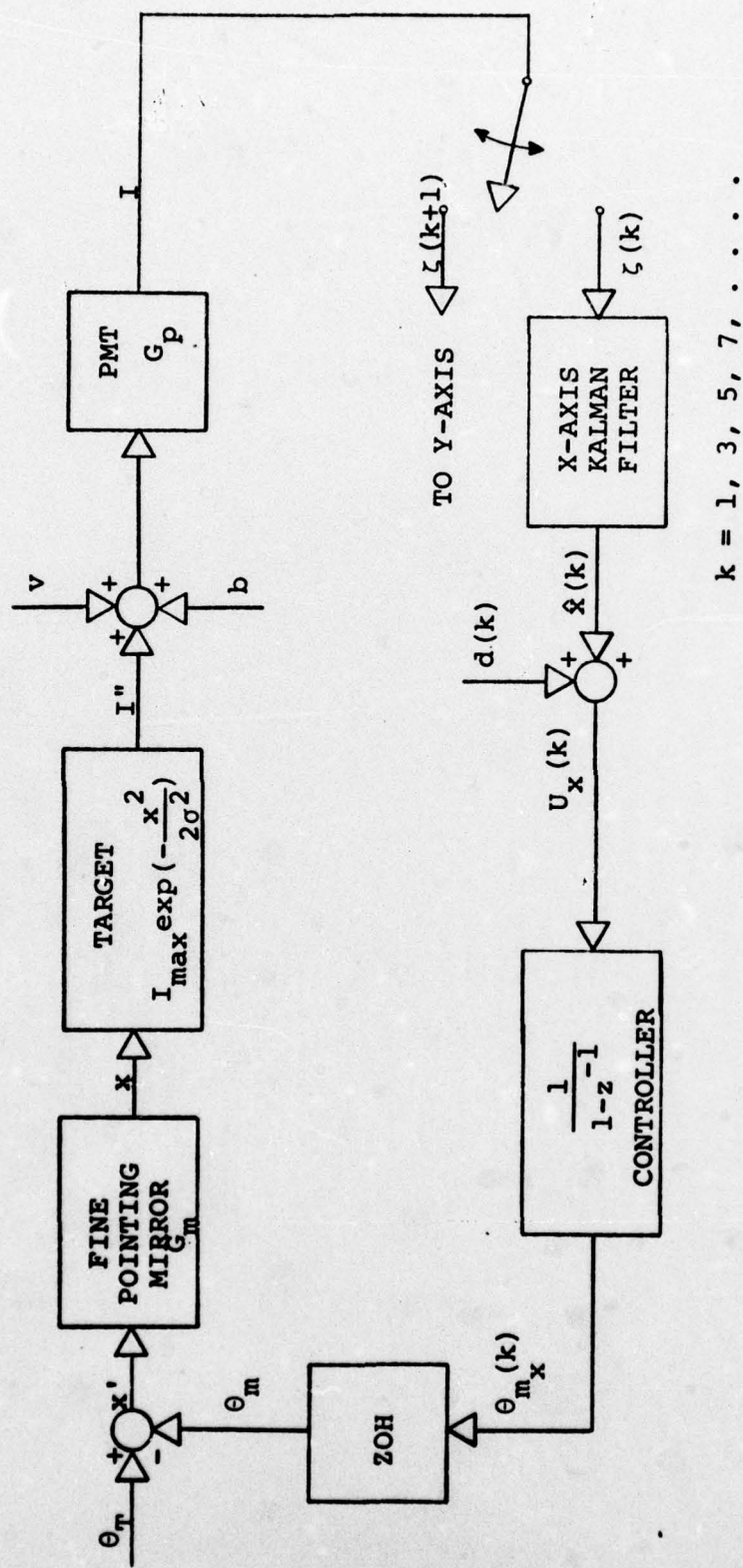
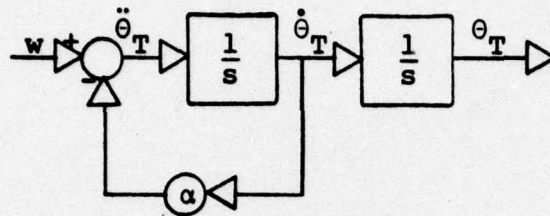


Figure 17. Simplified Digital ALOT with Kalman Filter

First, what is the least order of shaping filter that will be adequate? Second, what is the bandwidth of this shaping filter? And third, what is the white noise strength driving the shaping filter? Considerable attention was given to the initial shaping filter. The random disturbance process, or the relative motion between the tilt mirror and the target, consists of random motions of the target, mirror, mirror platform, and the atmospheric disturbances to the beam propagation path. It seemed logical to think that a proper model of this disturbance process would be a second order shaping filter driven by white noise at the acceleration level as shown in Figure 18a. Another shaping filter in Figure 18b is similar to the one above, but has an additional noise source at the velocity level. Finally, in Figure 18c, is a first order shaping filter with the white noise driving the velocity. The three candidates for a shaping filter model were proposed for various reasons. The first order shaping filter is often an adequate model for a particular disturbance process and is the simplest to implement. The other two shaping filters are variations of disturbance models sometimes used to describe the relative motion between two airborne vehicles. The shaping filter that produces the best error rejection is chosen experimentally as discussed in Chapter V. Each of the above shaping filters has been used in the Kalman filter algorithm, however the first order shaping filter was



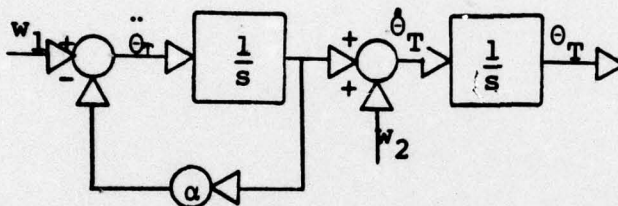
$$E\{w(t)\} = 0$$

$$E\{w(t)w(t-5)\} = Q\delta(t-5)$$

$$\begin{bmatrix} \dot{\theta}_T \\ \ddot{\theta}_T \\ \theta_T \end{bmatrix} = \begin{bmatrix} 0 & 1 \\ 0 & -\alpha \end{bmatrix} \begin{bmatrix} \theta_T \\ \dot{\theta}_T \end{bmatrix} + \begin{bmatrix} 0 \\ 1 \end{bmatrix} w$$

$\begin{matrix} \text{F} & \text{G} \end{matrix}$

a. Single Noise Source--Second Order Shaping Filter



$$E\{w_1(t)\} = E\{w_2(t)\} = E\{w_1(t)w_2(t)\} = 0$$

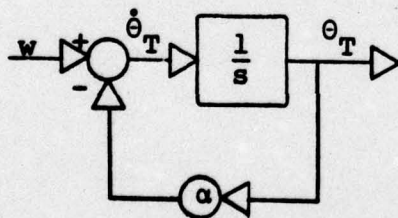
$$E\{w_1(t)w_1(t-s)\} = Q_1\delta(t-s)$$

$$E\{w_2(t)w_2(t-s)\} = Q_2\delta(t-s)$$

$$\begin{bmatrix} \dot{\theta}_T \\ \ddot{\theta}_T \\ \theta_T \end{bmatrix} = \begin{bmatrix} 0 & 1 \\ 0 & -\alpha \end{bmatrix} \begin{bmatrix} \theta_T \\ \dot{\theta}_T \end{bmatrix} + \begin{bmatrix} 1 & 0 \\ 0 & 1 \end{bmatrix} \begin{bmatrix} w_2 \\ w_1 \end{bmatrix}$$

$\begin{matrix} \text{F} & \text{G} \end{matrix}$

b. Two Noise Source--Second Order Shaping Filter



$$E\{w(t)\} = 0$$

$$E\{w(t)w(t-s)\} = Q\delta(t-s)$$

$$\begin{bmatrix} \dot{\theta}_T \\ \theta_T \end{bmatrix} = \begin{bmatrix} -\alpha \end{bmatrix} \begin{bmatrix} \theta_T \end{bmatrix} + \begin{bmatrix} 1 \end{bmatrix} w$$

$\begin{matrix} \text{F} & \text{G} \end{matrix}$

c. First Order Shaping Filter

Figure 18. Possible Shaping Filters

experimentally shown to result in at least as good error rejection as the other two. Consequently, the following Kalman filter development is based on the first order shaping filter model. The bandwidth of the shaping filter and the strength of the driving white noise were perturbed experimentally until best ALOT control loop response was achieved.

The measurement noise v presented earlier from experimental data is wide band. Therefore, it will be modeled as a white noise of a given strength.

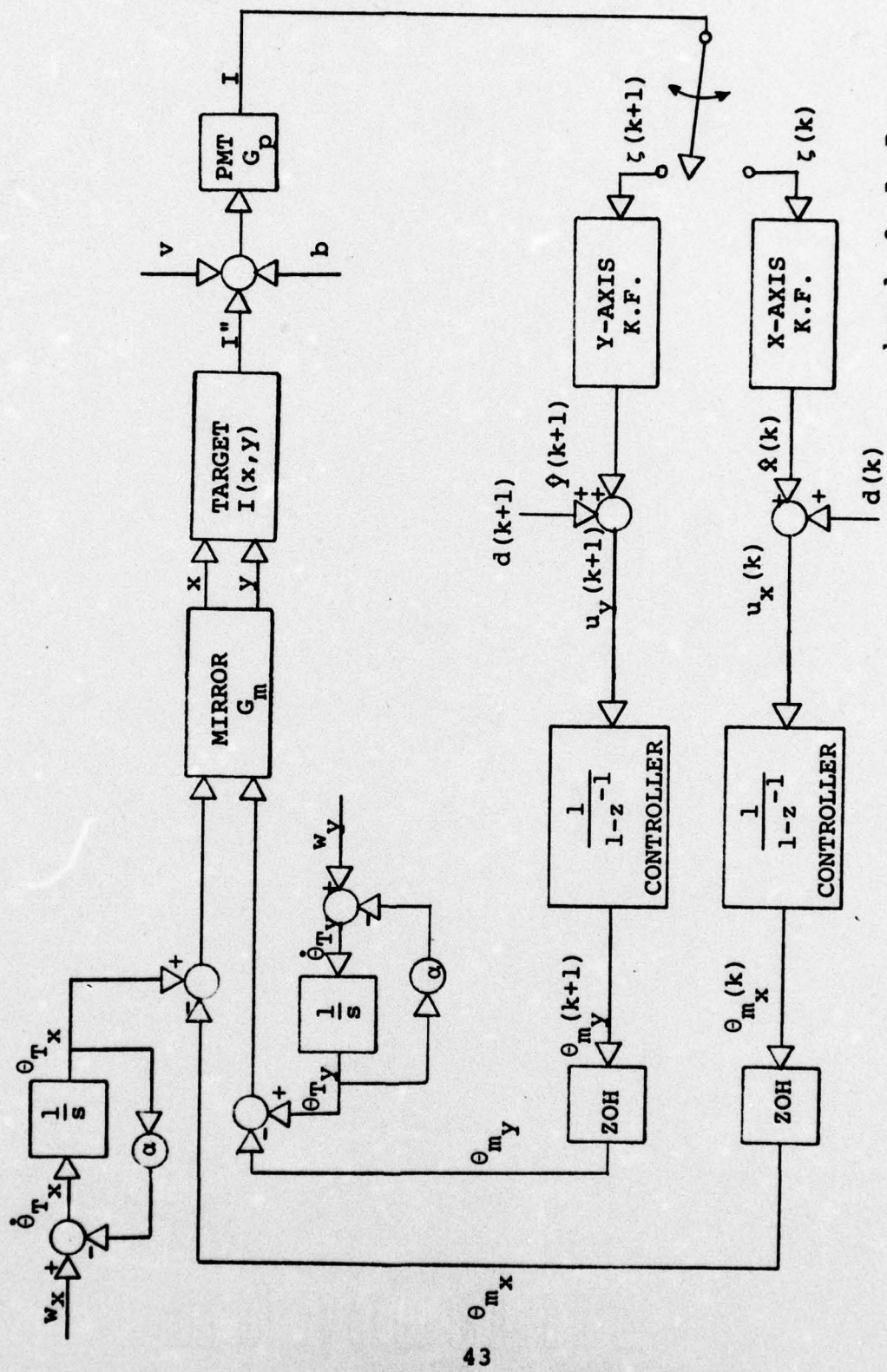
Filter Equations. Combining the simplified ALOT control loop model in Figure 17 with the first order shaping filter in Figure 18c, the entire two axes first order (in each axis) model is presented in Figure 19. The x and y sub-loops in that figure are identical except for the sample timing, thus only one loop is developed.

The equations describing a single loop are given. The target motion $\theta_T'(t)$ with respect to the mirror base as seen in Figure 19 is given by: .

$$\begin{aligned}\dot{\theta}_T'(t) &= F \theta_T'(t) + G w'(t) \\ &= -\alpha \theta_T'(t) + 1 w'(t)\end{aligned}\tag{7}$$

Where $F = -\alpha$, and $G = 1$. Discretizing this equation:

$$\theta_T'(k+1) = \phi(k+1,k) \theta_T'(k) + \int_k^{k+1} \phi(k+1,\tau) G(\tau) w'(\tau) d\tau \tag{8}$$



$k = 1, 3, 5, 7, \dots$

Figure 19. Two Axes ALOT Model with First Order Shaping Filters

Where $\phi = e^{FT}$, and T is the sampling period. The discrete motion of the fine pointing mirror with respect to the mirror base is given by:

$$\theta_m(k+1) = \phi_m \theta_m(k) + B_m u_x(k) \quad (9)$$

where $\phi_m = 1$, and $B_m = 1$.

The discrete input $u_x(k)$ contains the pointing error estimate and the dither $d(-1)^k$.

From Figure 19 it is evident that the pointing error x is:

$$x(k+1) = \theta_T'(k+1) - \theta_m(k+1)$$

and

$$\theta_m(k) = \theta_T'(k) - x(k)$$

Then subtracting Eq (9) from Eq (8) and substituting

$$x(k+1) = (e^{-\alpha T} - 1) \theta_T'(k) + x(k) - u_x(k) + \int_k^{k+1} \phi(k+1, \tau) G(\tau) w'(\tau) d\tau \quad (10)$$

The relative motion between the fine pointing mirror and the target can be arbitrarily modeled as target motion alone with respect to the mirror. The mirror is being controlled by a discrete controller. Then $\theta_m(k)$ changes with respect to the mirror base only at the sampling times k . Since it is difficult to work with $\theta_T'(k)$ it is replaced by $\theta_m(k) + x(k)$. But the mirror position $\theta_m(k)$ is a random variable and is combined under the stochastic integral in Eq (10). The

pointing geometry is seen in Figure 20. Additionally,
the statistics of the disturbance process driving target

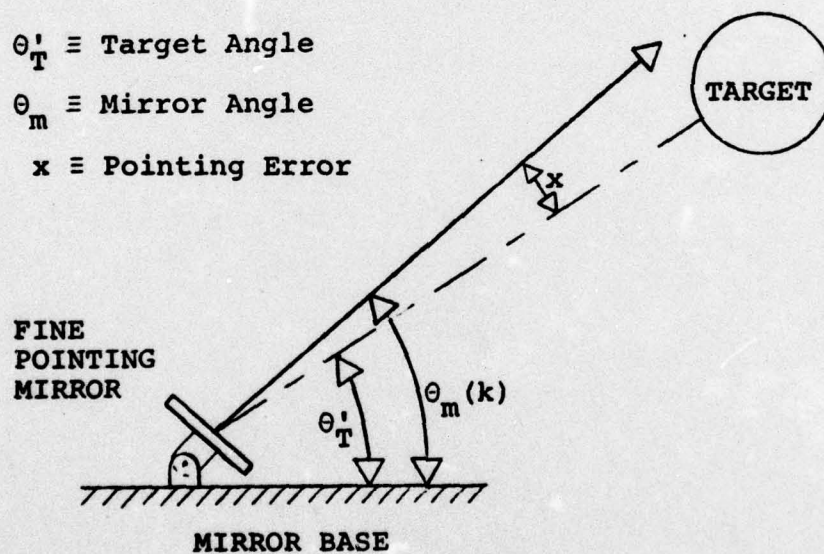


Figure 20. Beam Pointing Angle Geometry

change, and are reflected by a change of variable from $w'(t)$ to $w(t)$. Equation (10) then is rewritten:

$$x(k+1) = \phi x(k) + Bu_x(k) + \int_k^{k+1} \phi(k+1, \tau) G(\tau) w(\tau) d\tau \quad (11)$$

where $\phi = e^{-\alpha T}$, and $B = -1$. The measurement equation is

$$z(k) = I_{\max} \exp\left(-\frac{x^2(k) + y^2(k)}{2\sigma_G^2}\right) + b + v(k) \quad (12)$$

Where the bias b is assumed to be a measurable constant, and $v(k)$ is the white measurement noise. It is important to remember that the stochastic noise driving the shaping filter is no longer described by the statistics of the target motion with respect to the mirror base directly. The proper modeling of this random motion must include the statistics of the target motion with respect to the mirror base and subtracted from it is the statistical motion of the mirror as it is driven by known inputs. These known inputs, however, are dependent on the statistics of the target motion.

The filter equations, (Eq 13-19), are recursively computed (Ref 4:187,188). The mean and the variance of the conditional probability density function which describe the statistics of the pointing error $x(k)$ are propagated forward from time k^+ to time $k+1^-$ and then updated at time $k+1^+$ by incorporating the measurement at time $k+1$. The term $\hat{x}(k)$

denotes the estimate of x . The propagation of the estimate is given by

$$\hat{x}(k+1^-) = e^{-\alpha T} \hat{x}(k^+) + u_x(k) \quad (13)$$

The propagation of variance P is given by

$$\begin{aligned} P(k+1^-) &= \phi^2 P(k^+) + \int_0^T \phi^2 G^2 Q d\tau \\ &= e^{-2\alpha T} P(k^+) + \frac{Q}{2\alpha} (1 - e^{-2\alpha T}) \end{aligned} \quad (14)$$

where Q is the strength of the disturbance process $\theta_T - \theta_m$.

The predicted measurement at time k is given by

$$h(\hat{x}_k^-, \hat{y}_k^-) = I_{\max} \exp\left(-\frac{\hat{x}_k^{-2} + \hat{y}_k^{-2}}{2\sigma_G^2}\right) + b \quad (15)$$

where $\hat{x}_k^- = \hat{x}(k^-)$ and $\hat{y}_k^- = 0$ for single axis. The linearization of Eq (15), based upon the predicted pointing error, is

$$\begin{aligned} H(\hat{x}_k^-) &= \left. \frac{\delta h}{\delta x} \right|_{\hat{x}_k^-} = -\frac{\hat{x}_k^-}{\sigma_G^2} I_{\max} \exp\left(-\frac{\hat{x}_k^{-2} + \hat{y}_k^{-2}}{2\sigma_G^2}\right) \\ &= -\frac{\hat{x}_k^-}{\sigma_G^2} \left\{ h(\hat{x}_k^-) - b \right\} \end{aligned} \quad (16)$$

The update (with the measurement) of the mean $\hat{x}(k^+)$ and the

variance $P(k^+)$ is performed using the Kalman gain $K(k)$

$$K(k) = \frac{P(k^-)H(\hat{x}_{k^-})}{H^2(\hat{x}_{k^-})P(k^-) + R(k)} \quad (17)$$

where $R(k)$ is the strength of the measurement noise $v(k)$.

The update of the variance is

$$P(k^+) = P(k^-) \left[1 - K(k)H(\hat{x}_{k^-}) \right] \quad (18)$$

The update of the mean is accomplished at the very end of this algorithm, immediately after the measurement $z(k)$ is taken.

$$\hat{x}(k^+) = \hat{x}(k^-) + K(k) \left[z(k) - h(\hat{x}_{k^-}) \right] \quad (19)$$

The recursive solution of this algorithm begins at the specified initial conditions:

$$\hat{x}(0^+) = 0$$

$$P(0^+) = \frac{4}{9} \sigma_G^2$$

The initial guess of zero pointing error is better than attempting to determine from the first measurement(s) the deterministic pointing error. The algorithm initially "searches" the target area for an intensity measurement that is greater than a preset bound, thus assuring that the laser beam is initially on the target (on the glint). The step size of search algorithm is approximately equal to the dispersion ($1\sigma_G$) of the glint. The probability density

function, that describes the possible initial pointing error based on the fact that the initial measurement $\zeta(0)$ is above a certain bound, is nearly a uniform function. For computational ease it is assumed that this uniform density function can be approximated by a Gaussian curve. Then the pointing error is unknown but within certain bounds. If the $\zeta(0)$ threshold is set to coincide with $|x| \leq 2\sigma_G$ then this would correspond to the 3σ point on the Gaussian probability density function. Then

$$3\sigma(0^+) = 2\sigma_G$$

$$P(0^+) = \sigma^2(0^+) = \frac{4}{9} \sigma_G$$

is the initial condition deemed appropriate to initialize the algorithm.

Pointing Error Sign Estimation. The estimation algorithm was simulated on the CDC 6600 computer. During the early efforts it became clear that the algorithm did not properly estimate the sign of the pointing error. This is the result of the single axis argument x^2 in the measurement equation, Eq (12), for $y=0$. But $\sqrt{x^2} = \pm x$, that is, the solution has two roots and the algorithm, starting from an arbitrary initial pointing error $x(0)$, does not receive sufficient information to converge on the proper sign. In Eq (19), the term $\zeta(k) - h(\hat{x}_k^-)$ is called the residual. If the estimate of the pointing error $\hat{x}(k^-)$ is close to the true

pointing error, then the predicted measurement $h(\hat{x}_k^-)$ is close to the true measurement $z(k)$. As a result, the residual is small. Conversely, if the estimate of the pointing error in sign or in magnitude is not good, the residual is large. An upper bound is calculated for a "normal" range of the residual magnitude. Then during the initial ten iterations of the filter the sign of the pointing error estimate $\hat{x}(k^-)$ is forcibly changed whenever the filtered residual magnitude exceeds that bound. The residual magnitude is passed through a low bandwidth low pass filter to prevent sign changes for any single large residual. This allows the sign change to take place only on a consistently large residual. Once the filter converges on the proper pointing error, it is no longer necessary to keep testing the residual.

The extended Kalman filter algorithm described above provides us with the best possible estimate, in the MMSE sense, of the pointing error. This optimal estimate is, of course, confined to within the limits of the goodness of the system model and the available measurement.

Optimal Controller

According to the separation theorem

the optimal stochastic controller for a linear system driven by white Gaussian noise, subject to a quadratic cost criterion, consists of an optimal linear Kalman filter cascaded with the optimal feedback gain matrix of the corresponding deterministic optimal control problem (Ref 5:16).

This quotation is summarized by the key words: linear, quadratic, Gaussian (LQG).

In the problem development we have already made the Gaussian assumption. The ALOT control loop model is a linear one, however, the measurement equation is highly non-linear. The extended Kalman filter linearizes this non-linearity at each current operating point and is hence treated as a linear system. A quadratic performance index "J" is used to describe the cost function. This estimation and control problem meets the requirements of Gaussian noise and quadratic cost criteria. However, the relinearization about the current operating point does not satisfy the criterion of linearity. Thus because of the lack of a better approach a "forced" separation design is presented, where linearity is simply assumed. Thus the LQG assumptions are forcibly met. The development of the LQG problem is referred to Ref 5:9-18. The cost function is written in general as:

$$J = E \left\{ \sum_{i=0}^N \frac{1}{2} \left[\underline{x}^T(i) \underline{X}(i) \underline{x}(i) + \underline{u}^T(i) \underline{U}(i) \underline{u}(i) \right] + \frac{1}{2} \underline{x}^T(N+1) \underline{S} \underline{x}(N+1) \right\} \quad (20)$$

where \underline{X} , \underline{U} , and \underline{S} are weighing matrices penalizing the cost for deviations in the state \underline{x} , large control inputs \underline{u} , and the missing of the terminal state $\underline{x}(N+1)$, respectively. In this regulator problem, the terminal state is assumed to

exist at the infinite time ($N=\infty$). This implies that the terminal condition is of no interest, and therefore the terminal state weighing matrix \underline{S} is set at zero. Without intermediate steps we will state the optimal control law for a scalar problem (Ref 5:14-15):

$$U^*[\hat{x}(k^+), k] = -G_C^*(k) \hat{x}(k^+) \quad (21)$$

where

$$G_C^*(k) = \frac{B_m K(k+1) \phi_m}{U + B_m^2 K(k+1)}$$

$G_C^*(k)$ is the optimal feedback gain, B_m is the control constant from Eq (3), ϕ_m is the state transition constant from Eq (3), and $K(k+1)$ is a state of the backward solved Riccati equation.

In this problem the fine pointing mirror has a settling time that is much less than the sample period used. Thus it is reasonable to assume that infinite control power is available as the mirror can reach the command position within one sampling period. (This is a dead-beat controller). Therefore the control weighing U is equal to zero. Since $\phi_m=1$, and $B_m=1$, $G_C^*(k)$ becomes unity and Eq (21) reduces to:

$$U^*[\hat{x}(k^+), k] = -[1] \hat{x}(k^+) \quad (22)$$

This control law is the degenerate case where $U=0$. This result is intuitively predicted as for a mirror of a

negligible mass and essentially instantaneous response, whenever a best estimate of the pointing error $\hat{x}(k)$ is available, the best we can do is to immediately drive the mirror with a control in an opposite direction by an amount exactly equal to the sensed error. This concept is clearly evident in Eq (22) and is implemented in the control law Eq (3), except that the dither is also included in the mirror drive command.

Although the result above is trivial, the fine pointing mirror will not always be as quickly responding, and the infinite control power assumption will not be valid. In that case the "forced" L-Q-G controller may be the most practical to implement.

The presentation of the concepts of application of the LQG solution to the ALOT control loop has not assured us of improved performance. This assurance can come only from a simulation on a large scale data processing system, such as our CDC 6600 computer system, or from an actual hardware implementation of the algorithm. Both the simulation and the hardware implementation were accomplished. First, the simulation techniques are presented in the next chapter.

III. Simulation of Kalman Filter in the ALOT Control Loop

The simulation was performed to verify the theoretical development of the ALOT control loop model and to gain insight into the behavior of the modeling parameters. The open loop simulation was performed to test the algorithm's ability to converge on the proper value of the pointing error, to observe the dynamics of the variance and Kalman gain, and to determine the filter's sensitivity to variations in dither amplitude, noise strength values, and other parameters.

Simulation Concepts

A single program approach is taken when building the simulation program. This CDC 6600 computer simulation is performed for the single axis only. Each significant point of simulation techniques is briefly discussed, but the results are deferred until a later chapter.

White Noise v. The FORTRAN library includes a random number generator with a uniform probability density function for numbers between 0 and 1, and therefore a mean of 0.5. Twelve random samples from this function are passed through the algorithm

$$v(k) = \sigma_R \sum_{i=1}^{12} [v_u\{12(k-1)+i\}-0.5] \quad (23)$$

for $k = 1, 2, 3 \dots$

where $v_u(k)$ is the random number, and σ_R is the variance of the desired white noise. This algorithm produces a relative frequency of the amplitude that is a very much Gaussian distributed white sequence $v(k)$.

Disturbance Process $\theta_T(k)$. Two approaches are considered in the generation of the disturbance process θ_T , a model of relative motion between the fine pointing mirror and the target. The first approach is to pass a white Gaussian sequence, similar to that produced by Eq (23), through a digital first order filter of variable bandwidth. The output of this filter is the exponentially time-correlated disturbance process θ_T . The second, and the adopted approach, is a generated sinusoid of a given amplitude and increasing frequency in a controllable manner. The second approach is chosen because the simulation results are compared to the results produced by a frequency response analyzer used for experimental analyses. The frequency analyzer generates the disturbance process as a sinusoid of a given amplitude and varying frequency. It should be noted that the two approaches would be equivalent, by superposition, in a linear system, for the purpose of measuring the error rejection of the closed loop. Since in this problem a significant non-linearity exists in the measurement of the pointing error, the superposition does not apply. Thus the two approaches are only approximately equivalent.

Frequency Response Algorithm. This algorithm is used in generating frequency response plots presented in a later chapter. The algorithm employs the Fourier coefficients in calculating the log-magnitude of the response ratio. Given that $\theta_T(k)$ is the controlled sinusoidal disturbance signal, and $r(k)$ the signal of interest, the Fourier coefficients are defined:

$$a_1(i) = \frac{1}{NT} \sum_{k=1}^N r(k) \sin(2\pi f_i kT) \quad (24a)$$

$$b_1(i) = \frac{1}{NT} \sum_{k=1}^N r(k) \cos(2\pi f_i kT) \quad (24b)$$

$$c_1(i) = \frac{1}{NT} \sum_{k=1}^N \theta_T(k) \sin(2\pi f_i kT) \quad (24c)$$

$$d_1(i) = \frac{1}{NT} \sum_{k=1}^N \theta_T(k) \cos(2\pi f_i kT) \quad (24d)$$

where f_i is a discrete frequency being considered, and T is the sampling period. Then the log-magnitude is computed:

$$L_m(i) = 20 \log \frac{a_1^2(i) + b_1^2(i)}{c_1^2(i) + d_1^2(i)} \quad (25)$$

where i indicates the frequency f_i . A value $N = 350$ is chosen for frequencies $f_i \leq 80\text{Hz}$.

Operation of the Simulation Program

The simulation program is sufficiently flexible to permit evaluation of many parameters without reprogramming.

In the initial phases of simulation, the convergence of the Kalman filter in the ALOT open control loop is accomplished. The glint is stationary for that simulation. The glint is then "disturbed" by driving the pointing direction with a sinusoidal θ_T . In the final step the loop is closed and the simulated ALOT control system performance is observed. A perturbation analysis is then performed on the key model parameters, Q--the strength of the disturbance process, R--the strength of the measurement noise, and the dither size.

Three different model versions of the Kalman filter are simulated. First, a first-order square-root extended Kalman filter is simulated, where the square root of the variance $P(k)$ is propagated in time. Then two second order filters with a single noise source (Fig 18a) and with two noise sources (Fig 18b) are analyzed. Finally, after the hardware implementation, a first order filter (Fig 18c) is simulated.

The real test of the LQG algorithm is in its implementation on the Nova 800 minicomputer at the AFWL ALOT laboratory breadboard.

IV. Implementation of the Algorithm

The extended-Kalman-filter ALOT control loop is demonstrated on the AFWL ALOT breadboard at Kirtland AFB. The estimation and control algorithm is implemented on a Data General Corporation Nova 800 minicomputer, and an Electronic Associates, Inc. TR-48 analog computer. The TR-48 is used primarily as an analog interface between the Nova 800 and both the fine pointing mirror power amplifiers and the PMT sensor output. Using R-C components, the PMT and the D/A filters (Fig 6), are built on the TR-48 patchboard. The analog computer potentiometers serve as gain selectors in the ALOT control loop. The Nova 800 is a 16-bit processor with an instruction time (other than a memory-reference or multiply/divide) of 0.8 μ sec. A memory reference instruction takes 1.6 μ sec, and a divide/multiply--8.8 μ sec. The Nova assembly language is very flexible allowing relatively complex logic operations in few instructions. The memory core is 20,000₈ word capacity, although only a small fraction, less than 7%, of the core was occupied by the algorithm. The digital control implementation presented some special programming problems.

Implementation Problems

In general the problems involved in the implementation of a complex estimation and control algorithm are significant. The complexity and the size of the program generally increase considerably with the increase of the number of states in the control loop and the filter model. This fact is the primary motivation for using simplest possible models in the algorithm. Although a second order filter is the highest filter order implemented, the programming in assembly language on the Nova 800 presents a number of challenges. These challenges are primarily in the precision of arithmetic operations, scaling from floating point decimal to binary integer arithmetic, round-off, and the logical flow of the digital program. The methods used in meeting those challenges are presented in the following discussion.

Precision. The Nova 800 has, as do most other general purpose minicomputers, a fixed wordlength of 16 bits. This includes the 15 magnitude bits and 1 sign bit. The quantization precision of the least significant bit is $(2^{15} - 1)^{-1}$, or .0000305. This is poor by comparison to the precision of large data processing computers, but it is adequate for many accuracy requirements of control algorithms. This precision, with proper scaling (discussed in the next section) proved sufficient for all but one set of variables in this algorithm. The variance $P(k)$ has a numerical dynamic range from 10.0 to 10^{-6} depending on the choice of values of the

model parameters. This accuracy is outside the accuracy range of 16 binary bits, however, well inside the accuracy range of 32 bits, i.e., double-word precision. The arithmetic manipulation, specifically multiplication and division, involving double words became cumbersome and time consuming.

Scaling. Due to a large numerical range of the variables, three scale factors, including a variable scale factor, are employed. The architecture of the Nova 800 performs the multiplication operation by multiplying the contents of two single-words with the result becoming a double word. Conversely, a double-word is divided by a single-word and the result is a single word. Then if a double-word variance $P(k)$ is to be multiplied by another single-word variable $K(k)$, the $P(k)$ first has to be divided by an appropriate scale factor, then multiplied by $K(k)$. The variable scale factor is used in $P(k)$ computation to prevent a possible zero intermediate result when a small, but significant, double-word number is divided by a large single-word number. A possibility exists of an intermediate result being zero, which in turn would erroneously render a zero final result. The variable scaling is accomplished by shifting left, or right as necessary, to perform multiplication, or division respectively, by integer powers of two. The necessity of scaling introduces numerous multiply and divide operations in addition to those required by the algorithm itself. Specifically, 12 multiply/divide operations

are necessary in one cycle of the single state filter algorithm however, with the scaling/descaling operations the number of multiply/divide operations rises to 26. For a two state filter algorithm this number rises to approximately 55. In the one state filter algorithm the single axis computation time is 228.8 μ sec for the multiply/divide arithmetic operations alone. One cycle computation time for the entire algorithm, including the adaptation schemes to be discussed later, was at approximately 750 μ sec/axis as compared to an algorithm sample period at 5 μ sec/axis.

Round-off and Truncation. Truncation error is introduced during division operations with finite word lengths. It is modeled as a stochastic process described by a uniform probability density function with a mean of 0.5 bits. In general this mean is inadvertently summed, and significant bias errors can result. To eliminate the truncation errors, the division result can be rounded-off. This shifts the mean of the uniform probability density function to the zero point. Thus the truncation error is not cumulative, and is essentially eliminated. Only a few quotients, those in sensitive calculations, are rounded-off, because to round-off all quotients would result in a significant computation time increase.

Exponential Evaluation. The evaluation of the exponential function poses a peculiar problem. The evaluation needs to be accurate as well as rapid in computation.

Several schemes are considered, however, the scheme chosen is a table look-up of $\exp(-z)$ for $0 \leq z \leq 8.0$. This provides a range for the pointing error $-4 \leq x \leq 4$, or for a bivariate argument $-4 \leq \sqrt{x^2 + y^2} \leq 4$. It is not necessary to consider values of x beyond 4.0 as the glint essentially does not exist beyond that point, also the value of $\exp(-z) = 0$ for $z > 8$. A table of $2^8 = 256$ entries is generated. Then each computed argument is split into 2 8-bit bytes. The most significant byte is then the relative address within the table. The least significant byte is multiplied by the slope between the addressed and adjacent points within the look-up table. This interpolation is then added to the base value for $\exp(-z)$ with accuracy better than the 16 bits permit. The speed of this exponential evaluation is less than 30 μsec , far less than for any other scheme considered.

Program Modularity. Due to the program complexity it is necessary to use subroutines for essentially all calculations. The main program then merely consists of a number of subroutine calls. All subroutines are called with the pertinent arguments passed in a similar manner that a FORTRAN subroutine call passes arguments. This is necessary as the arguments differ from one axis to the other. The modularity of the program lends itself well to debugging of errors as each subroutine can be debugged separately.

Two Axis Program

The algorithm is coded in the Nova assembly language. The program is structured to provide flexibility to the user.

Program Flexibility. The program is logically organized and easy to use. After entry of the few algorithm parameters, the program computes all of the necessary constants internally allowing frequent and rapid changes of any parameters between runs. After the computation of constants, all of the variables are initialized as necessary. The main program follows the initialization; it is composed mostly of subroutine call statements, so it is short and easy to follow. In the main program, first the x-axis then the y-axis algorithms are computed, then the main program recycles through the loop. This can be seen in the program listing in the Appendix.

Monitor Table. Since the program execution rate is much faster than the transfer rate of the available input/output devices, a method is devised to record the time histories of variables of interest. Two tables of 256 words each are filled with the specified variables, thus recording the time histories of the initial 256 values of these variables. The contents of these tables are recorded through a hard copy unit for analyses.

Flow Diagram. A functional flow diagram is presented in Figure 21. This flow diagram omits the details of the

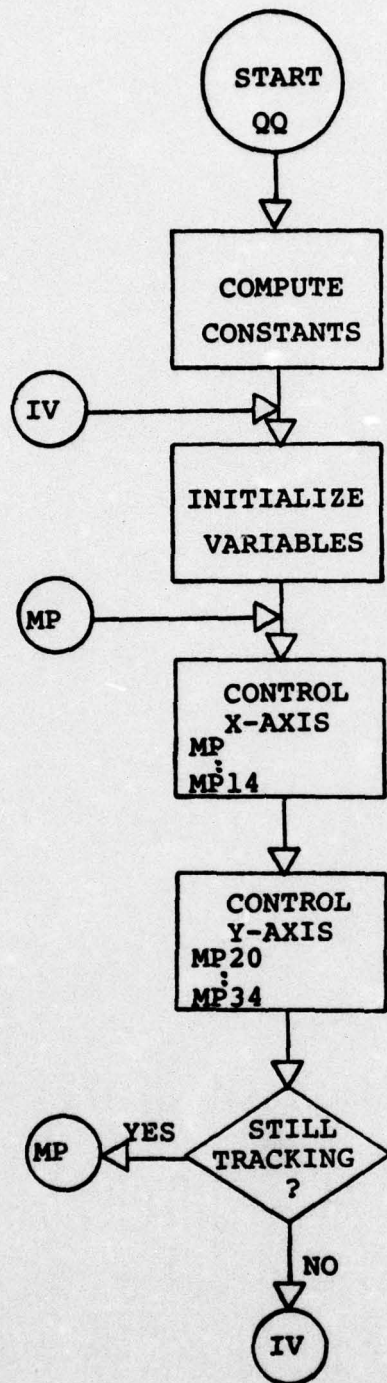


Figure 21. Main Program Functional Diagram

specific programming language. The specific details of the Nova 800 assembly language program are available in the program listing in the Appendix.

Error Rejection Bode Plots

The experimental error rejection Bode plot data are generated by an "x-y plotter" attached to the BAFCO frequency analyzer. The BAFCO provides a sinusoidal disturbance input, $\theta_T \propto \cos \omega t$ to the control loop and measures the log-magnitude of the ratio of the Fourier coefficients of pointing error x and disturbance θ_T at each discrete frequency ω_i . The frequency ω_i is increased discretely over a preselected range, and at each point the log-magnitude is evaluated and plotted (also displayed digitally).

The effectiveness of the algorithm is tested in an experimental implementation. The results of the simulation and implementation are presented in the next chapter.

V. Results

The simulation and experiment results are presented in this chapter. The simulation results establish the basis for model choices and parameter selections subsequently applied in the filter control algorithm on the ALOT breadboard.

CDC 6600 Simulation

A significant amount of simulation was performed for a single axis estimation model. In the early stages of simulation, qualitative analysis was performed on a first order Kalman filter, to observe the effects of different parameters on the quality of the estimation.

Open Loop Simulation. With the strength Q of the disturbance process model set non-zero, a 20 Hz sinusoidal motion θ_T is applied to the simulated fine pointing mirror. With the measurement noise strength R set at a small value, and the sampling period T set at .002 sec, the estimation is performed in an open loop configuration. The goodness of the estimation is observed by comparing the history of the estimated error to the true pointing error. The algorithm "tracks" θ_T quite well in an open loop configuration. At this disturbance frequency, the error in estimation is less than 5% of θ_T amplitude. The shaping filter is a part

of the Kalman filter design, i.e., different shaping filters output different stochastic processes as models for θ_T .

Choice of Shaping Filter. A number of choices of shaping filter are available, as models for the disturbance process. First order shaping filter, as presented in Figure 18c, is relatively easy to implement and very often adequate for a given application. Other shaping filters such as the one in Figure 18a, are often used in modeling of disturbances of airborne targets. No data representing the real world disturbance process is available for comparison with the hypothesized models. The second order shaping filter (Figure 18a) is appealing because it can provide velocity estimates as well as position estimates. It is intuitively obvious that a good velocity estimate can improve a position estimate--a desirable goal. However, the first order filter (Figure 18c) is much simpler to implement. Since the implementation on the minicomputer deals with a finite word length, either double word precision, as discussed in the previous chapter, or a square-root version of the extended Kalman filter variance has to be implemented. The square root filter is a Kalman filter version which propagates the square root of the variance $\sqrt{P(k)}$ (Ref 4:88-118). This form reduces the accuracy requirement at the expense of the algorithm complexity. The square root version of the first order Kalman filter in the ALOT closed loop was simulated. The filter converges; however, it estimates poorly for

other than low frequencies. The second order shaping filter works reasonably well in the estimation of position but provides a very poor velocity estimate. The velocity estimate is essentially zero for all circumstances. A noise source added to the velocity level, thus modifying the shaping filter to that shown in Figure 18b, does not improve the velocity estimate. At this point it appears that a velocity estimate is not possible as the velocity state is not measurable. Additionally, when the noise strength Q_2 is adjusted to produce good filter performance, the value (including zero) of the noise strength Q_1 does not alter the filter performance. This implies that only the integrator driven by white noise w_2 is a good model of the stochastic process θ_T . But this is the same shaping filter as the one in Figure 18c with α set at zero. At this point it can only be speculated that the simulation of the square-root version of the first-order filter had a programming error or other problems.

The discussion in the above paragraph presents the background information that led to the final implementation on the Nova 800 of the first-order shaping-filter extended Kalman filter. Double word precision, instead of square-root filtering, is used to obtain the necessary accuracy for the propagation of the variance $P(k)$. The above evidence that the two state shaping filter is not as good a representation of the real world disturbance process θ_T

characteristics as the one state shaping filter dictates the choice of the first-order shaping-filter model, such as in Figure 18c. The bandwidth of this filter can be varied by choosing the appropriate α and gain.

First Order Filter Simulation. The first order shaping filter in the ALOT closed loop is simulated, and the Kalman filter variance and gain time-histories are plotted. Also a log-magnitude plot versus frequency of the error rejection is obtained. The Kalman gain $K(k)$ and filter variance $P(k)$ are shown in Figures 22 and 23 respectively. Both plots show the rapid transition from the initial to the steady-state condition. Essentially steady-state values are reached by the filter in one iteration. This rapid transition is due to the small correlation between the previous measurement history and the current measurements, as reflected in a small value of the measurement variance $R(k)$ in Eq (17). This effect causes a rapid gain in the estimation confidence as reflected by this rapid variance convergence. For greater values of $R(k)$, both the variance and the filter gain would have a slower transient to steady state.

In general, the variance and gain of the Kalman filter for a non-linear system do not have a steady state solution, because the linearized term $H(\hat{x}_{k-})$ is not constant as can be seen in Eq (16). Then the variance $P(k)$ cannot have a steady state solution because $H(\hat{x}_{k-})$ appears in the

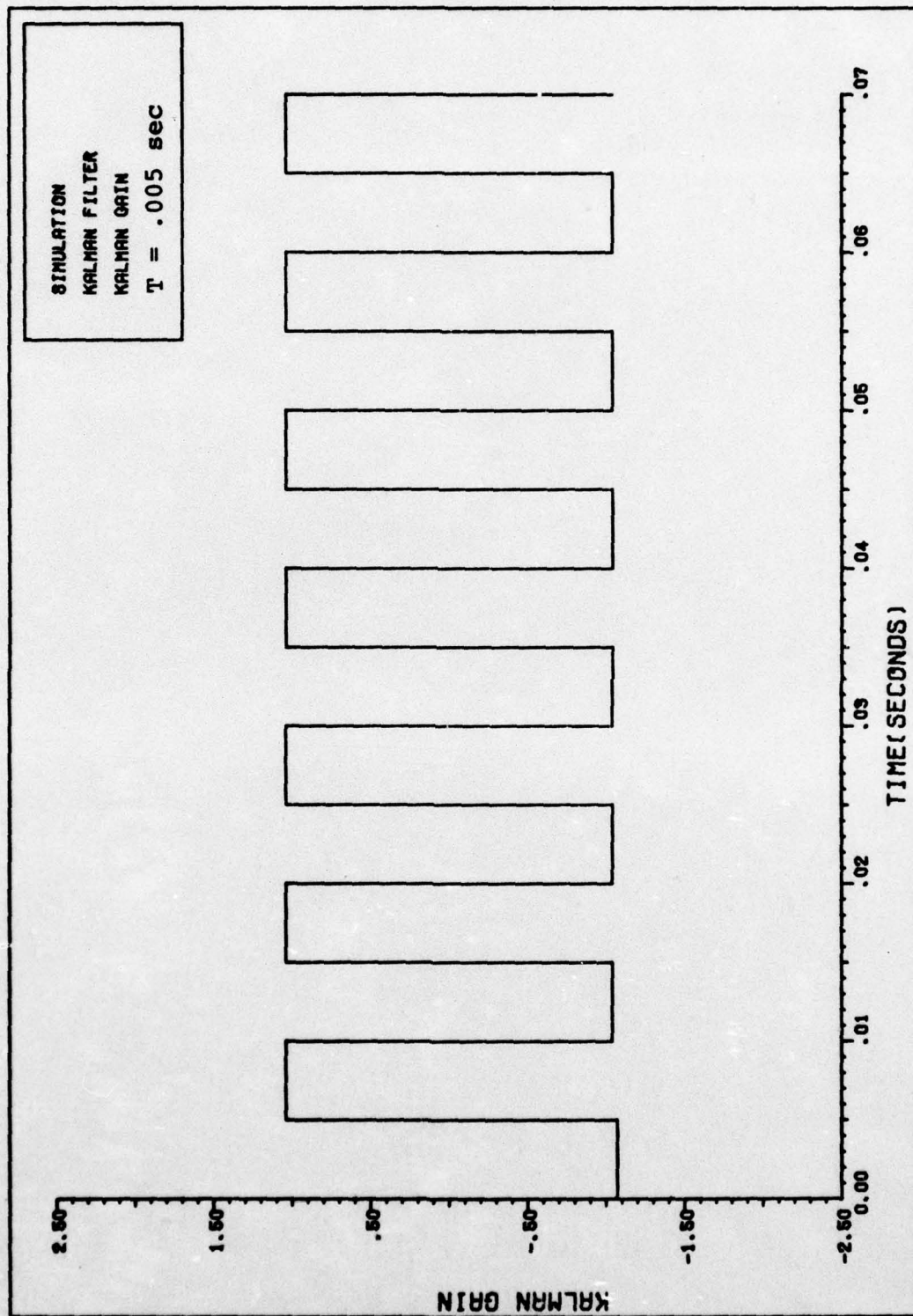


FIGURE 22. KALMAN GAIN TIME HISTORY

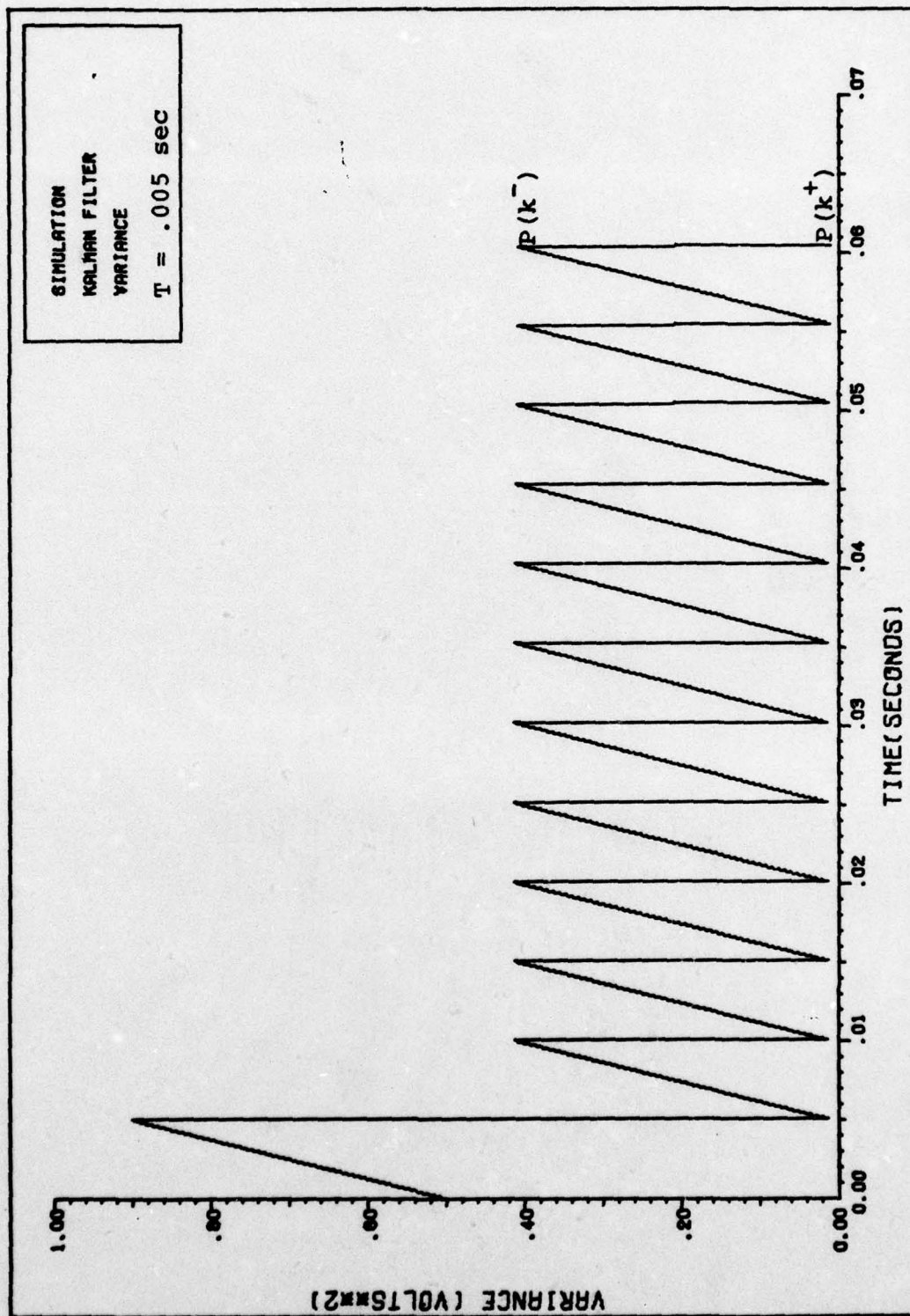


FIGURE 23. SINGLE STATE FILTER VARIANCE

intermediate Kalman gain Eq (17). However, in this problem it is our desire to zero out the error by allowing $u(k) = -\hat{x}(k^+) \pm d(k)$, where d is the dither constant. Then for the case where $\alpha = 0$, ($e^{-\alpha T} = 1$), Eq (13) becomes:

$$\begin{aligned}\hat{x}(k+1^-) &= \hat{x}(k^+) - \hat{x}(k^+) \pm d(k) \\ &= \pm d(k) = \pm d_k\end{aligned}$$

The linearized observation $H(\hat{x}_k^-)$ evaluated at $\pm d$ then becomes $H(\pm d_k)$, where \pm implies alternating sign of the dither. For this special case the magnitude of $H(\pm d_k)$ is constant, but the sign of $H(\pm d_k)$ varies with the changing sign of the dither as seen in Eq (16)

$$H(\pm d_k) = -\frac{\pm d_k}{\sigma_G^2} [h(\pm d_k) - b]$$

Consequently the magnitude of the Kalman gain solution $K(k)$ is constant, although its sign changes with the change of the sign of the linearized observation parameter $H(\pm d_k)$ as it is evident from Eq (17). Since the magnitudes of $H(\pm d_k)$ and $K(k)$ are constant, then the variance propagation $P(k^-)$ and the variance update $P(k^+)$ have steady state solutions, as evident in Figures 22 and 23. Filter stability and dynamics are important in the system analysis, but the effectiveness of the Kalman filter in the ALOT closed loop needs to be measured.

Error Rejection. The measure of "goodness" of the ALOT control loop is the ratio of the dither frequency to the error-rejection bandwidth. The error rejection has been obtained using the method presented in Eqs. (24) and (25). The simulated control loop error-rejection curve is plotted in Figure 24. The initial slope is 20 dB per decade indicating a first order response. The -3dB point occurs at 41 Hz--indicating that the error-rejection bandwidth is 41 Hz. The dither frequency of 100 Hz (200 samples per second) is used in this simulation. The dither to response ratio is 2.44:1. For frequencies above 40 Hz, the Bode plot indicates higher order dynamics that are probably induced by a combination of filter dynamics and non-linearity effects. No analysis has been performed to determine the source of this phenomenon. Phase angle is not computed for this simulation. Additionally, this one axis simulation of the ALOT loop is not tuned for best performance. The parameters I_{\max} , σ_G , Q , R , and dither size are approximately the same as the parameters in the experimental control loop. In the simulation these parameters are perturbed in the small to maximize the ALOT control loop bandwidth. These parameters are not perturbed in the large to globally maximize these parameters for a maximum bandwidth performance as this is not within the scope of this feasibility study.

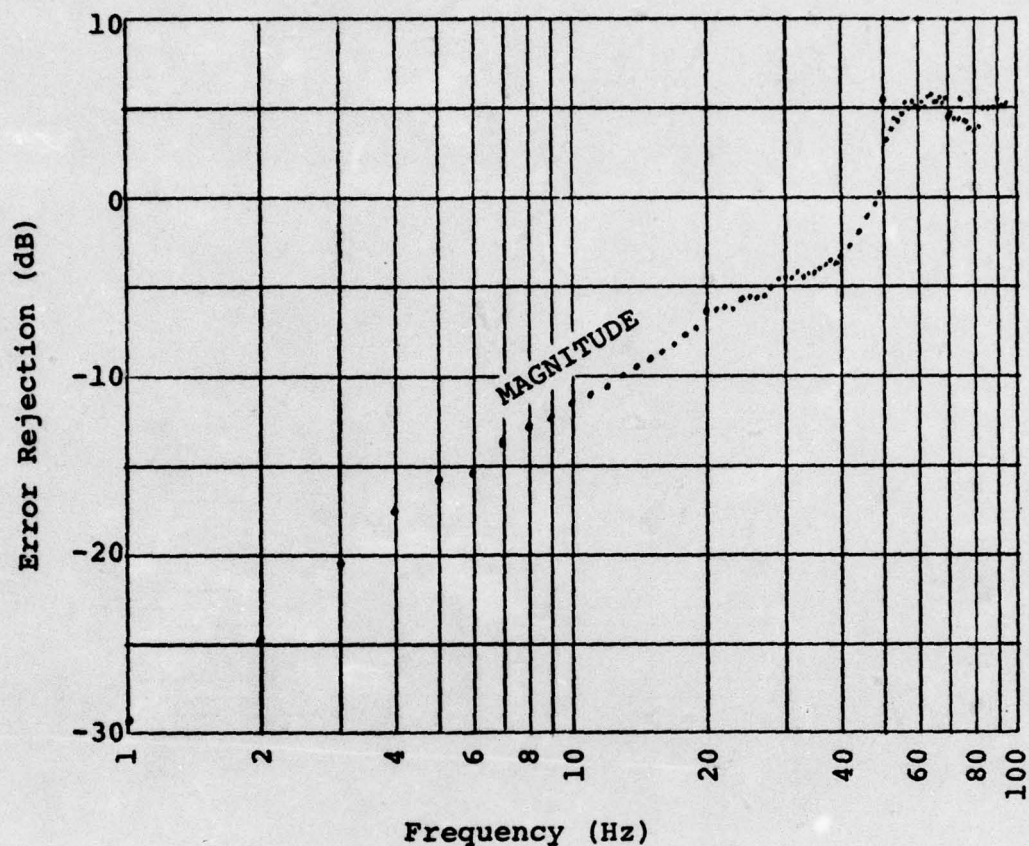


Figure 24. Simulated Error Rejection

ALOT Laboratory Results

The algorithm first is implemented in single axis using a pipe for a target. The pipe is held in a vise with the pipe axis perpendicular to the laser beam plane of movement. The glint from the laser beam sweeping across the pipe is modeled very well by a Gaussian function.

Single Axis Results. The results of the single axis Kalman filter implementation are discussed in this section. The error rejection plot in Figure 25 shows that the bandwidth (-3dB point) is 62 Hz. This bandwidth translates into a dither-to-response ratio of 1.61:1. Considerable time was spent "tuning" the filter and control loop to obtain this response. It must be remembered that the theoretical limit is at best a dither-to-response ratio of 1:1 due to Shanon's sampling theorem. The dither-to-response ratio of 1.61:1 is better than the 2.44:1 obtained in simulation. However, it must be remembered that simulation algorithm was not nearly as well tuned as the experimental filter. The important point to be observed is that the shape of the experimental log-magnitude plot (Figure 25) compares quite favorably with the shape of the simulated plot (Figure 24).

The time history of the variance is shown in Figure 26. This plot shows that the variance reaches steady state within two iterations, very much like the simulated variance in Figure 23. The experimental gain time history in Figure 27 shows essentially steady state Kalman gain magnitude. This is an important point. In this algorithm the discrete-time Riccati equation is solved for each iteration to provide the Kalman gain. However, if the Kalman gain is essentially constant, then it can be approximated by a constant, and thus reduce the algorithm computation time by approximately

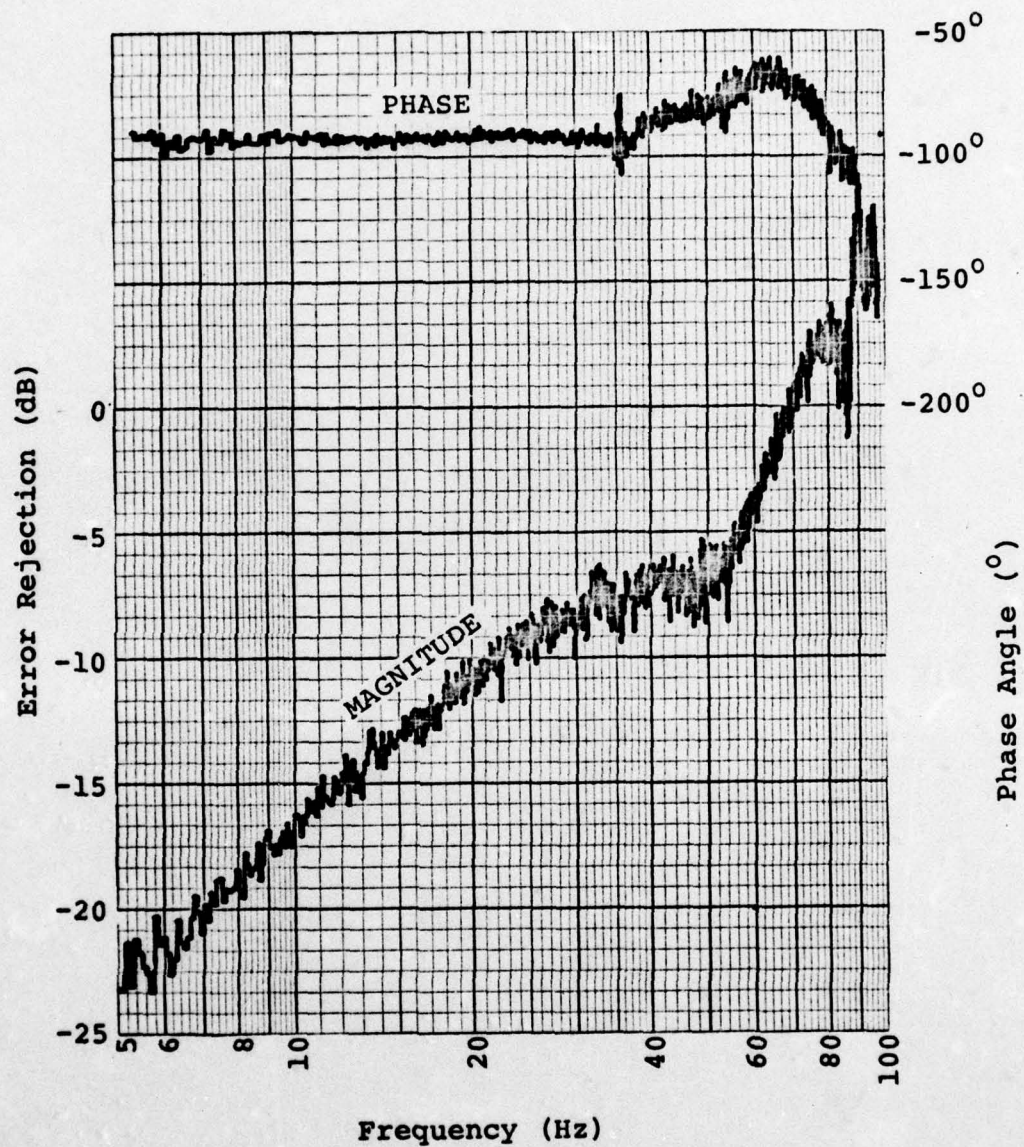


Figure 25. Single Axis Error Rejection

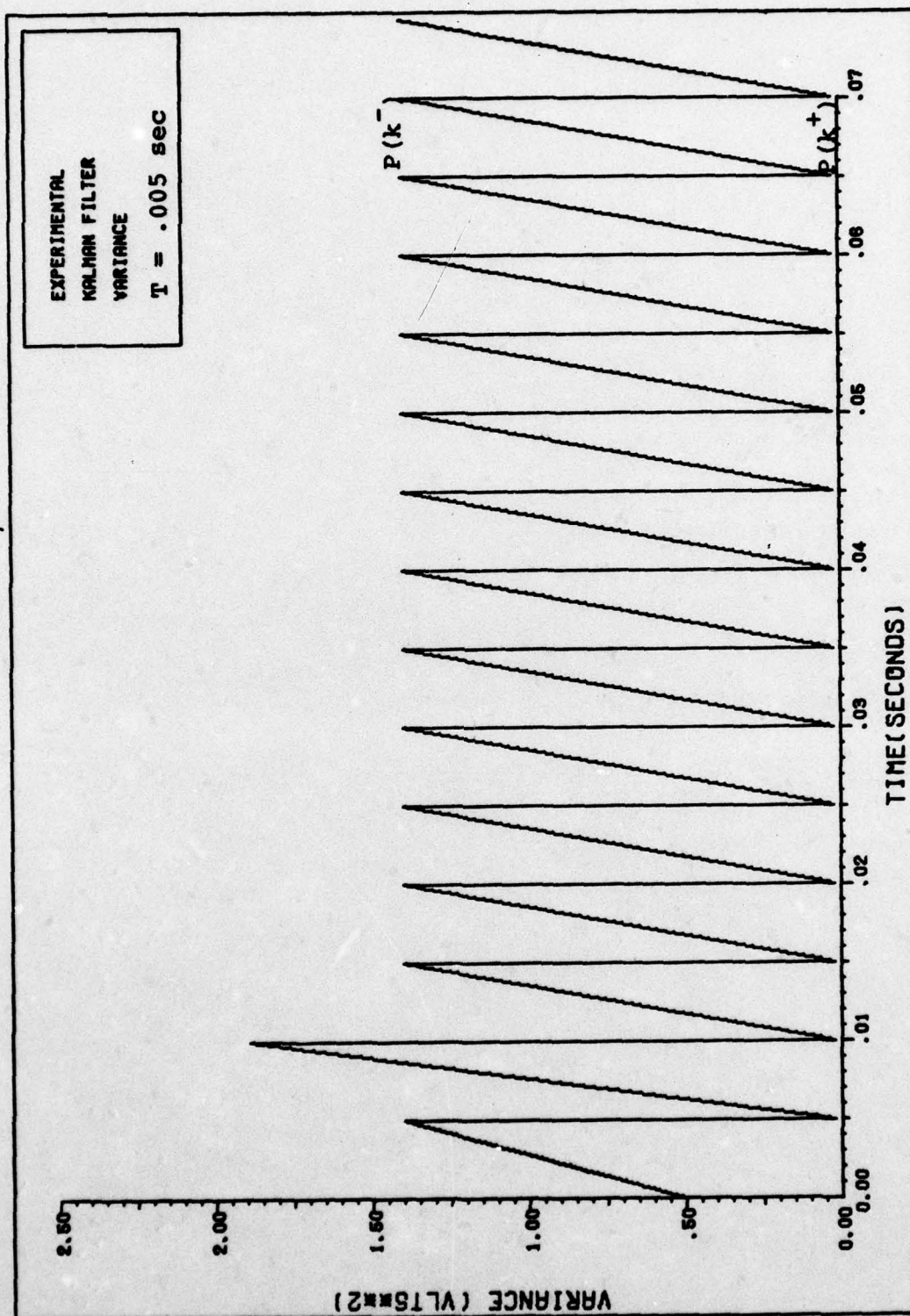


FIGURE 26. VARIANCE TIME HISTORY

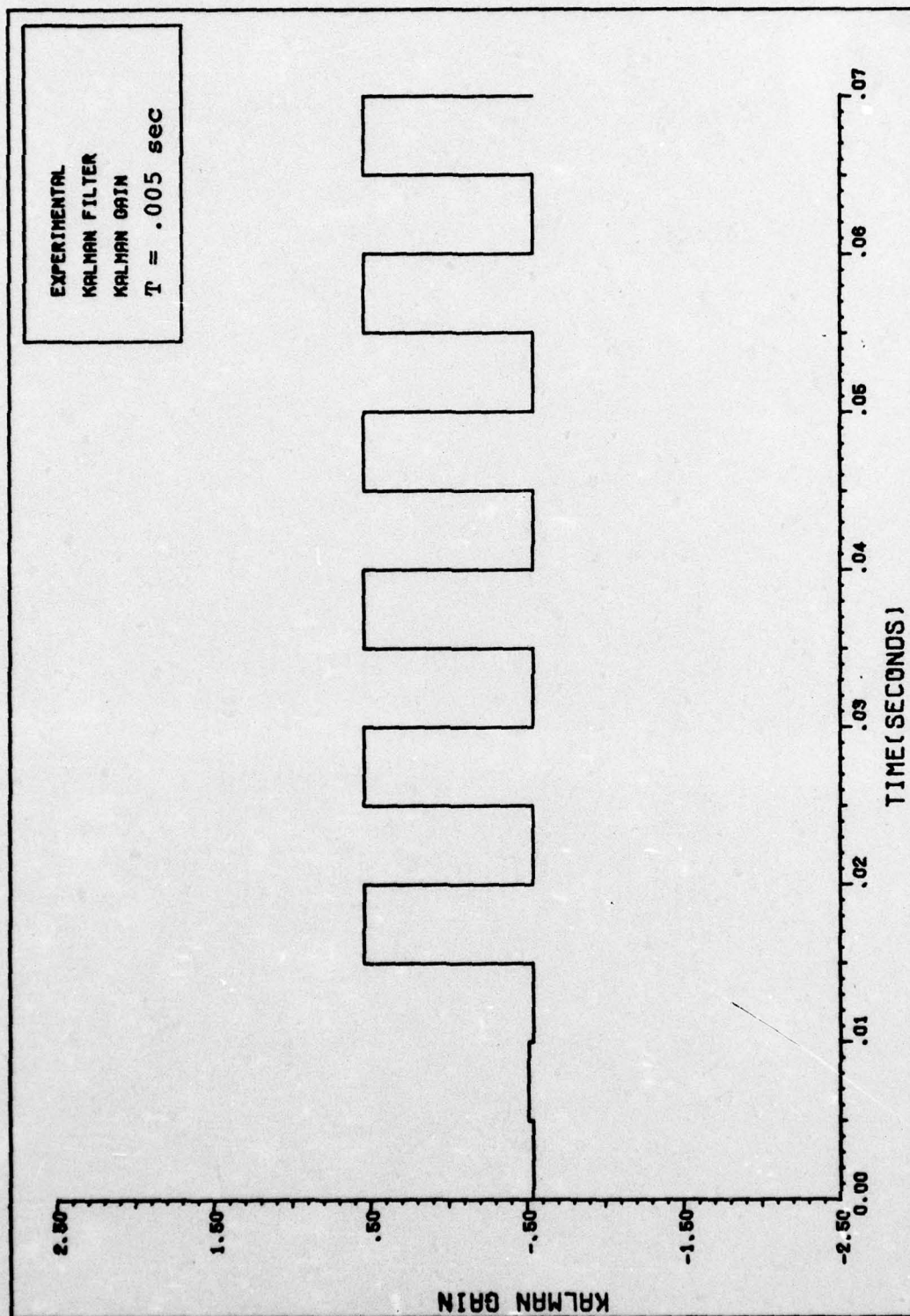
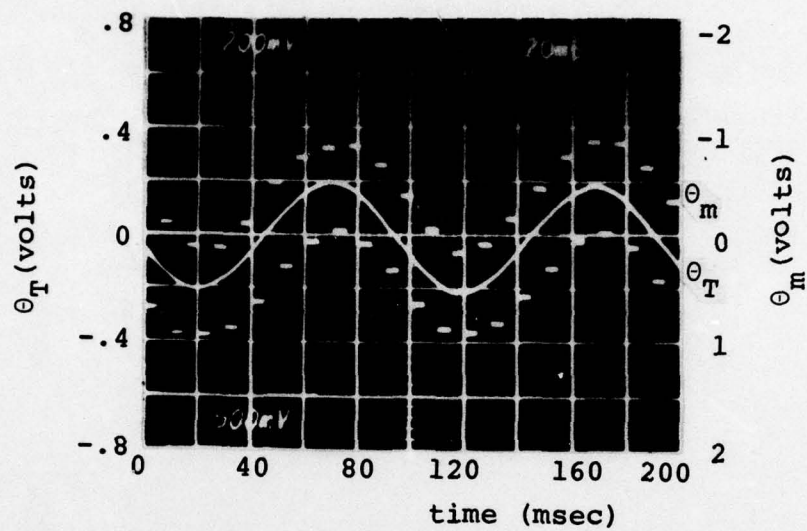


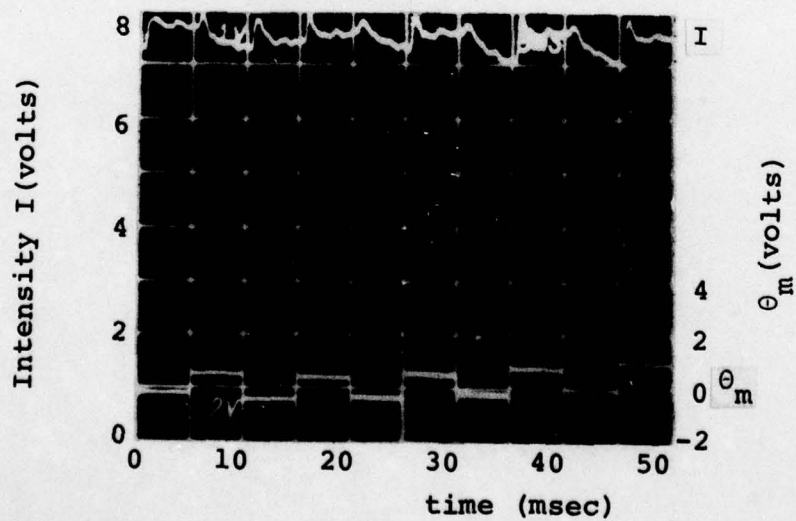
FIGURE 27. KALMAN GAIN TIME HISTORY

50% as well as eliminate the wordlength problem in the variance computation.

The "goodness" of the single axis estimation and control algorithm is presented in the following series of photographs of signals recorded on a storage oscilloscope. Figure 28a shows the amplitude and frequency of the disturbance sinusoid $\theta_T = .2 \sin(2\pi 10t)$ volts (smooth curve). Superimposed on top of it is the feedback signal θ_m with the discrete dither added. The dither frequency is 100 Hz (sampling period $T = .005$ sec). The mean of θ_m appears not to deviate from θ_T . This indicates that the laser beam is tracking the center of the steel pipe (top of the glint) despite the 10 Hz disturbance. This fact is indeed evident in Figure 28b. The feedback signal θ_m is shown in the bottom of the photograph; the change in both the vertical and horizontal scales for Figure 28a to Figure 28b should be noted. In the top of the photograph is the output of the PMT filter, or the measurement sampled by the A/D converter. I_{max} is set equal to 8 volts. In this photo the PMT filter output does not indicate that the laser beam is precisely at the top of the glint which would be represented by 8 volts, but it indicates the effect of the dither. The dither causes the laser beam to "jump" on either side of the glint peak. The important point to notice, however, is that this "jumping" on either side of the glint peak is quite

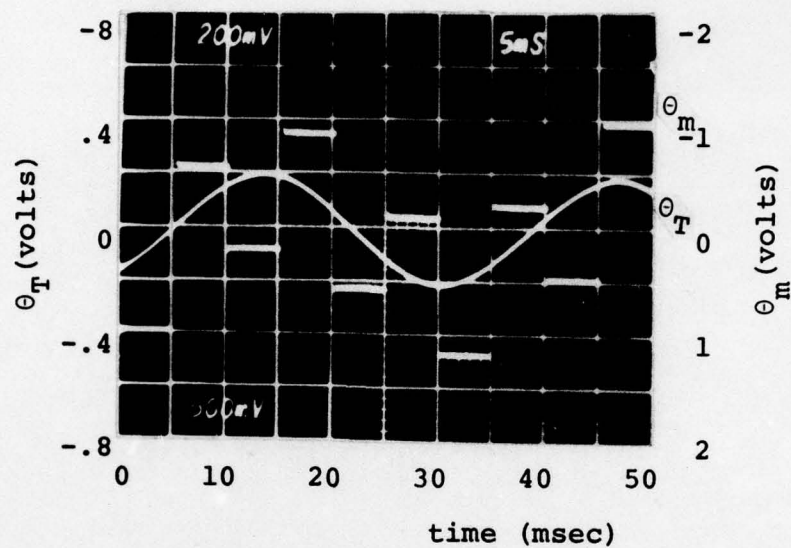


a. $f_{\theta_T} = 10\text{Hz}$

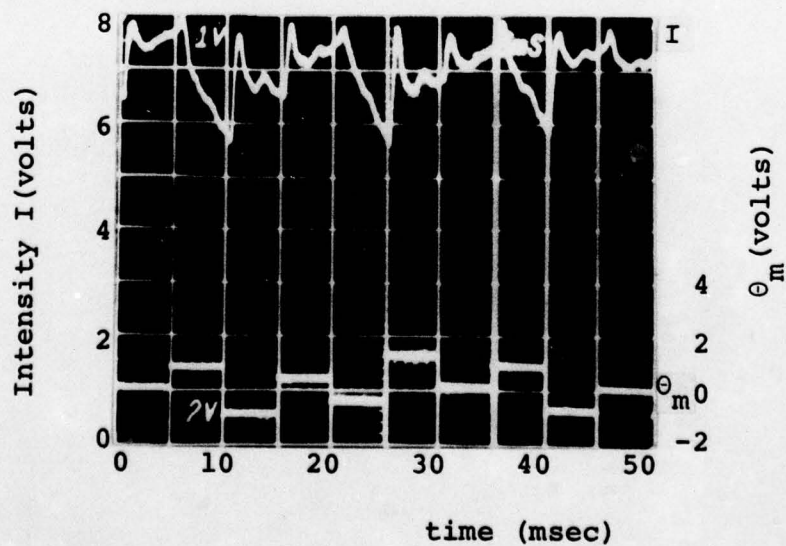


b. $f_{\theta_T} = 10\text{Hz}$

Figure 28. Tracking Photographs (Non-Adaptive)



c. $f_{\theta_T} = 30\text{Hz}$



d. $f_{\theta_T} = 30\text{Hz}$

Figure 28 (continued)

AD-A035 275

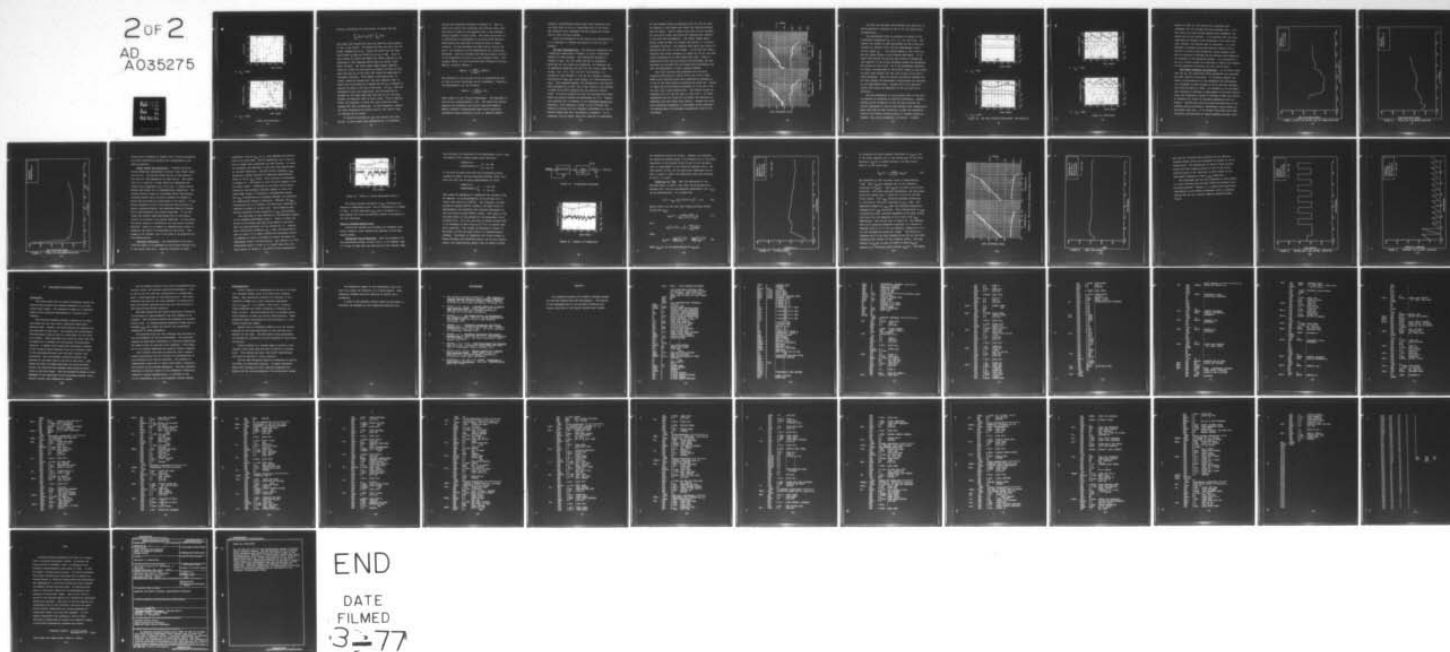
AIR FORCE INST OF TECH WRIGHT-PATTERSON AFB OHIO SCH--ETC F/G 20/5
LASER POINTING AND TRACKING USING AN ADAPTIVE EXTENDED KALMAN F--ETC(U)
DEC 76 Z H LEWANTOWICZ

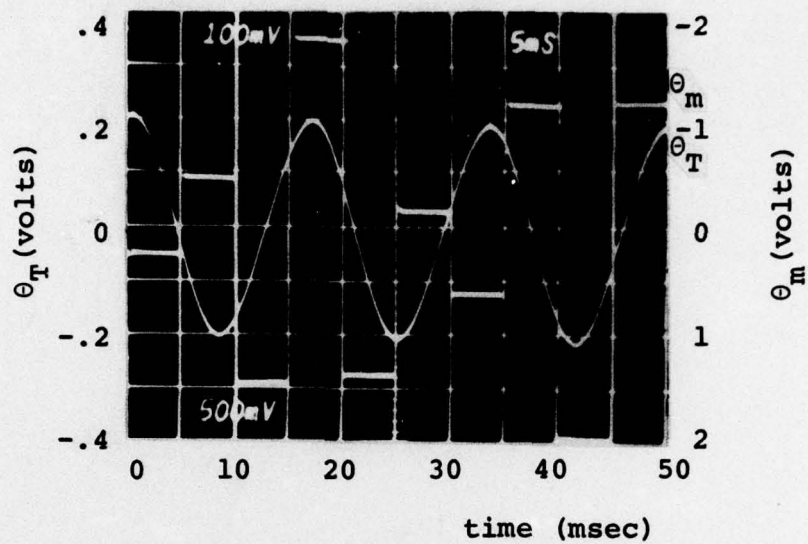
UNCLASSIFIED

06/EE/76-29

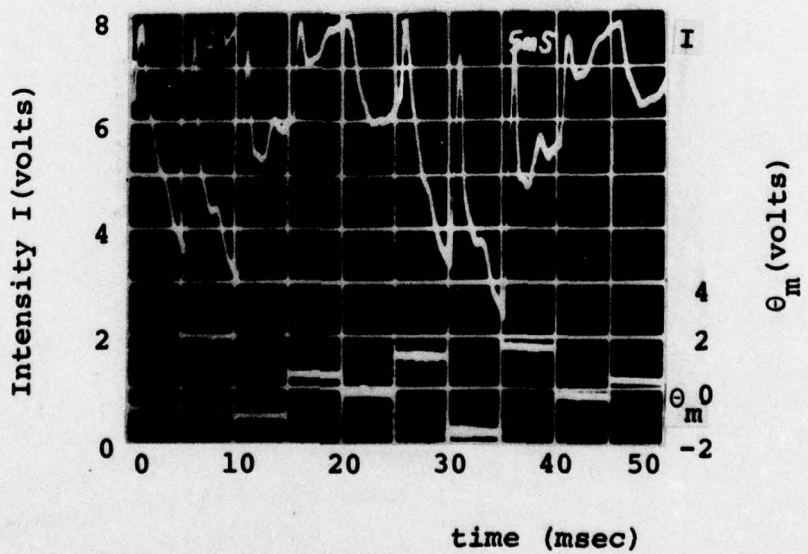
NL

2 of 2
AD
A035275





e. $f_{\theta_T} = 60\text{Hz}$



f. $f_{\theta_T} = 60\text{Hz}$

Figure 28 (continued)

uniform, confirming the observations in Figure 28a that

$$\sum_{k=1}^N \left[\theta_T(k) - \theta_m(k) \right]^2 \approx \sum_{k=1}^N d^2(k)$$

This means that essentially the only pointing error present is due to the dither. Of course this does not hold true for higher frequencies of θ_T . Figure 28c shows that the feedback signal θ_m does not follow θ_T at $f_{\theta_T} = 30\text{Hz}$. This is also evident in Figure 28d where the control applied at the beginning of each sampling period does not evenly "jump" about the mean. The three steep ramps between sampling times are created by the motion θ_T causing the beam to move away from the top of the glint and reduce the magnitude of reflected intensity. This change in pointing error, of course, cannot be sensed until the next sampling time, at which time this deviation is sensed and the θ_m is changed to restore the beam to the top of the glint. At $f_{\theta_T} = 60\text{Hz}$ the estimation errors are significant, and the magnitude of movement of the laser beam away from the top of the glint between the sampling times is quite large. This is approximately the frequency at which the error rejection curve reaches the -3dB log-magnitude. At this frequency, despite the above estimation and control errors, the control loop is tracking and is stable.

It should be pointed out that the initial sign estimation, in this single axis implementation, is performed

through the technique discussed in Chapter II. That is, during the initial ten iterations the pointing error estimate sign is forced to the opposite sign if the residual history exceeds a certain bound. This works quite well as no hesitations in convergence on the glint were observed. Additionally the algorithm is restarted when it ceases tracking. To help determine the ALOT control lock-on the glint, the residuals and the measurements are continually monitored. Both are filtered with low pass digital filters of low bandwidth to extract the time averaged values. The residual $RES(k)$ is first rectified then filtered to provide $SRES(k)$ (filtered $|RES(k)|$).

$$SRES(k) = \frac{.014}{1-.986z^{-1}} |RES(k)|$$

The bandwidth of the low pass filter is approximately 1Hz, so that only slow variations are not attenuated. Similarly the measurements $\zeta(k)$ are filtered

$$SZET(k) = \frac{.023}{1-.977z^{-1}} \zeta(k)$$

where $SZET(k)$ is the filtered measurement. The bandwidth of this filter is approximately 1.5Hz. The break-lock monitor restarts the estimation and control algorithm whenever $SRES(k)$ exceeds a predetermined upper bound indicating excessively large estimation errors, or whenever $SZET(k)$

exceeds a predetermined lower bound, thus indicating that the laser beam is not on a measurable part of the glint. The low-pass filter constants and the bounds were chosen with a trial and error method.

After the discussion of the single axis implementation, it is necessary to examine the results of the two axis problem.

Two-Axes Implementation. The modeling assumptions for a spherical target made in Chapter II allow a simplified approach to this problem. This simplified approach is evident in Eqs. (13)-(19) where one set of estimation equations for the x-axis are presented. An identical set of estimation equations are used for the y-axis except that in Eqs. (13), (17), (18), and (19) the variable x is replaced by the variable y, also Eq (16) becomes a partial derivative of $h(\hat{x}_k, \hat{y}_k)$ with respect to y and evaluated at $y = \hat{y}_k$. This approach permits the decoupling of the disturbance processes θ_T in the x and y axes, which in turn permits to model the control problem with two parallel control loops. It must be pointed out that the pointing error estimates are coupled through the measurement Eq (15). However, this coupling was not modeled in the covariance propagation equations. This coupling is shown in the following discussion to be weak for low frequency disturbance θ_T , and it becomes significant with increasing θ_T frequency. It is suspected, but not shown, that this coupling is responsible

for the reduced dither-to-response ratio for the two axes as compared to the single axis where the coupling problem does not exist. Each of these loops with its own estimator and controller would time share the computational capacity of the Nova 800 minicomputer. The dither scheme implemented moved the beam in a square box pattern in a counter-clockwise direction. One complete path about this square is defined as one cycle of the dither. In the two-axis implementation the dither frequency is chosen as 100 Hz--the same dither frequency as for the single axis case. Since no simulation of the two axis control was performed, the comparisons will be made with the single axis performance and with the performance of other tracking schemes.

The first two-axis data presented are the error rejection Bode plots in Figure 29 for the x and y axes. These error rejection plots were generated by applying θ_T to one of the axes without disturbing the other one. Figure 29 shows the error-rejection bandwidth is 34 Hz and 36 Hz for the x and y axes respectively. The average dither-to-response ratio for the two axes is then 2.86:1. No clear explanation was yet found for the almost 50% reduction in bandwidth from the single axis results. Perhaps the cross axis uncoupling assumption in the Kalman filter equations is breaking down at disturbance frequencies around 30 Hz and above.

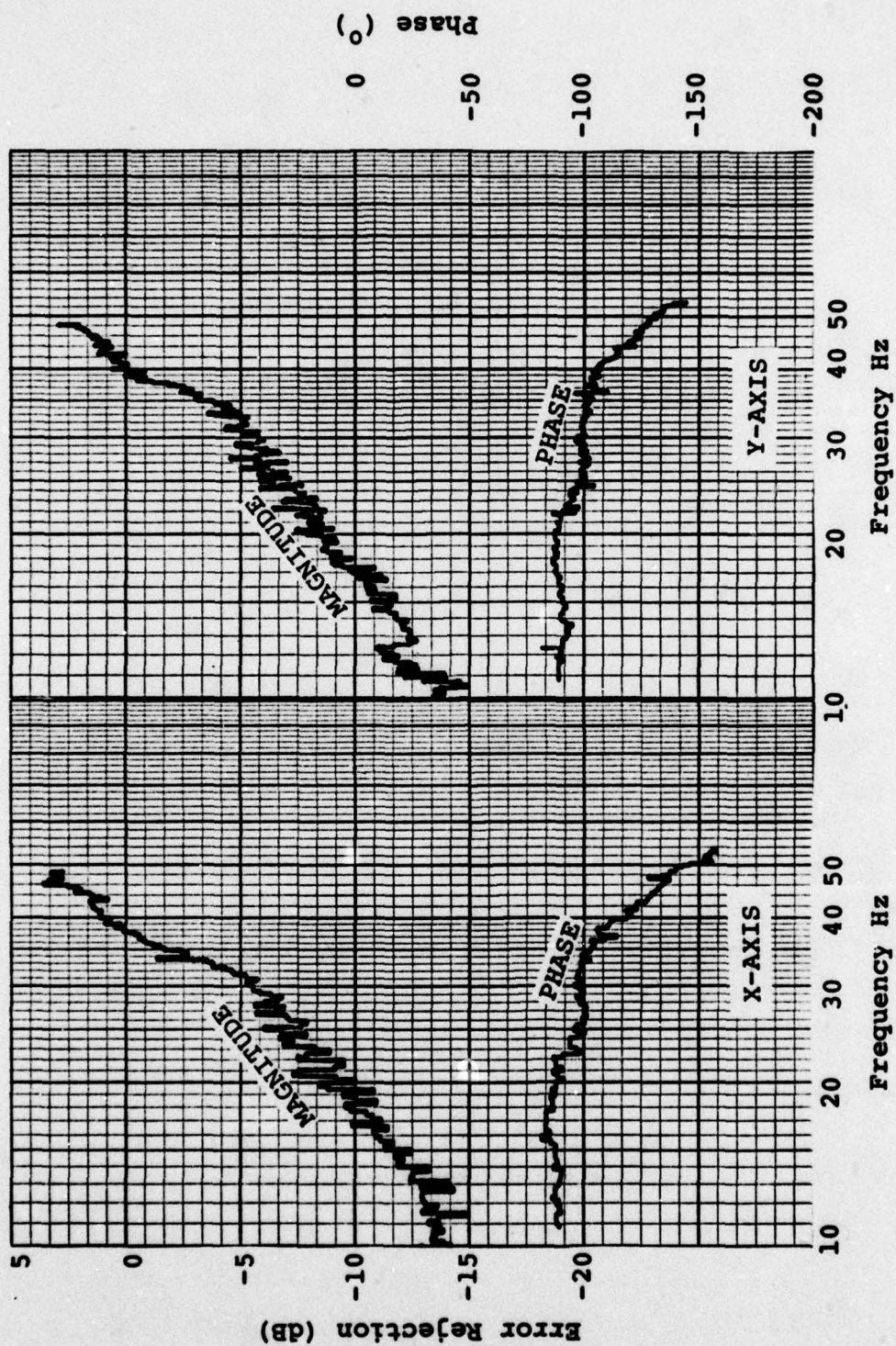
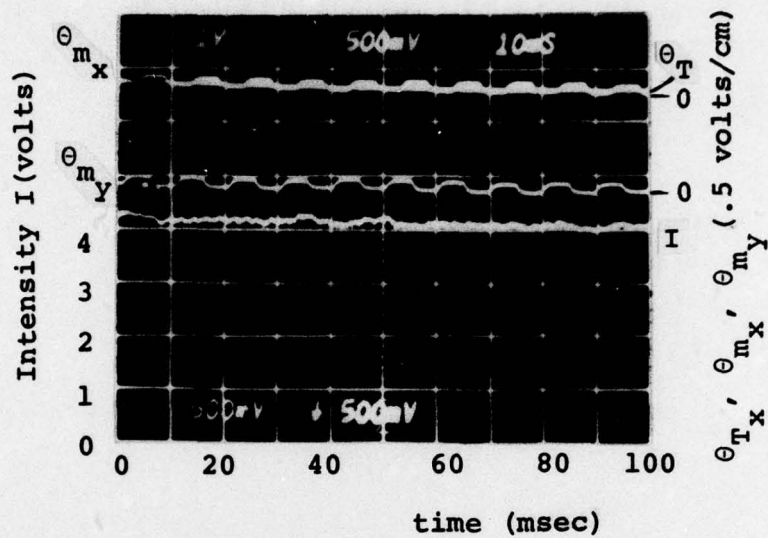


Figure 29. Two Axis Error Rejection

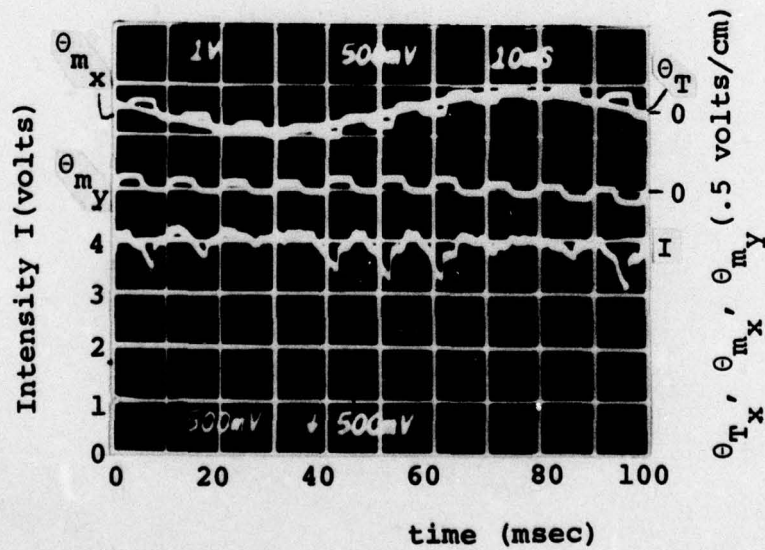
The gain and variance time histories are identical to those presented in Figures 22 and 23 for the single axis implementation.

The photographic data is presented in Figure 30 for disturbance frequencies θ_T , of 0, 10, 30, and 40 Hz. The topmost two signals in each photograph are the x-axis disturbance θ_T (smooth curve) and the superimposed x-axis control signal θ_m . The middle signal is the y-axis θ_m and the lowest signal is the filtered PMT output. It is clear from Figures 30c and 30d that errors in estimation (and control) in the x-axis adversely affect the estimation and control of the y-axis. At 30 Hz disturbance frequency to x-axis, the magnitude of the control signal in the y-axis is quite large despite the fact that y-axis is not externally disturbed. There is obvious correlation between the two axes through the measurement relationships as confirmed by the experimental data. Perhaps this is an important factor that limits the bandwidth of the two-axes error rejection.

The sign estimation of the pointing error in one axis is feasible as evidenced in previous discussions. However, pointing error estimation in the two axis involves the correct estimation of one of four possible sign combinations. Again this must be done initially, as when the estimation locks-on the correct pointing errors it remains locked on. However, the initial estimation is crucial. A method

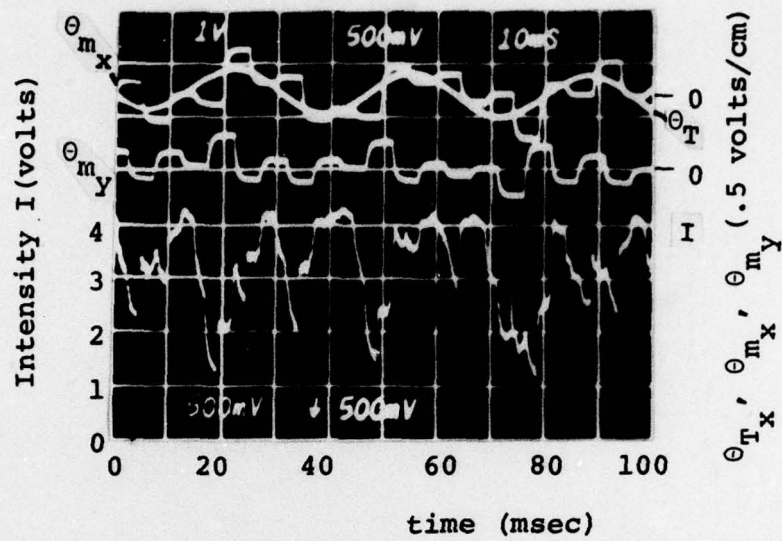


a. $f_{\theta_T} = 0\text{Hz}$

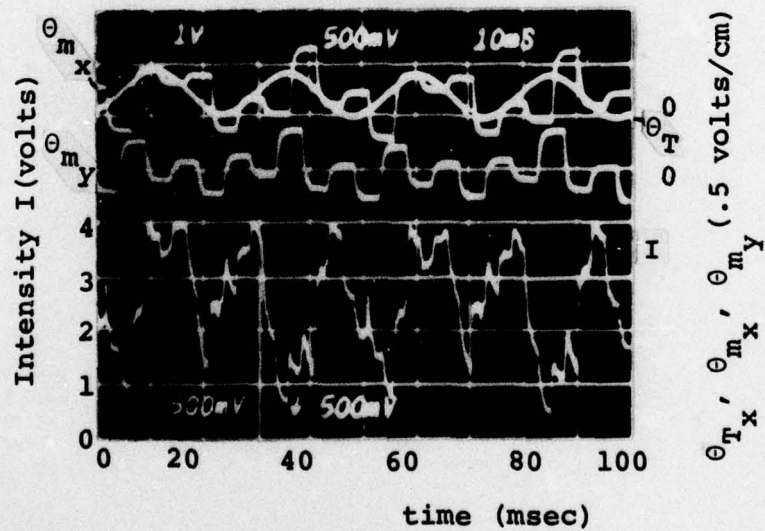


b. $f_{\theta_T} = 10\text{Hz}$

Figure 30. Two Axes Tracking Photographs (Non-Adaptive)



c. $f_{\theta_T} = 30\text{Hz}$



d. $f_{\theta_T} = 40\text{Hz}$

Figure 30 (continued)

similar to that for the single axis estimation was attempted, but its success rate was extremely poor. As a last resort all sign forcing schemes were abandoned; the result was a total success. It is possible that the algorithm may not succeed in the estimation of the sign each time, however, its success rate is excellent. It is not possible to perceive algorithm restarts visually due to failure in correct sign estimation, either because there were no failures or because the few failures were masked by the rapidity of the algorithm restart. It is possible to set up a monitor within the algorithm to observe the numbers of sign estimation failures, but this was not done.

ALOT Model Parameter Perturbations. In the ALOT closed loop set up, the significant model parameters are perturbed and their effects are plotted. To uniformly measure the effect of perturbations of the parameters the disturbance (θ_T) frequency is held constant at 20 Hz and the log-magnitude from the BAFCO is noted. An increase in the log-magnitude indicates a decrease in performance of the ALOT control loop, and conversely, Figures 31 through 33 show the effects of changing the values of the model parameters from the nominal. Specifically the plots show perturbations of disturbance process strength Q , measurement noise strength R , and dither step size. It is evident from these plots that individual perturbations of these parameters produce local

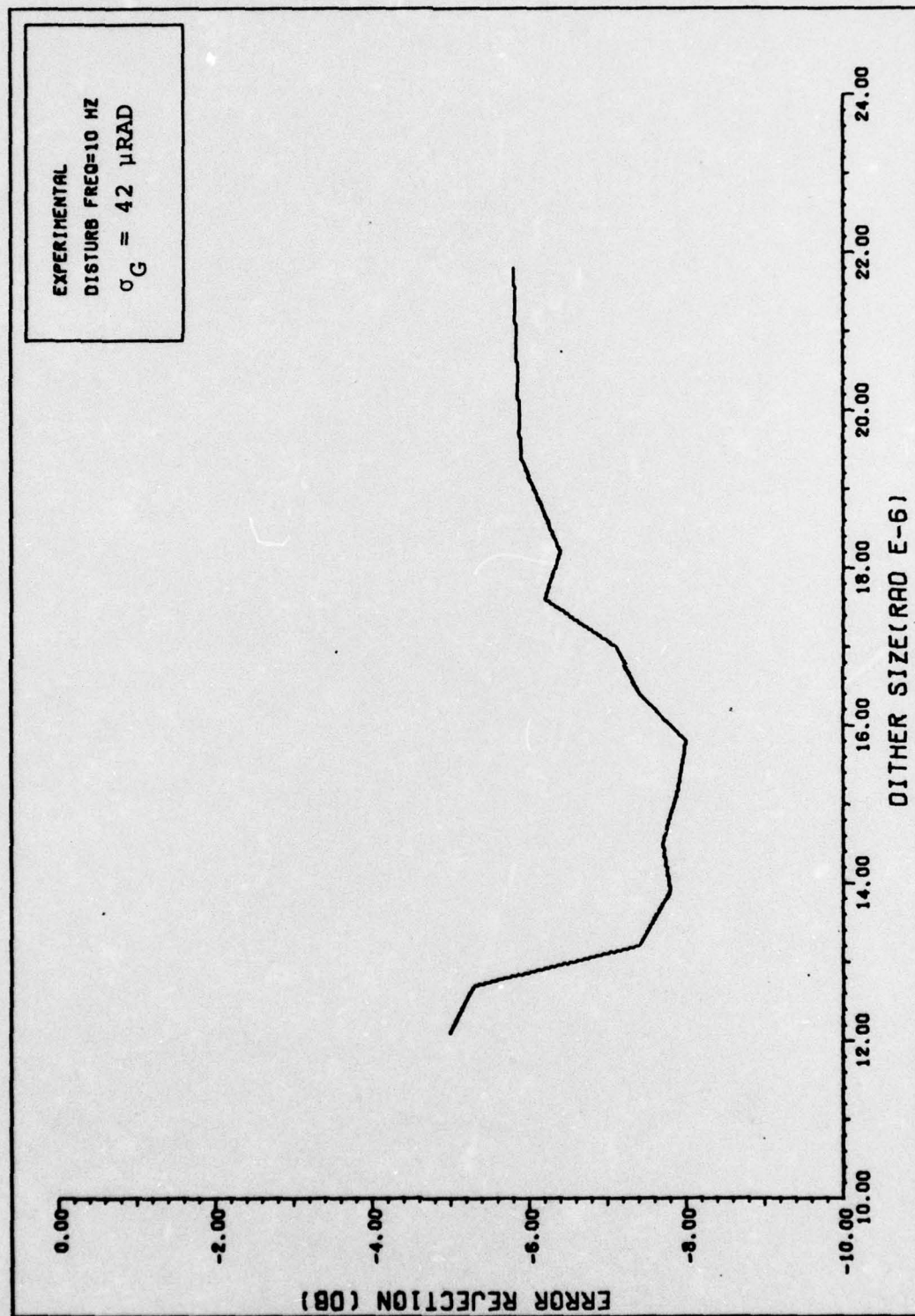


FIGURE 31. EFFECT OF DITHER SIZE ON ERROR REJECTION

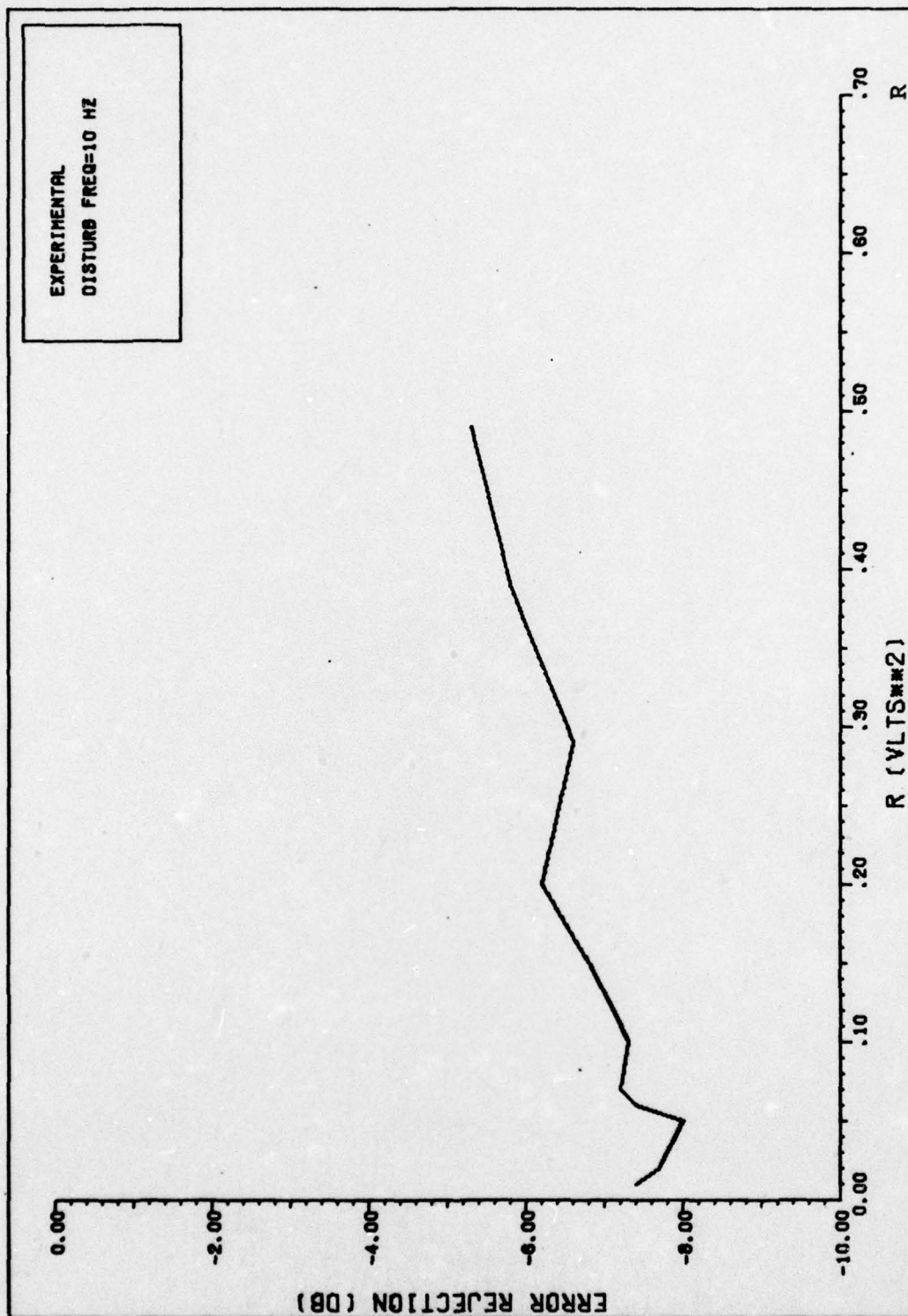


FIGURE 32. EFFECT OF R ON ERROR REJECTION

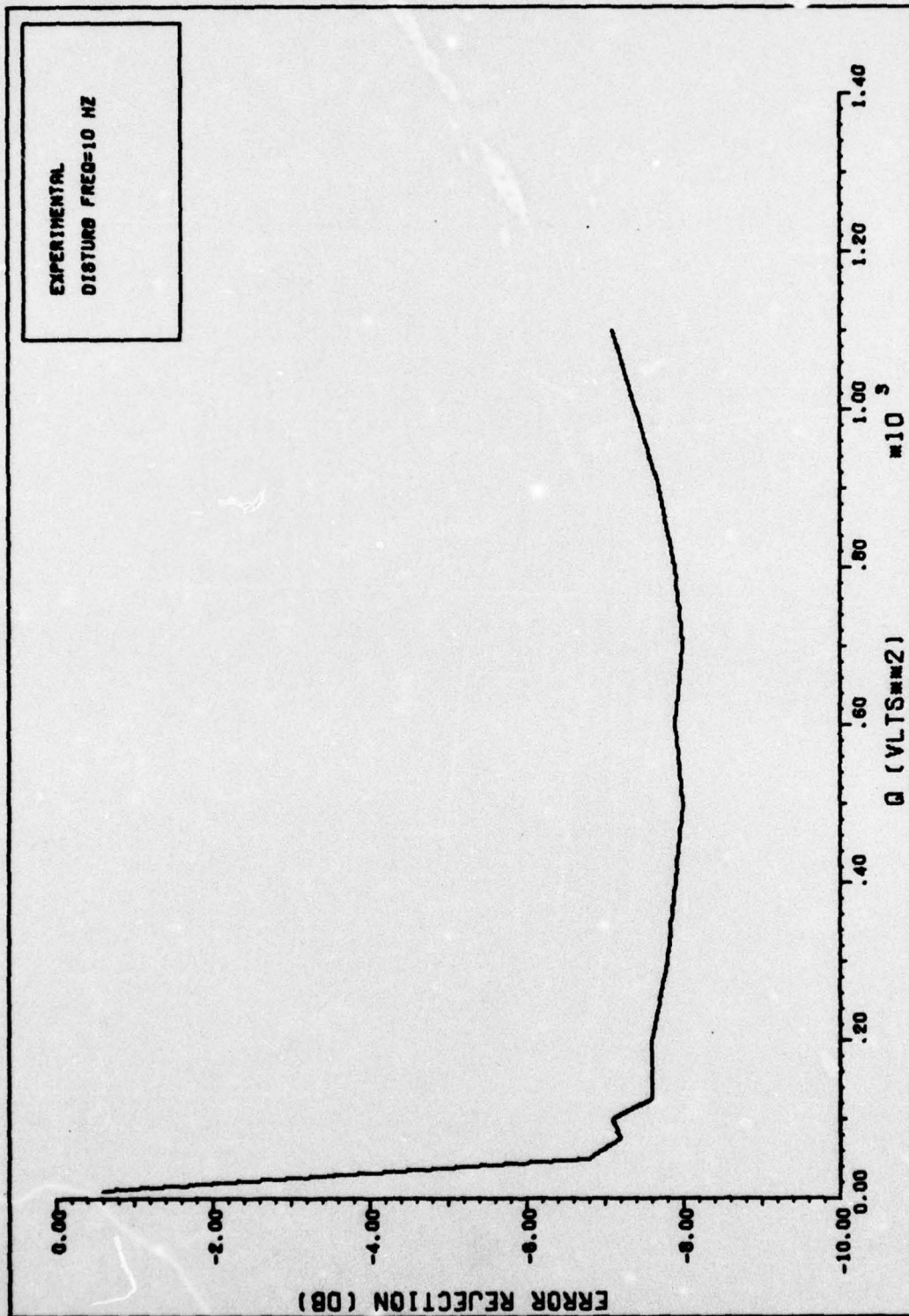


FIGURE 33. EFFECT OF Q ON ERROR REJECTION

minima that correspond to highest error rejection bandwidth. No global perturbation analysis was accomplished on the model parameters.

Target Search and Acquisition. A search and acquisition scheme was implemented to permit rapid target search and lock on. The search window was set at the limits of the field of view imposed by the ALOT optics. The window size is 1.2 mrad by 1.2 mrad, where for comparison the target glint dispersion (σ_G) is 42 μ rad. A spiral search pattern was chosen for its implementation simplicity. The initial search is begun at the window center and spirally diverged outward until the outer boundary is reached at which time the search is reinitiated at the center. If the return intensity at any of the discrete search points is above a preset threshold, the algorithm control is handed-off to the estimation and control algorithm. If for any reason the control algorithm breaks lock on the target, control is returned to the search algorithm. At this point the spiral search is initiated at the last mirror pointing position. Again if a boundary is reached before target is acquired, the search is reinitiated at the origin. This scheme is not optimal, but it was found to be effective for this demonstration.

Algorithm Sensitivity. The performance of the algorithm was shown to be dependent on the correct choices of Q, R, and dither step size. Incorrect selection of other

parameters, such as I_{\max} or σ_G , also degrades the performance of the algorithm. This is especially true if one or more of these other parameters are time varying. At least one parameter was observed to vary with time significantly in the ALOT laboratory. The peak return intensity, I_{\max} , contained a random variation of amplitude approximately equal to 15% of I_{\max} itself. This variation is discussed in Chapter II. The source of this variation appears to be the laser itself. Vibrations of the laser cavity optics induced by the building vibrations appear to cause the laser power output to fluctuate a corresponding amount. The I_{\max} fluctuations are strongest whenever the laboratory air conditioning system is operating. Whenever the I_{\max} fluctuations are at a minimum, the best error rejection is achieved in single or in dual axis. The estimation and control algorithm is most sensitive to I_{\max} fluctuations.

The algorithm is also sensitive to the assumed strength of the wideband measurement noise v . Figure 34 shows the effect of the strong wide band noise added to the glint when the algorithm model did not account for it. Despite small disturbance frequency, $f_{\theta_T} = 10\text{Hz}$, the algorithm is seen in Figure 34 to commit significant estimation errors as compared to errors in evident in Figure 30b where the measurement noise v is much smaller. The variance R of the measurement noise v is set at $.01 \text{ volts}^2$ while for this large amount of noise $R = .20 \text{ volts}^2$ is more appropriate.

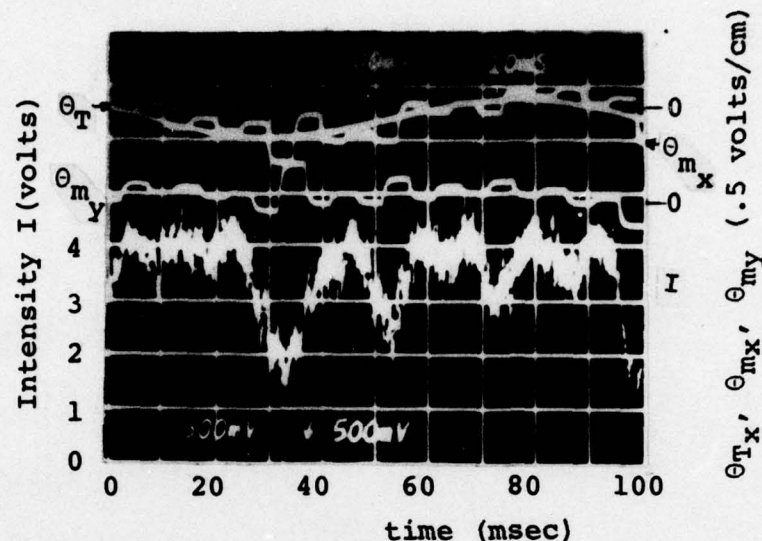


Figure 34. Effect of Strong Measurement Noise v

The strong adverse influence of I_{\max} variations and changes of measurement noise v can be attenuated in a number of ways. In this experiment I_{\max} and R (strength of v) were adapted for using conventional methods as presented in the next paragraph.

Adaptive Extended Kalman Filter

Statistical methods are available for parameter estimation, however, other methods were applied in this adaptation scheme.

Measurement Noise Adaptation. When the strength Q of the disturbance process is zero, and it is so modeled, then it is easy to show that the statistics of the residual (RES)

are precisely the statistics of the measurement noise v when the Kalman filter reaches steady state operation.

$$\begin{aligned} E\{\text{RES}(k)\} &= 0 \\ E\{\text{RES}(k)\text{RES}(l)\} &= \begin{cases} 0 & \text{for } l \neq k \\ R & \text{for } l = k \end{cases} \end{aligned}$$

It can also be shown that when the disturbance process strength is small, and the algorithm provides "good" estimates for $Q \neq 0$, the following approximation is valid:

$$\begin{aligned} E\{\text{RES}(k)\} &= 0 \\ E\{\text{RES}(k)\text{RES}(l)\} &\begin{cases} = & 0 & \text{for } l \neq k \\ \approx & R & \text{for } l = k \end{cases} \end{aligned}$$

Then under the assumption of ergodicity the variance R can be computed, in an approximation, as an average over a finite time interval of $\text{RES}^2(k)$. The averaging is accomplished by passing $\text{RES}^2(k)$ through a low pass filter of approximately 1Hz bandwidth thus allowing convergence on only the slowly varying $\text{RES}^2(k)$ signal. The output of the low pass filter is the estimate of the measurement noise variance $\hat{R}'(k)$. By trial and error it became evident that it is necessary to add a bias R_0 to $\hat{R}'(k)$ to achieve good error rejection. This scheme is presented in Figure 35. The gain m of this low pass filter is a proportionality constant. The effect of adaptation for R can be seen in Figure 36 where the estimation errors, and in turn control errors, are significantly smaller than in Figure 34 where

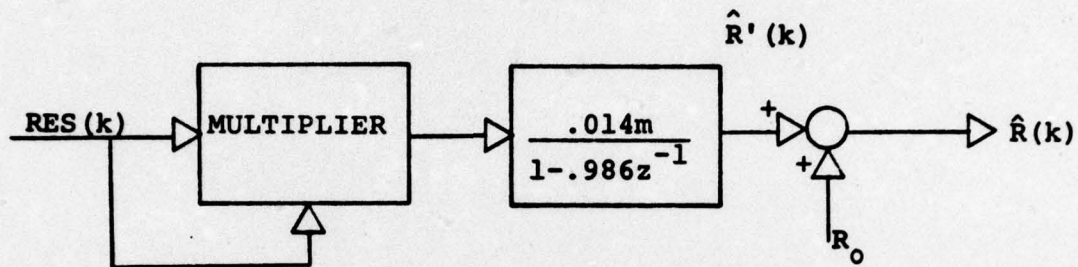


Figure 35. R Adaptation Algorithm

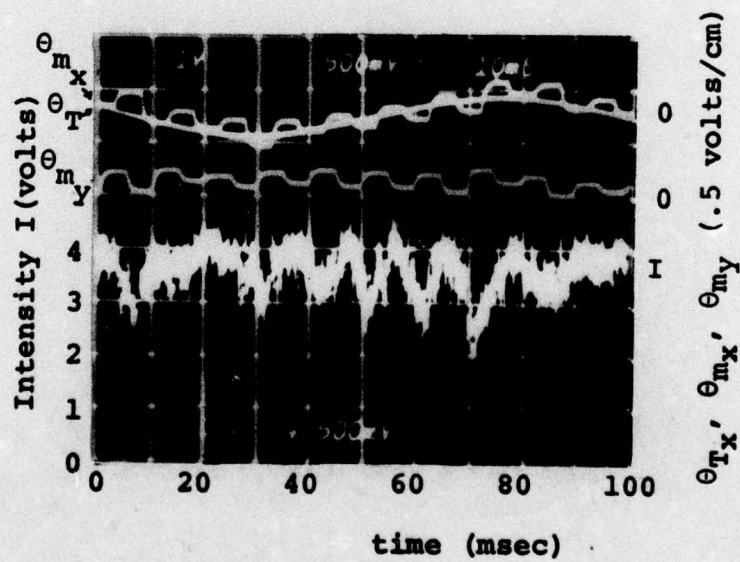


Figure 36. Effect of R Adaptation

the estimation errors are larger. Despite its crudeness, the adaptation scheme proved to be effective as in the above comparison of the Figures 36 and 34 and as will be shown later in improvement of the dither-to-response ratio. The time history of $\hat{R}(k)$ for one particular experiment can be seen in Figure 37 where the adaptation algorithm converges on $\hat{R}(k) \approx .17 \text{ volts}^2$.

Adaptation for I_{\max} . When the estimation of the pointing error is "good", then given the pointing error estimate $\hat{x}(k^-)$ and the corresponding measurement $\zeta(k)$, I_{\max} can be reconstructed. It is known that

$$\zeta(k) = I_{\max} \exp \left[-(x^2 + y^2) / 2\sigma_G^2 \right] + v(k) \quad (26)$$

Where x and y are the true time varying pointing errors. Solving for I_{\max} :

$$I_{\max}(k) = \frac{\zeta(k) - v(k)}{\exp \left[-(x^2 + y^2) / 2\sigma_G^2 \right]} \quad (27)$$

But:

$$\exp \left[-(x^2 + y^2) / 2\sigma_G^2 \right] \approx \frac{h(\hat{x}_{k-}, \hat{y}_{k-})}{I'_{\max}(k-1)}$$

Then:

$$I'_{\max}(k) = \frac{I'_{\max}(k-1) \zeta(k)}{h(\hat{x}_{k-}, \hat{y}_{k-})} - \frac{I'_{\max}(k-1) v(k)}{h(\hat{x}_{k-}, \hat{y}_{k-})} \quad (28)$$

Where $I'_{\max}(k)$ is the approximation of $I_{\max}(k)$.

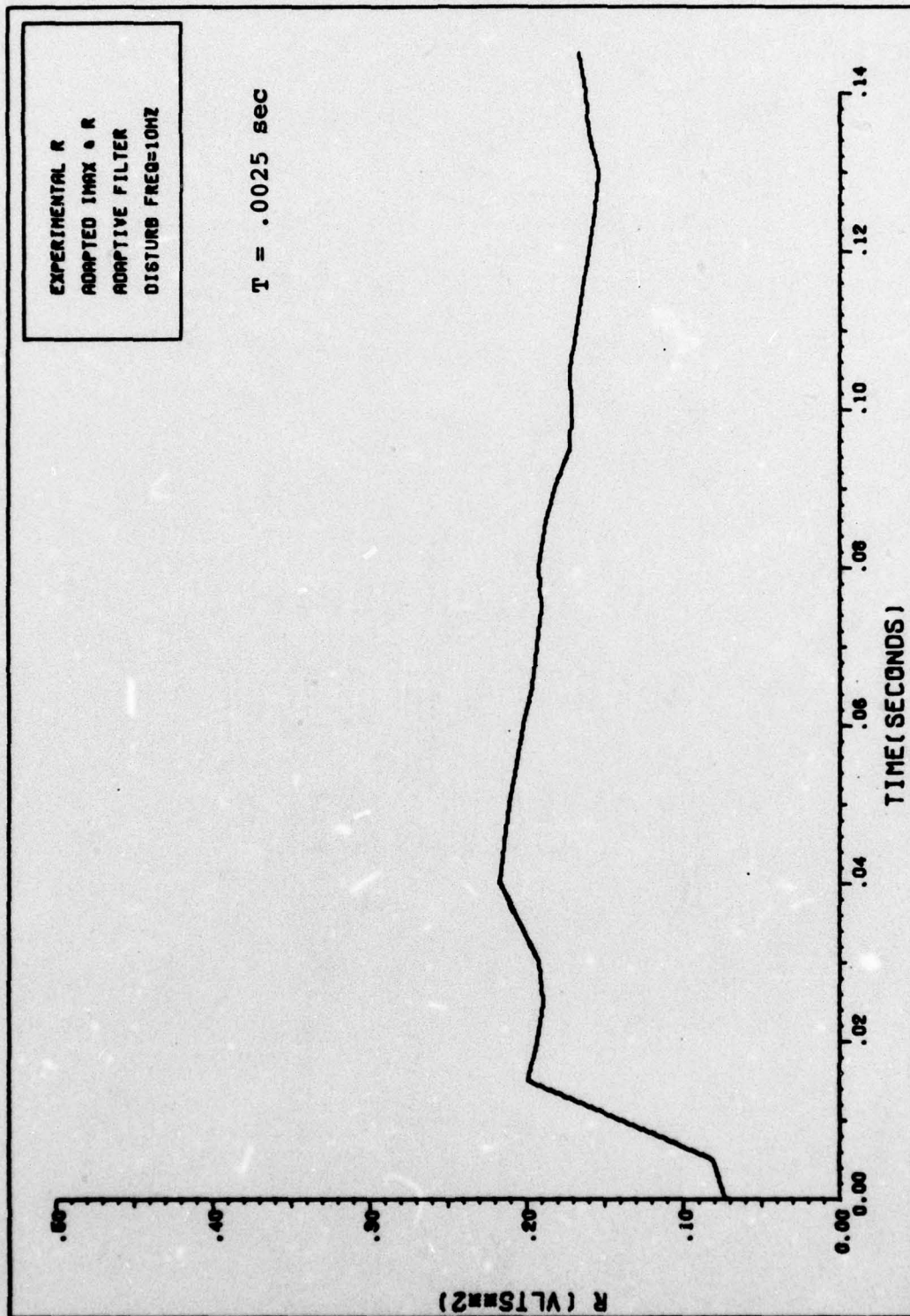


FIGURE 37. R TIME HISTORY

To eliminate the high frequency variations of $I_{\max}(k)$ due to the white sequence $v(k)$ in the second part of the above equation, $I'_{\max}(k)$ is passed through a low pass filter, where S is the filter gain.

$$\hat{I}_{\max}(k) = \frac{.023S}{1-.977z^{-1}} I'_{\max}(k) \quad (29)$$

The bandwidth of this low pass filter is approximately 1.5Hz. Thus, $\hat{I}_{\max}(k)$ responds only to low frequency variations of $I'_{\max}(k)$. Then $\hat{I}_{\max}(k)$ is used in the filter algorithm. With this algorithm implemented, the laser beam output was varied from .5 volts to 9.0 volts at the PMT filter output. This I_{\max} variation produced essentially no variation in the error rejection at $f_{\theta T} = 10\text{Hz}$. The adaptation scheme for I_{\max} made the algorithm essentially insensitive to I_{\max} variations. This insensitivity to I_{\max} increased the error rejection bandwidth of the ALOT control loop from 35 Hz non-adaptive to 40 Hz with R and I_{\max} adaptations. This can be seen in Figure 38. The improved ALOT error-rejection bandwidth translates to a dither-to-response ratio of 2.5:1 for the adaptive, compared to 2.9:1 for the non-adaptive estimation scheme. This dither-to-response ratio is the best documented for the two axis ALOT estimation and control in this research effort. The time history of $\hat{I}_{\max}(k)$ is seen in Figure 39 where $\hat{I}_{\max}(k)$ appears to be following slowly varying $I_{\max}(k)$. The Kalman

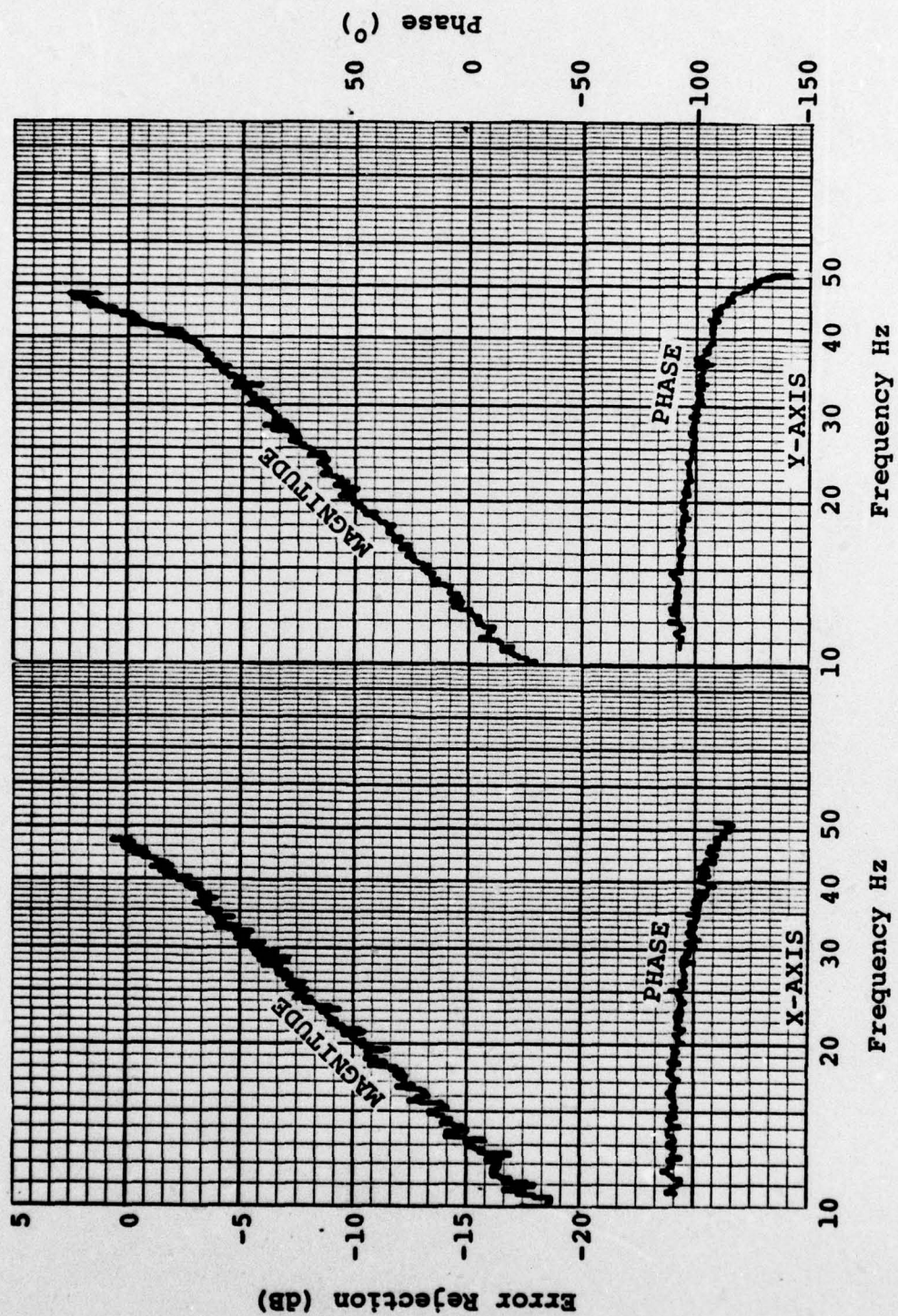


Figure 38. Two Axis Error Rejection--Adaptive Filter

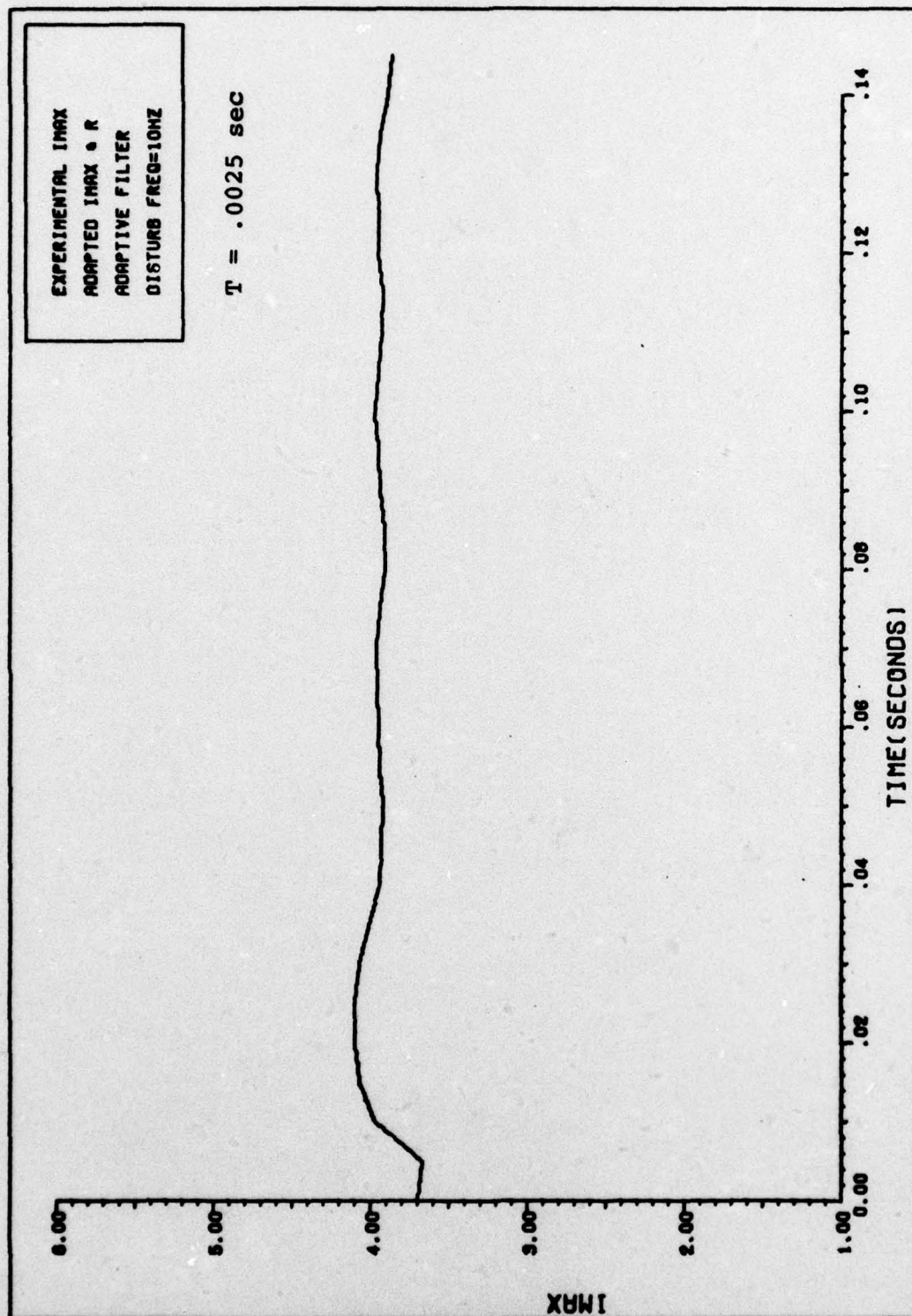


FIGURE 39. IMAX TIME HISTORY

gain and the variance time histories for the adaptive extended Kalman filter are presented in Figures 40 and 41 respectively. The abnormality in each of these figures during the first sampling period is due to the filter starting delay of one iteration to allow taking of one measurement necessary to begin I_{\max} adaptation.

The discussion and the data presented in this chapter in no way indicate that the best dither-to-response ratio has been achieved. However, it is shown that significant improvement in the dither-to-response ratio is feasible through the use of a digital adaptive extended Kalman filter.

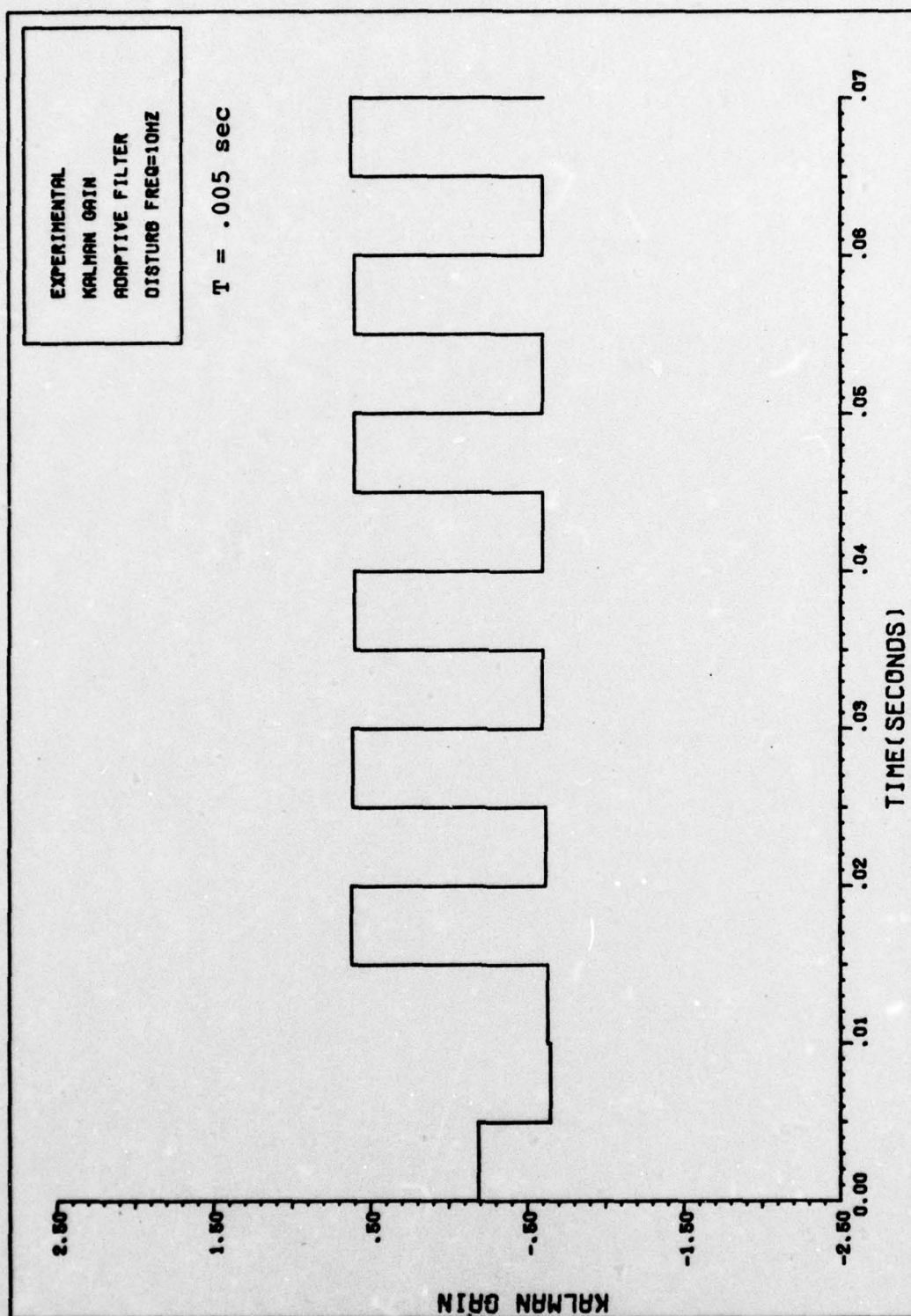


FIGURE 40. KALMAN GAIN TIME HISTORY (ADAPTIVE)

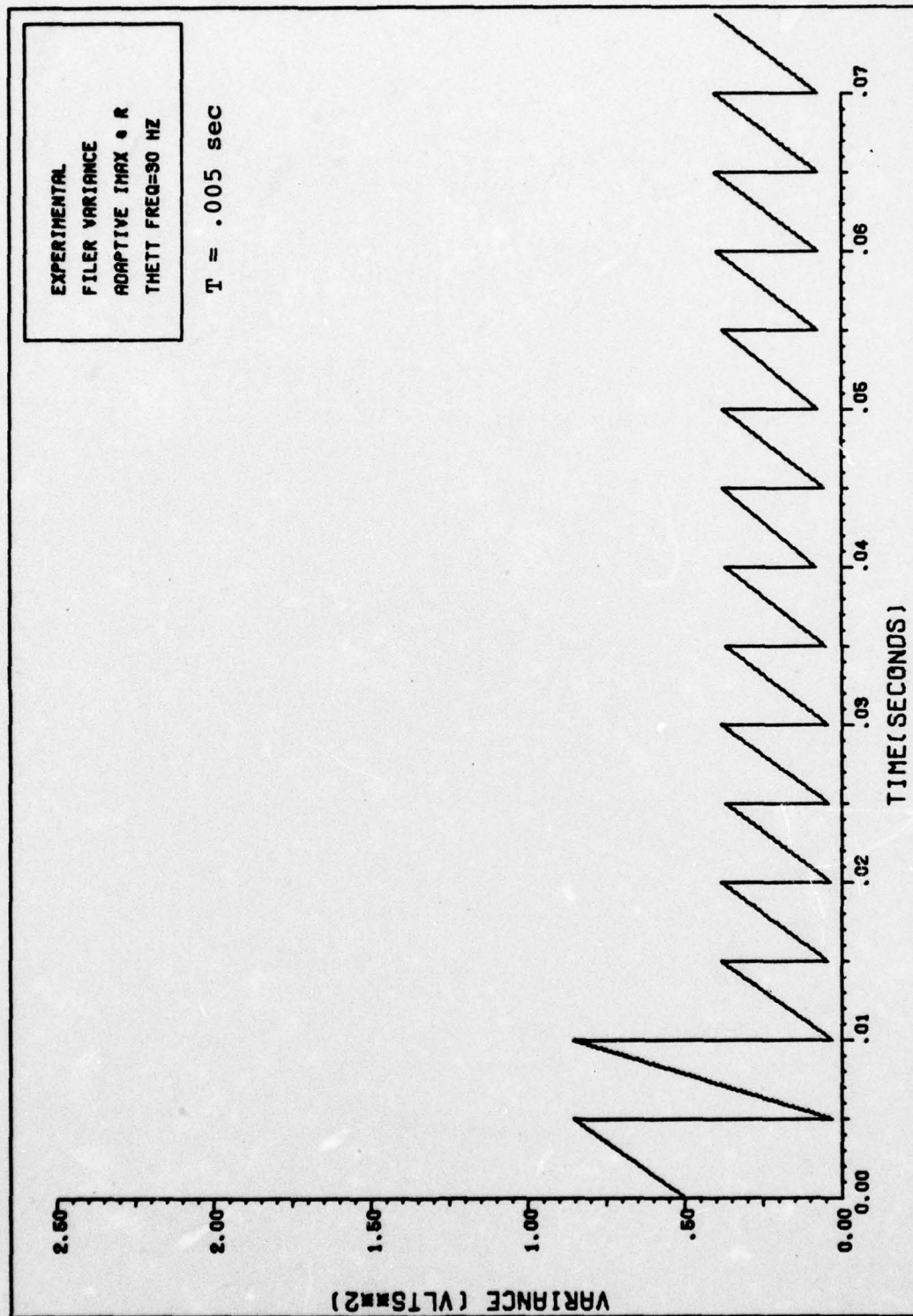


FIGURE 41. VARIANCE TIME HISTORY (ADAPTIVE)

VI. Conclusions and Recommendations

Conclusions

This study shows that an optimal estimation scheme can improve significantly the response bandwidth of the ALOT closed loop tracker. The estimation scheme is an extended Kalman filter algorithm implemented on a digital mini-computer.

The bivariate Gaussian (Normal) function is an excellent model for the glint from a spherical target and a Gaussian beam. However, the glint need not be Gaussian for the algorithm to work well. Any unimodal and continuously differentiable function that is a good model for the glint will suffice. This algorithm will track any glint that can be modeled by a unimodal and continuously differentiable function. A simple (first order pure integrator) shaping filter driven by white Gaussian noise is an adequate model of the disturbance process that the ALOT tracking loop attenuates. This disturbance attenuation permits the pointing of the laser beam at the top of the glint. Even though the glint is highly nonlinear for large pointing errors, the algorithm can estimate these pointing errors close to the glint edges. Thus the estimation scheme is less dependent on the amplitude of the disturbance process than a typical conical scan demodulation scheme.

The non-adaptive Kalman filter can be implemented using constant gains, and constant predicted measurements. This is due to the fact that the linearization is accomplished about a fixed magnitude of the pointing error. This would eliminate the need for the time consuming re-linearization about the nominal pointing error and real time solution of the discrete-time Riccati equation.

The ALOT estimation and control algorithm is sensitive to variations of some parameters that were assumed to be constant. This variation reduces the bandwidth of the ALOT control loop. An unsophisticated adaptation scheme used to estimate I_{\max} and R makes the control loop essentially insensitive to these parameters.

The pointing error has four possible sign solutions in the two arguments for any one measurement. The algorithm requires no additional information in correctly identifying the signs of the two pointing error arguments. This behavior is not totally explained and requires further research.

This research also shows conclusively that a general purpose minicomputer can be utilized for implementation of this estimation and control algorithm. The problems of computational errors due to finite word-length, truncation, and scaling can be overcome adequately. The most important advantage of digital control is the tremendous flexibility, compared to analog implementation, it afforded in the initial programming and in the subsequent program changes.

Recommendations

Further research is recommended in the use of an adaptive extended Kalman filter in an ALOT glint tracking scheme. Most significant should be an analysis of full estimation scheme for a given intensity measurement $I(x, y, \sigma_G, I_{\max}, b)$. In a general "real world" situation these parameters are either variables or constants not known a priori. The goal would be then to estimate parameters essential to meet the control specifications. These parameters should be modeled as state variables in a stochastic estimation scheme.

Another area of suggested research is in the correct modeling of the cross-correlation of the pointing error between the two axes. The ALOT control loop performance can possibly be improved by correct modeling of this cross-correlation.

Offset tracking is a concept where a portion of the unimodal glint other than the peak is used as a tracking point. This concept may have "real world" applications and could be explored in future research.

The two axes estimation should be simulated to explore the effect of cross-axis coupling. A proper stochastic model that includes the cross coupling parameters may improve the two axis performance of this estimation scheme.

The adaptation scheme for the measurement noise variance R is crude, but effective to a limited degree. Other adaptation schemes should be explored to improve the R estimation.

A study of the possible targets should be performed to determine the adequacy of this simplified modeling form.

Bibliography

1. The Analytic Sciences Corporation. TASC Proposal to Develop Advanced Adaptive Optics Control Techniques. Prepared for the Air Force Special Weapons Center, Kirtland Air Force Base, New Mexico, 10 August 1976.
2. Dillow, J. D., et al. A Control Model for a Conical Scan Tracking System. Laser Digest, July 1976, AFWL-TR-76-131, Air Force Weapons Laboratory, Kirtland Air Force Base, New Mexico.
3. Maybeck, P. S. The Kalman Filter, An Introduction for Potential Users. TM-72-3. Wright-Patterson Air Force Base, Ohio: Air Force Flight Dynamics Laboratory, 1972.
4. Maybeck, P. S. Stochastic Estimation and Control Systems Part II (Course notes for EE 7.66). Wright-Patterson Air Force Base, Ohio: Air Force Institute of Technology, February 1975.
5. Maybeck, P. S. Stochastic Estimation and Control Systems Part II (Notes for EE 7.12). Wright-Patterson Air Force Base, Ohio: Air Force Institute of Technology, July 1975.
6. Pearson, J. E., et al. COAT Measurements and Analysis. RADC-TR-75-303. Griffiss Air Force Base, New York: Rome Air Development Center, November 1975.
7. Potter, R. M., et al. Digital Control of a Conical Scan Pointing System. Laser Digest, July 1976, AFWL-TR-76-131, Air Force Weapons Laboratory, Kirtland Air Force Base, New Mexico.
8. Wozencraft, J. M. and I. M. Jacobs. Principles of Communication Engineering. New York: John Wiley and Sons, Inc., 1967.

Appendix

This appendix presents the assembly language program for the Data General-Nova 800 minicomputer. The program is the implementation of the two-axes estimation and control algorithm of the digital conical scan tracker.


```

.TITL  AXIS2  ;THIS PROGRAM ESTIMATES

;THE LASER BEAM POINTING ERROR
;IN TWO AXIS.  THIS ERROR IS USED
;AS A CONTROL INPUT IN A FEED-
;BACK LOOP TO ZERO OUT THAT ERROR.

.EXTN  DEBUG
.ENT   QQ
.EXTU
.ZREL  ;ALL CONSTANTS AND VARIABLES
ALPH:  0  ;=2*PI*F
IMAX0: 10240. ;INITIAL IMAX
SIGNT: 1400. ;GLINT SIGMA #####
T:      4.   ;SAMPLING PERIOD #####
R0:     100. ;INITIAL R #####
CT0:    1.   ;INITIAL COUNT #####
D:      3200. ;DITL FACTOR #####
Q:      200. ;NOISE STRENGTH (DIST) ###
GI:     0    ;IMAX FLTR GAIN (1-GIX)
GII:    2048. ;FLTR GAIN MULTPLR
GIX:    1800. ;IMAX FLTR TIME CONST
GR:     0    ;R FLTR GAIN (1-GRX)
GRI:    2048. ;FLTR GAIN MLTPLR
GRX:    1800. ;R FLTR TIME CONSTANT
GS:     0    ;SZET FILTER GAIN
GSX:    1024. ;SZET FILTER TIME CONSTANT
TABC:   0    ;STORE TABLE COUNTER
TABCO:  -301 ;INITIAL TABLE COUNTER
SF11:   2048. ;SCALE FACTORS
SF3:    8.   ;      "
SF7:    16.  ;      "
SF15:   32768. ;      "
SFOUT:  10.  ;D/A SCALE FACTOR
BLB:    600. ;BREAK LOCK BOUND
P0:     32.  ;P(0) MSW
P01:    0    ;      LSW
TRES:   1600. ;RES FLTR TIME CONSTANT
GRES:   0    ;GAIN OF RES FLTR
RPROP:  18432. ;REST PROPORTIONALITY CONST
G:      0    ;QQG MSW
G1:     0    ;      LSW
A:      0    ;EXP(-ALPH*T)
B:      0    ;A**2
DITL:   400. ;DITHER SIZE
SHFT:   11.  ;SHIFT COUNTER
SIGS:   0    ;SIGNT**2
SIGS2:  0    ;2*SIGS
UX:     0    ;X-AXIS CONTROL
DAX:    0    ;X-AXIS OUTPUT REGISTER
UY:     0    ;Y-AXIS CONTROL
DAY:    0    ;Y-AXIS OUTPUT REGISTER

```

IMAX:	0	;CURRENT IMAX
R:	0	;CURRENT R
BOUND:	8000.	;.9*IMAX
MSK:	177400	;BYTE MASK
MSK1:	177740	;SHIFT MASK
MSK2:	177000	;SHIFT MASK
MSK4:	140000	;EXPONENT ARGUMENT MASK
MSKB:	174000	;BOUNDARY MASK
XM:	0	;X-ERROR AT T-
XP:	0	;X-ERROR AT T+
YM:	0	;Y-ERROR AT T-
YP:	0	;Y-ERROR AT T+
PXM:	0	;X-VARIANCE AT T- MSW
PXM1:	0	; LSW
PXP:	0	;X-VARIANCE AT T+ MSW
PXP1:	0	; LSW
PYM:	0	;Y-VARIANCE AT T- MSW
PYM1:	0	; LSW
PYP:	0	;Y-VARIANCE AT T+ MSW
PYP1:	0	; LSW
KX:	0	;X-FILTER GAIN
KY:	0	;Y-FILTER GAIN
AK:	0	;ABS(KX OR KY)
HX:	0	;H(X,Y) IN X
HY:	0	;H(X,Y) IN Y
HHX:	0	;LINEARIZED H ABOUT X
HHY:	0	;LINEARIZED H ABOUT Y
AHH:	0	;ABS(HHX OR HHY)
ZETA:	0	;MEASUREMENT
SZET:	0	;SUM OF ZETAS
XRES:	0	;RESIDUAL IN X
SXRES:	0	;SUM OF X RESIDUALS
AXRES:	0	;ABS(XRES)
YRES:	0	;RESIDUAL IN Y
SYRES:	0	;SUM OF Y RESIDUALS
AYRES:	0	;ABS(YRES)
HP:	0	;TEMP STORE FOR H*P MSW
HP1:	0	; LSW
TEM:	0	;SUBROUTINE RTN ADDR STORE
TEM1:	0	;TEMPORARY STORAGE
TEM2:	0	; "
TEM3:	0	; "
TEM10:	18000.	; "
TEM11:	0	; "
TEM12:	0	; "
TEM13:	0	; "
TEM14:	0	; "
COUNX:	0	;CONVERGENCE TIME COUNTER
COUNY:	0	; "
ZERO:	0	;DUMMY LOCATION
SGN:	0	;SIGN FLAG


```

ARG:      0      ;EXPONENTIAL ARGUMENT (X**2+Y**2)
EXPT:     0      ;VALUE OF EXPONENT
TAB:      0      ;TEMPORARY STORAGE
ZER:      0      ;VALUE OF ZERO
ONE:      1.     ;VALUE OF ONE
BIAS:     820.   ;I=IMAX*EXP(-(X**2+Y**2)/SIGS2))+BIAS
PTSIX:    1050.  ;SRES FACTOR
DITIV:    0      ;INITIAL DITHER SIZE
SLPE:     1092.  ;BOUND SLOPE
MIN:      750.   ;BOUND BIAS
NO:       1.     ;INITIAL # OF STEPS
N:        0      ;CURRENT # OF STEPS
NC:       0      ;STEP COUNTER
TEST:     2000.  ;SEARCH THRESHOLD
STP:      2000.  ;STEP SIZE
MPP:      MP
IVV:      IV
MP35M:    MP35   ;
           .NREL  ;COMPUTE CONSTANTS *****
           .BLK   20
QQ:        LDA    1,ALPH  ;LOAD ALPH
           LDA    2,T      ;LOAD T
           SUBO    0,0     ;CLR AC0
           MUL     ;
           STA    1,TEM1  ;STORE ARGMNT
           JSR    @EXP    ;A=EXP(-ALPH*T)
           TEM1    ;EXP ARGUMENT
QQ1:       A      ;STORE RSLT IN A
           .BLK   10
           LDA    1,A      ;LOAD A
           MOV    1,2      ;DUPLCT A
           SUBO    0,0     ;CLR AC0
           MUL     ;
           LDA    2,SF11   ;LOAD SF11
           DIV     ;
           MOVZL   0,0     ;ROUND OFF
           SUBZL#  0,2,SZC ;
           INC     1,1     ;
QQ2:       STA    1,B      ;STORE B
           LDA    2,ALPH   ;LOAD ALPH
           MOVL#   2,2,SZR ;IS ALPH=0?
           JMP     QQ3     ;NO, JMP QQ3
           LDA    1,T      ;YES,LOAD T
           LDA    2,SF11   ;LOAD SF11
           SUBO    0,0     ;CLR AC0
           MUL     ;
           LDA    2,Q      ;LOAD Q
           MUL     ;
           JMP     QQ33    ;JMP AND STORE G
QQ3:       LDA    1,SF11   ;LOAD SF11

```



```

LDA      2,B      ;LOAD B
SUB      2,1      ;1-B
LDA      2,SF11   ;LOAD SF11
SUBO     0,0      ;CLR AC0
MUL      ;
LDA      2,ALPH   ;LOAD ALPH
DIV      ;
MOVZR    1,1      ;DIV BY 2
LDA      2,Q      ;LOAD Q
SUBO     0,0      ;CLR AC0
MUL      ;
QQ33:    STA      0,G      ;STORE G MSW
        STA      1,G1     ;      LSW
        JMP      QQ4      ;
        .BLK     20
QQ4:     LDA      1,SIGNT ;LOAD SIGNT
        MOV      1,2      ;DUPLCT SIGNT
        SUBO     0,0      ;CLR AC0
        MUL      ;
        LDA      2,SF11   ;LOAD SF11
        DIV      ;
        STA      1,SIGS   ;STORE SIGS
        MOVZL    1,1      ;MULT BY 2
        STA      1,SIGS2  ;STORE SIGS**2
QQ5:     LDA      1,GIX   ;LOAD GIX
        LDA      2,SF11   ;LOAD SF11
        MOV      2,3      ;DUPLCT SF11 IN AC3
        SUB      1,2      ;1-GIX
        LDA      1,GII   ;LOAD GII
        SUBO     0,0      ;CLR AC0
        MUL      ;
        LDA      2,SF11   ;LOAD SF11
        DIV      ;
        STA      1,GI     ;STORE GI
QQ6:     LDA      1,GRX   ;LOAD GRX
        SUB      1,3      ;1-GRX
        MOV      3,1      ;MOV AC3 TO AC1
        LDA      2,GRI   ;LOAD GRI
        SUBO     0,0      ;CLR AC0
        MUL      ;
        LDA      2,SF11   ;LOAD SF11
        DIV      ;
        STA      1,GR     ;STORE GR
QQ7:     LDA      1,GSX   ;LOAD GSX
        LDA      2,SF11   ;LOAD SF11
        SUB      1,2      ;1-GSX=GS
        STA      2,GS     ;STORE GS
        LDA      1,SF11   ;LOAD SF11
        LDA      2,TRES   ;LOAD TRES
        SUB      2,1      ;1-TRES
        STA      1,GRES   ;STORE GRES

```

```

LDA      1,SIGNT ;LOAD SIGNT
LDA      2,D      ;LOAD D
SUBO     0,0      ;CLR AC0
MUL      ;
LDA      2,IMAX0 ;LOAD IMAX0
DIV      ;
STA      1,DITIV ;STORE DITIV
SUBO     0,0      ;CLR AC0
STA      0,DAX    ;RESET X-AXIS
STA      0,DAY    ;RESET Y-AXIS
IV:      SUBO     0,0 ;INITIALIZE THE VARIABLES
STA      0,UX     ;
STA      0,UY     ;
STA      0,XM     ;
STA      0,XP     ;
STA      0,YM     ;
STA      0,YP     ;
IV1:     STA      0,ZETA ;
IV2:     LDA      1,IMAX0 ;
STA      1,IMAX   ;
STA      1,SZET   ;
LDA      1,R0     ;
STA      1,R      ;
LDA      0,P0     ;
LDA      1,P01    ;
STA      0,PXP    ;
STA      0,PYP    ;
IV3:     STA      1,PXP1 ;
STA      1,PYP1   ;
LDA      1,CT0    ;
STA      1,COUNX  ;
STA      1,COUNY  ;
LDA      1,DITIV  ;
STA      1,DITL   ;
STA      1,UX     ;
STA      1,UY     ;
LDA      1,TABC0  ;
STA      1,TABC   ;
IV4:     LDA      1,MP7 ;
STA      1,MP8    ;
LDA      1,IMAX0  ;
MOVZR    1,1      ;
STA      1, SXRES ;
STA      1, SYRES ;
JMP      MP9+4    ;
IV5:     JSR      @SRCH ;FIND THE GLINT
IV6:     JMP      MP      ;
        .BLK      20
        .ZREL
P20:     MP20
        .NREL

```



```

MP:      JSR      @TABLS      ;MAIN PROGRAM *****
        PXM              ;STORE 264 SPECFD VLS
        PXM1             ;
        PYM              ;
        PYM1             ;
        JSR      @PROP      ;PROPAGATE X-AXIS
        XP              ;SUBROUTINE ARGUMENTS
        UX              ;
        XM              ;
        PXP             ;
        PXP1            ;
        PXM              ;
        PXM1             ;
        .BLK      20
MP1:     JSR      @ARGM      ;COMPUTE ARGUMENT
        JSR      @EXP      ;COMPUTE EXPONENTIAL
        ARG              ;ARGUMENTS
        EXPT            ;
        .BLK      10
MP2:     JSR      @HHHH      ;COMPUTE H,HH
        XM              ;ARGUMENTS
        HHX             ;
        HX              ;
        .BLK      10
MP3:     JSR      @UPDT      ;COMPUTE K,P
        PXM              ;ARGUMENTS
        PXM1             ;
        KX              ;
        PXP             ;
        PXP1            ;
        HHX             ;
        .BLK      10
MP4:     JSR      @CLCK      ;SAMPLE AND COMPUTE:
        XRES              ;  XP, XRES, SXRES
        AXRES            ;
        KX              ;
        XM              ;
        XP              ;
        SXRES            ;
        HX              ;
        .BLK      10
        JSR      @SZETA     ;COMPUTE SUM OF ZETAS
MP5:     JMP      MP8        ;BYPASS TWO DUMMIES
MP6:     JMP      MP10-2     ;
MP7:     DSZ      COUNX      ;
MP8:     DSZ      COUNX      ;DECR. CONVERGENCE COUNTER
        JMP      MP9        ;COUNT NOT=0, CONTINUE
        LDA      1,MP6      ;COUNT=0, SET UP BYPASS
        STA      1,MP8      ;
        JMP      MP10      ;CONTINUE

```



```

MP9:   JSR    @BOUN    ; COMPUTE BOUND
       JSR    @TEN     ; IF COUNT NOT=0, FORCE SIGN
       SXRES   ; ON XP, OR YP
       XP      ;
       LDA     1,MP27   ; RESTART Y-AXIS BYPASS
       STA     1,MP28   ;
       JMP     IV5      ;
       .BLK    5
       LDA     2,DITL   ; LOAD DITL
       STA     2,UX     ; STORE UX=DITL
       JMP     MP11     ; JMP MP11
MP10:  LDA     1,XP     ; LOAD XP
       LDA     2,DITL   ; LOAD DITL
       SUB     1,2      ; UX=-XP+DITL
       STA     2,UX     ; STORE UX
MP11:  LDA     1,DAX     ; LOAD DAX
       ADD     2,1      ; DAX=DAX+UX
       STA     1,DAX     ; STORE DAX
MP12:  JSR     @OUTPT   ; OUTPUT X CHANNEL
       ZER     ;
       DAX     ;
       .BLK    10
MP13:  LDA     1,COUNX   ; LOAD COUNT
       MOV     1,1,SZR  ; IS COUNT=0?
       JMP     MP20     ; NO, JMP MP20
MP14:  JSR     @IEST    ; ESTIMATE IMAX
       HX      ;
       JSR     @REST    ; ESTIMATE R
       AXRES   ;
       RPROP   ;
       .BLK    10
MP20:  JSR     @PROP    ; PROPAGATE Y-AXIS
       YP      ; ARGUMENTS
       UY      ;
       YM      ;
       PYP     ;
       PYP1    ;
       PYM     ;
       PYM1    ;
       .BLK    20
MP21:  JSR     @ARGM    ; COMPUTE ARGUMENT
       JSR     @EXP     ; COMPUTE EXPONENTIAL
       ARG     ;
       EXPT    ;
       .BLK    10
MP22:  JSR     @HHH     ; COMPUTE H,HH
       YM      ;
       HHY     ;
       HY      ;
       .BLK    10
MP23:  JSR     @UPDT    ; COMPUTE K,P

```

```

PYM ;
PYM1 ;
KY ;
PYP ;
PYP1 ;
HHY ;
.BLK 10
MP24: JSR @CLCK ;SAMPLE AND COMPUTE
YRES ; YP, YRES, AND SYRES
AYRES ;
KY ;
YM ;
YP ;
SYRES ;
HY ;
.BLK 10
MP25: JSR @SZETA ;COMPUTE SZET
JMP MP28 ;BYPASS TWO DUMMIES
MP26: JMP MP30-2 ; "
MP27: DSZ COUNY ; "
MP28: DSZ COUNY ;DECR CONVER COUNTER
JMP MP29 ;COUNT NOT=0, CONTINUE
LDA 1,MP26 ;COUNT=0, SET UP BYPASS
STA 1,MP28 ; "
JMP MP30 ;YES, JMP MP30
MP29: JSR @BOUN ;COMPUTE SZET
JSR @TEN ;NO, FORCE SIGN
SYRES ;
YP ;
.BLK 10
LDA 2,DITL ;LOAD DITL
STA 2,UY ;STORE UY=DITL
JMP MP31 ;
MP30: LDA 1,YP ;LOAD YP
LDA 2,DITL ;LOAD DITL
SUB 1,2 ;UY=-YP+DITL
STA 2,UY ;STORE UY
MP31: LDA 1,DAY ;LOAD DAY
ADD 2,1 ;DAY=DAY+UY
STA 1,DAY ;STORE DAY
MP32: JSR @OUTPT ;OUTPUT Y-AXIS
ONE ;
DAY ;
.BLK 10
MP33: LDA 1,COUNY ;LOAD COUNT
MOV 1,1,SZR ;IS COUNT=0?
JMP MP35 ;NO, JMP MP35
MP34: JSR @IEST ;ESTIMATE IMAX
HY ;
JSR @REST ;ESTIMATE R
AYRES ;

```



```

RPROP      ;
      .BLK 10
MP35: JSR @DITS ; COMPUTE DITL AND NEG IT
      LDA 1,COUNX ; LOAD X-COUNTER
      MOV 1,1,SNR ; IS X-COUNTER=0?
      JSR @BREAK ; IT IS=0, TEST FOR BREAK
      JMP @MPP ; NOT=0, CONTINUE
MP36: JSR @BREAK ; IS IT STILL TRACKING?
      JMP @MPP ;
      .BLK 20
      .ZREL ; PROPAGATE SUBROUTINE *****
PROP: PRO ; IT PROPAGATES THE MEAN AND
      .NREL ; THE VARIANCE
PRO: STA 3,TEM ; STORE RTN ADDR
      LDA 1,@0,3 ; LOAD XP OR YP
      SUBO 3,3 ; CLR AC0
      MOVZL# 1,1,SNC ; TEST SIGN
      INC 3,3,SKP ; POS, SET FLAG
      NEG 1,1 ; NEG, NEGATE
      LDA 2,A ; LOAD A
      SUBO 0,0 ; CLR AC0
      MUL ;
P1: LDA 2,SF11 ; LOAD SF11
      DIV ;
      MOVZR 3,3,SNC ; IS FLAG SET?
      NEG 1,1 ; NO, NEGATE
      LDA 3,TEM ; RESTORE RTN ADDR
      LDA 2,@1,3 ; LOAD UX OR UY
      ADD 2,1 ;
P2: STA 1,@2,3 ; STORE XM OR YM
      LDA 0,@3,3 ; LOAD PP MSW
      LDA 1,@4,3 ; LSW
      MOV 0,0,SZR ; IS MSW=0?
PRO1: JMP PRO2-1 ; NO, JMP PRO2
      LDA 2,B ; YES, LOAD B
      MUL ;
      LDA 2,SF11 ; LOAD SF11
      DIV ;
      SUBO 0,0 ; CLR AC0
      STA 3,TEM ; STORE RTN ADDRESS
      JMP PRO6 ; JMP TO ADD G
      SUBO 3,3 ; CLR SHFT COUNTER
PRO2: INC 3,3 ; INC SHFT COUNTER
      MOVZR 0,0,SZR ; IS MSW=0?
      JMP PRO3 ; NO, JMP PRO3
      MOVR 1,1 ; YES, MOVE LSW
      JMP PRO4-2 ; JMP DESHIFT
PRO3: MOVR 1,1 ; MOVE LSW
      JMP PRO2 ; MSW NOT=0, GO BACK
      LDA 2,B ; LOAD B
      MUL ;

```



```

PRO4:  NEG      3,3      ;NEG SHFT COUNTER
        LDA      2,SHFT  ;LOAD SHIFT
        ADD      2,3      ;
        MOVZL#   3,3,SNC ;DSHFT LFT OR RGHT?
        MOV      3,3,SNR ;NO SHFTS?
        JMP      PRO6     ;NO SHFTS, JMP PRO6
        JMP      .+6      ;POS, DSHFT RGHT
        MOVZL    1,1      ;NEG, LFT; MOV LSW
        MOVL     0,0      ;      MSW
P3:     INC      3,3,SZR  ;INC COUNTER
        JMP      .-3      ;GO BACK
        JMP      PRO6     ;JMP TO PRO6
        NEG      3,3      ;NEG COUNTER
        MOVZR    0,0      ;MOVR MSW
        MOVR     1,1      ;      LSW
        INC      3,3,SZR  ;INC COUNTER
        JMP      .-3      ;GO BACK
PRO6:   LDA      3,TEM     ;RESTORE RTN ADDR
        LDA      2,G       ;LOAD G MSW
        ADD      2,0       ;ADD MSW
        LDA      2,G1      ;LOAD G LSW
        ADD      2,1       ;ADD LSW
        STA      0,@5,3    ;STORE PXM MSW
        STA      1,@6,3    ;      LSW
        JMP      27,3      ;RETURN
        .BLK     20
        .ZREL    ;ARGUMENT SUBROUTINE *****
ARGM:   AR       ;CALCULATES (X**2+Y**2)/2SIGs
        .NREL    ;
AR:     STA      3,TEM     ;STORE RTN ADDR
        LDA      1,XM      ;LOAD XM
        MOVZL#   1,1,SCZ  ;TEST DIGN
        NEG      1,1      ;NEG, NEGATE
        MOV      1,2      ;DUP XM
        SUBO     0,0      ;CLR AC0
        MUL      ;
AR1:    STA      0,TEM1    ;TEMPOR STORE MSW
        STA      1,TEM2    ; AND LSW OF XM**2
        LDA      1,YM      ;LOAD YM
        MOVZL#   1,1,SZC  ;TEST SIGN
        NEG      1,1      ;NEG, NEGATE
        MOV      1,2      ;DUPLICATE YM
        SUBO     0,0      ;CLR AC0
        MUL      ;
AR2:    LDA      2,TEM1    ;LOAD MSW OF XM**2
        ADD      2,0       ; ADD
        LDA      2,TEM2    ;LOAD LSW OF XM**2
        ADD      2,1       ; ADD
        LDA      2,SIGS2   ;LOAD 2*SIGs
        DIV      ;
        STA      1,ARG     ;STORE EXP ARGUMENT

```

```

AR3:   JMP      @TEM      ;RETURN
       .BLK      20
       .ZREL      ;H, HH SUBROUTINE *****
HHHH:   HHH      ;CALCULATES H, AND HH FOR GIVEN
       .NREL      ;ARGUMENTS IN CALLING STATEMENT
HHH:    STA      3,TEM      ;STORE RTN ADDR
       LDA      1,EXPT      ;LOAD EXPT
       LDA      2,IMAX      ;LOAD IMAX
       SUBO      0,0        ;CLR AC0
       MUL
       LDA      2,SF11      ;LOAD SF11
       DIV
       LDA      2,BIAS      ;LOAD I BIAS
       ADD      1,2        ;ADD
H1:     STA      2,@2,3      ;STORE HX
       LDA      2,@0,3      ;LOAD XM OR YM
       SUBO      3,3        ;CLR AC3
       MOVZL#    2,2,SNC    ;TEST SIGN
       INC      3,3,SKP     ;POS, SET FLAG
       NEG      2,2        ;NEG, NEGATE
       SUBO      0,0        ;CLR, AC0
H2:     MUL
       LDA      2,SIGS      ;LOAD SIGS
       DIV
       MOVZR     3,3,SZC    ;TEST FLAG
       NEG      1,1        ;NEG, NEGATE
       LDA      3,TEM      ;RESTORE RTN ADDR
       STA      1,@1,3      ;STORE HHX OR HHY
H3:     JMP      13,3        ;RETURN
       .BLK      20
       .ZREL      ;UPDATE SUBROUTINE *****:
UPDT:   UPD      ;UPDATES K AND P
       .NREL
UPD:     STA      3,TEM      ;STORE RTN ADDR
       LDA      0,@0,3      ;LOAD PKM OR PYM MSW
       LDA      1,@1,3      ;      LSW
       LDA      2,MSK2      ;LOAD SHFT MASK
       JSR      @SCL        ;SHIFT P
       STA      0,TEM13     ;STORE SHIFTED PM MSW
       STA      1,TEM14     ;      LSW
       STA      3,TEM12     ;STORE SHFT #
U1:     LDA      2,SF11      ;LOAD SF11
       DIV
       LDA      3,TEM      ;RESTORE RTN ADDR
       LDA      2,@5,3      ;LOAD HHX OR HHY
       SUBO      0,0        ;CLR AC0
       MOVZL#    2,2,SNC    ;TEST SIGN
       INC      0,0,SKP     ;POS, SET FLAG
       NEG      2,2        ;NEG, NEGATE
U2:     STA      0,SGN      ;STORE SIGN FLAG

```



```

          STA      2,AHH      ;STORE ABS (HHX)
          SUBO     0,0        ;CLR AC0
          MUL
          STA      0,TEM10    ;STORE H*P MSW
          STA      1,TEM11    ;      LSW
          LDA      2,SF11     ;LOAD SF11
U3:      DIV
          LDA      2,AHH      ;LOAD ABS (HHX)
          SUBO     0,0        ;CLR AC0
          MUL
          LDA      2,SF11     ;LOAD SF11
          DIV
          LDA      2,TEM12    ;LOAD SHFT #
U4:      SUBO     0,0        ;CLR AC0
          JSR      @DESC      ;DESHIFT SNGL WORD
          LDA      2,R        ;LOAD R
          ADD      1,2        ;ADD; =DENOMINATOR
          LDA      0,TEM10    ;LOAD NUM MSW
          LDA      1,TEM11    ;      LSW
          DIV
U5:      LDA      2,TEM12    ;LOAD SHFT #
          SUBO     0,0        ;CLR AC0
          JSR      @DESC      ;DESHIFT SINGLE WORD
          LDA      3,TEM      ;RESTORE RTN ADDR
          STA      1,AK       ;STORE ABS (KX)
          MOV      1,2        ;DUPLICATE ABS (KX)
          LDA      0,SGN      ;LOAD SIGN FLAG
U6:      MOVZR#   0,0,SNC    ;TEST SIGN
          NEG      1,1        ;NEG, NEGATE
          STA      1,@2,3     ;STORE KX OR KY
          LDA      1,AHH      ;LOAD ABS (HHX)
          SUBO     0,0        ;CLR AC0
          MUL
          LDA      2,SF11     ;LOAD SF11
U7:      DIV
          SUB      1,2        ;1-K*HH
          STA      2,TEM1     ;TEMP STORE 1-K*HH
          LDA      0,TEM13    ;LOAD PM MSW
          LDA      1,TEM14    ;      LSW
          LDA      2,SF11     ;LOAD SF11
          DIV
U8:      LDA      2,TEM1     ;LOAD 1-K*HH
          SUBO     0,0        ;CLR AC0
          MUL
          LDA      2,TEM12    ;LOAD SHFT #
          JSR      @DESC      ;DESHIFT
          LDA      3,TEM      ;RESTORE RTN ADDR
          STA      0,@3,3     ;STORE PXP MSW
          STA      1,@4,3     ;      LSW
          JMP      16,3       ;RETURN

```



```

        .BLK      20
        .ZREL     ;SHIFT SUBROUTINE *****
SCL:    SC        ;IT SHIFTS A DOUBLE WORD UNTIL THE
        .NREL     ;MSB IS MASK2 (IN AC2) JUSTIFIED.
SC:     STA       3,TAB    ;STORE RTN ADDR
        SUBO      3,3      ;CLR AC3
        MOVZ      0,0,SNR  ;IS MSW=0?
        MOVZ      1,1,SZR  ;YES, IS LSW=0?
        JMP       .+2      ;ONE IS NOZERO
        JMP       @TAB     ;BOTH=0, RETURN
        MOV       0,0,SNR  ;IS MSW=0?
        JMP       SC3      ;YES, JMP SC3
        AND#      0,2,SNR  ;SHFT LFT OR RT?
        JMP       SC2      ;LEFT
SC1:    MOVZR     0,0      ;MOVE RIGHT MSW
        MOVR      1,1      ;      LSW
        INC       3,3      ;INC AC3
        AND#      0,2,SZR  ;DONE?
        JMP       SC1      ;NO, GO BACK
        NEG       3,3      ;YES
        JMP       @TAB     ;RETURN
SC2:    MOVZR     2,2      ;SHIFT MASK
        MOVZL     1,1      ;SHIFT LSW
        MOVL      0,0      ;      MSW
        INC       3,3      ;INC SHFT COUNTER
        AND#      0,2,SNR  ;DONE?
        JMP       SC2+1    ;NO, DO IT AGAIN
        JMP       @TAB     ;YES, RETURN
SC3:    AND#      2,1,SZR  ;16 SHFTS OR LESS?
        JMP       SC2      ;LESS, JMP SC2
        MOV       1,0      ;SHFT LFT BY 16
        SUBO      1,1      ;      "
        LDA       3,SF7    ;LOAD SF=16.
        JMP       @TAB     ;RETURN
        .BLK      10
        .ZREL     ;DESHIFT SUBROUTINE *****
DESC:   DES       ; SHIFTS A DOUBLE WORD BY # OF BITS
        .NREL     ;SPECIFIED IN AC2 BY CALL.
DES:    STA       3,TAB    ;STORE RTN ADDR
        MOV       2,2,SNR  ;0 SHIFTS?
        JMP       @TAB     ;YES, 0 SHIFTS - RETURN
        MOVZL#    2,2,SZC  ;LEFT OR RIGHT SHIFT?
        JMP       DES2     ;LEFT SHIFT
        NEG       2,2      ;RIGHT SHIFT
DES1:   MOVZR     0,0      ;SHFT RT MSW
        MOVR      1,1      ;AND LSW
        INC       2,2,SZR  ;INC SHFT COUNTER
        JMP       DES1     ;NOT DONE, GO BACK
        JMP       @TAB     ;DONE, RETURN
DES2:   MOVZL     1,1      ;SHFT LFT LSW
        MOVL      0,0      ;      MSW

```

```

INC      2,2,SZR ;DONE?
JMP      DES2    ;NO, GO BACK FOR MORE
JMP      @TAB    ;YES, RETURN
.BLK     10
.ZREL    ;CLOCK SUBROUTINE *****
CLK:     CLK     ;IT SAMPLES DATA, UPDATES XP, YP,
.NREL    ;AND CALCULATES RESIDUES.
CLK:     STA     3,TEM ;STORE RTN ADDR
SUBO     0,0      ;CLR AC0
DOAS     0,ADCV   ;LOAD CHNL SELECT
SKPBZ    ADCV     ;IS DATA READY?
JMP      -1      ;NO, WAIT
DOAS     0,ADCV   ;DO IT TO KILL TIME
SKPBZ    ADCV     ;
JMP      -1      ;
DIC      1,ADCV   ;LOAD DATA
MOV      1,2      ;DUPLICATE DATA
C11:     ADDZL    1,1 ;*4
ADD      1,2      ;=5*DATA (SCALING)
STA      2,ZETA   ;STORE ZETA
LDA      1,@6,3   ;LOAD H
SUB      1,2      ;ZETA-H=RES
STA      2,@0,3   ;STORE XRES
SUBO     0,0      ;CLR AC0
C2:     MOVZL#    2,2,SNC ;TEST SIGN
INC      0,0,SKP  ;POS, SET FLAG
NEG      2,2      ;NEG, NEGATE
STA      2,@1,3   ;STORE ABS (XRES)
LDA      1,@2,3   ;LOAD KX
MOV      0,3      ;MOV SGN TO AC3
SUBO     0,0      ;CLR AC0
C3:     MOVZL#    1,1,SNC ;TEST SIGN
INC      3,3,SKP  ;POS, SET FLAG
NEG      1,1      ;NEG, NEGATE
MUL      ;
LDA      2,SF11   ;LOAD SF11
DIV      ;
MOVZR    3,3,SZC  ;TEST FLAG
C4:     NEG      1,1 ;NEG, NEGATE
LDA      3,TEM    ;RESTORE RTN ADDR
LDA      2,@3,3   ;LOAD XM
ADD      2,1      ;
STA      1,@4,3   ;STORE XP
LDA      1,@5,3   ;LOAD SXRES
LDA      2,TRES   ;LOAD TIME CONSTANT
SUBO     0,0      ;CLR AC0
C5:     MUL      ;
LDA      2,SF11   ;LOAD SF11
DIV      ;
STA      1,TEM1   ;TEMP STORE
LDA      1,@1,3   ;LOAD AXRES

```



```

C6:   LDA      2,GRES  ;LOAD GAIN
      SUBO     0,0    ;CLR AC0
      MUL      ;
      LDA      2,SF11 ;LOAD SF11
      DIV      ;
      LDA      2,TEM1 ;RETURN STORE
      ADD      2,1    ;
      STA      1,@5,3 ;STORE SXRES
      JMP      17,3   ;RETURN
      .BLK     20
      .ZREL    ;SIGN SUBROUTINE *****
TEN:  TE       ;IN 1ST 10 ITERATIONS, THE SIGN OF
      .NREL    ;ERROR EST. IS FORCED
TE:   STA      3,TEM  ;STORE RTN ADDR
      LDA      1,@0,3 ;LOAD AXRES
      LDA      0,BOUND ;LOAD BOUND
      SUBZ#    1,0,SZC ;IS SXRES GT BOUND?
      JMP      12,3   ;NO, RETURN
      LDA      0,@1,3 ;LOAD XP
T1:   NEG      0,0    ;NEGATE XP
      STA      0,@1,3 ;STORE NEW XP
      JMP      12,3   ;RETURN
      .BLK     20
      .ZREL    ;OUTPUT SUBROUTINE *****
OUTPT: OUT     ;OUTPUTS SPECIFIED DATA ON
      .NREL    ;SPECIFIED CHANNEL
OUT:  STA      3,TEM  ;STORE RTN ADDR
      LDA      1,@1,3 ;LOAD DATA
      SUBO     3,3    ;CLR FLAG
      MOVZL#   1,1,SNC ;TEST SIGN
      INC      3,3,SKP ;POS, SET FLAG
      NEG      1,1    ;NEG, NEGATE
      LDA      2,SFOUT ;LOAD D/A SCL FCTR
      SUBO     0,0    ;CLR AC0
      DIV      ;
      MOVR     3,3,SNC ;IS NEG POS FLAG SET?
      NEG      1,1    ;NO, NEGATE
      LDA      3,TEM  ;RESTORE RTN ADDR
      LDA      0,@0,3 ;LOAD CHANNEL SELECT
      DOB      0,DACV ;SPECIFY CHNL SELECT
      DOA      1,DACV ;OUTPUT D/A
      JMP      12,3   ;RETURN
      .BLK     10
      .ZREL    ;IMAX EST. SUBROUTINE *****
IEST: IES      ;CALCULATES THE FILTERED AVG OF
      .NREL    ;I(EST)=ZETA*IMAX/H
IES:  STA      3,TEM  ;STORE RTN ADDR
      LDA      1,ZETA ;LOAD ZETA
      LDA      0,BIAS ;LOAD BIAS
      SUB      0,1    ;SUBTRACT BIAS
      LDA      2,IMAX ;LOAD IMAX

```

```

SUBO 0,0 ;CLR AC0
MUL ;
LDA 2,@0,3 ;LOAD H
LDA 3,BIAS ;LOAD BIAS
SUB 3,2 ;SUBTRACT BIAS
DIV ;
LDA 2,GI ;LOAD FLTR GAIN
I1: SUBO 0,0 ;CLR AC0
MUL ;
LDA 2,SF11 ;LOAD SF11
DIV ;
STA 1,TEM1 ;TEMP STORE
LDA 1,IMAX ;LOAD IMAX
LDA 2,GIX ;LOAD TIME CONSTANT
I2: SUBO 0,0 ;CLR AC0
MUL ;
LDA 2,SF11 ;LOAD SF11
DIV ;
LDA 2,TEM1 ;RETURN TEMP STORE
ADD 2,1 ;
LDA 2,GII ;LOAD GII
LDA 0,R ;LOAD R
MOVZR 0,0 ;DIVIDE BY 128
MOVZR 0,0 ; "
MOVZR 0,0 ; "
MOVZR 0,0 ; "
MOVZR 0,0 ; "
MOVZR 0,0 ; "
JMP .+1 ;SAVE ROOM FOR MORE
JMP .+1 ; DIVIDES
ADD 0,2 ;
SUBO 0,0 ;CLR AC0
MUL ;
LDA 2,SF11 ;LOAD SF11
DIV ;
STA 1,IMAX ;STORE NEW IMAX ESTIMATE
LDA 3,TEM ;RESTORE RTN ADDR
I3: JMP 1,3 ;RETURN
.BLK 20
.ZREL ;R ESTIMATE SUBROUTINE *****
REST: RES ;R(EST)=FILTERED AVG OF (RES**2)/9
.NREL ;
RFS: LDA 1,@0,3 ;LOAD AXRES
MOV 1,2 ;DUPLICATE
SUBO 0,0 ;CLR AC0
MUL ;
LDA 2,@1,3 ;LOAD PROPRT. CONSTANT
DIV ;
LDA 2,GR ;OAD FILTER GAIN
REL: SUBO 0,0 ;CLR AC0

```



```

      MUL      ;
      LDA      2,SF11 ;LOAD SF11
      DIV      ;
      STA      1,TEM1 ;STORE TEMPORARY
      LDA      1,GRX  ;LOAD TIME CONSTANT
      LDA      2,R    ;LOAD R
RE2:  SUBO     0,0    ;CLR AC0
      MUL      ;
      LDA      2,SF11 ;LOAD SF11
      DIV      ;
      LDA      2,TEM1 ;RETURN TEMPOR STORAGE
      ADD      2,1    ;
      STA      1,R    ;STORE NEW R
RE3:  JMP      12,3   ;RETURN
      .BLK     20
      .ZREL    ;DITHER SUBROUTINE *****
DITS: DIT      ;IT COMPUTES DITL=SIGNT*D/IMAX
      .NREL    ;AND NEGATES NEXT DITL
DIT:  STA      3,TEM  ;STORE RTN ADDR
      LDA      1,DITL ;LOAD DITL
      SUBO     3,3    ;CLR SIGN FLAG
      MOVZL#   1,1,SZC ;IS DITL POS?
      INC      3,3    ;NO, SET FLAG
      LDA      1,SIGNT ;LOAD SIGNT
      LDA      2,D    ;LOAD D
D01:  SUBO     0,0    ;CLR AC0
      MUL      ;
      LDA      2,IMAX ;LOAD IMAX
      DIV      ;
      MOVR     3,3,SZC ;IS NEG FLAG SET?
      NEG      1,1    ;YES, NEGATE IT
      NEG      1,1    ;NEGATE FOR SIGN CHANGE
D2:   STA      1,DITL ;STORE DITL
      JMP      @TEM   ;RETURN
      .BLK     10
      .ZREL    ;BREAKLOCK SUBROUTINE *****
BREAK: BREA    ;CHECKS IF TRACKING BY LOOKING
      .NREL    ;AT HISTORY OF IMAX AND RESIDUES
BREA:  LDA      1,SZET ;LOAD SZET
      LDA      2,BLB  ;LOAD BLB
B1:   SUBZL    2,1,SZC ;IS S-B NEG? (S<B?)
      JMP      @IVV   ;YES RESTART
      LDA      1,SYRES ;LOAD SYRES
      LDA      2, SXRES ;LOAD SXRES
      ADD      2,1    ;SRES IN AC1
      LDA      2,PTSIX ;LOAD BOUND FACTOR
      SUBO     0,0    ;CLR AC0
      MUL      ;
      LDA      2,SF11 ;
      DIV      ;
      LDA      2,IMAX ;LOAD IMAX

```

```

B2:      SUBZL 1,2,SZC ;IS I-S NEG? (S>I?)
        JMP   @IVV   ;YES RESTART
        JMP   0,3     ;RETURN
        .BLK 20
        .ZREL ;SZETA SUBROUTINE*****
SZETA:   SZE    ;COMPUTES A FILTERED AVG OF
        .NREL   ;ZETAS (MEASUREMENTS)
SZE:     LDA    1,GSX ;LOAD GSX
        LDA    2,SZET ;LOAD SZET
        SUBO   0,0   ;CLR AC0
        MUL    ;
        LDA    2,SF11 ;LOAD SF11
        DIV    ;
        STA    1,TEM1 ;TEMPOR STORE RSLT
SZ1:     LDA    1,ZETA ;LOAD ZETA
        LDA    2,GS    ;LOAD GAIN
        SUBO   0,0   ;CLR AC0
        MUL    ;
        LDA    2,SF11 ;LOAD SF11
        DIV    ;
        LDA    2,TEM1 ;RETURN TEMPOR STORE
SZ2:     ADD    2,1   ;
        STA    1,SZET ;STORE SZET
        JMP    0,3   ;RETURN
        .BLK 20
        .ZREL ;BOUND SUBROUTINE*****
BOUN:    BOU    ;COMPUTES THE BOUND FOR SIGN
        .NREL   ;FORCING DURING CONVERGENCE
BOU:     LDA    1,SLPE ;LOAD SLOPE
        LDA    2,SZET ;LOAD SZET
        SUBO   0,0   ;CLR AC0
        MUL    ;
        LDA    2,SF11 ;LOAD SF11
        DIV    ;
        LDA    2,MIN  ;LOAD CONSTANT
BOU1:    ADD    2,1   ;
        STA    1,BOUND ;STORE BOUND
        JMP    0,3   ;RETURN
        .BLK 20
        .ZREL ;SEARCH SUBROUTINE*****
SRCH:    SRC    ;IT USES A SPIRAL SCAN TO LOCATE
        .NREL   ;THE TARGET BEFORE LOCK-ON
SRC:     STA    3,TAB ;STORE RTN ADDR
SR:      LDA    1,NO  ;INITIALIZE:
        STA    1,N    ;STEP COUNTER
SX:      LDA    0,N   ;LOAD COUNTER
        STA    0,NC  ;STORE IN X-COUNTER
SX1:     LDA    1,STP ;LOAD STEP
        LDA    2,DAX ;LOAD X-OUTPUT REGISTER
SX2:     ADD    2,1   ;NEW X-OUTPUT REGISTER
        STA    1,DAX ;STORE IT

```



```

        JSR      BNDRY      ;TEST FOR BOUNDARY
        DAX
        JSR      @OUTPT     ;OUTPUT X-CHNL
        ZER
        DAX
        .BLK      10
SX3:    JSR      TRSH       ;TEST FOR THRESHOLD
        DSZ      NC         ;DONE WITH X-AXIS?
        JMP      SX1        ;NO, CONTINUE
        ISZ      N          ;YES, INC N AND DO Y-AXIS
SY:     LDA      0,N        ;RESTORE NC
        STA      0,NC       ;
SY1:    LDA      1,STP      ;LOAD STEP INCREMENT
        LDA      2,DAY      ;LOAD Y-OUT REGISTER
SY2:    ADD      2,1        ;
        STA      1,DAY      ;STORE NEW Y-OUT RGSTR
        JSR      BNDRY      ;TEST FOR BOUNDARY
        DAY
        JSR      @OUTPT     ;OUTPUT Y-AXIS CONTROL
        ONE
        DAY
        .BLK      10
SY3:    JSR      TRSH       ;TEST FOR THRESHOLD
        DSZ      NC         ;DONE WITH Y-AXIS?
        JMP      SY1        ;NO, CONTINUE
        ISZ      N          ;INC N
        LDA      1,STP      ;REVERSE STEP DRCTN
        NEG      1,1        ;
        STA      1,STP      ;
        JMP      SX         ;DO IT AGAIN
        .BLK      20
BNDRY:  LDA      1,@0,3     ;LOAD DAX (OR Y)
        MOVZL#  1,1,SZC     ;TEST SIGN
        NEG      1,1        ;NEG, NEGATE IT
        LDA      2,SFOUT    ;LOAD D/A SF
        SUBO     0,0        ;CLR AC0
        DIV
        LDA      2,MSKB     ;LOAD BOUNDARY MASK
        AND      2,1,SNR    ;TEST FOR BOUNDARY
        JMP      1,3        ;NONE, RETURN
        SUBO     0,0        ;RESTART X & Y AXIS
        STA      0,DAX      ; AT ORIGIN
        STA      0,DAY      ;
        JMP      SR         ;
        .BLK      20
TRSH:   LDA      0,ZETA     ;TESTS FOR THRESHOLD
        MOVZR    0,0        ;FILTER THE MEASUREMENTS
        SUBO     1,1        ;SET A/D CODE
        DOAS     1,ADCV     ;START CONVERSION
        SKPBZ    ADCV       ;IS IT READY?
        JMP      -1        ;NO, WAIT

```

```

DIC      1,ADCV  ;LOAD DATA
MOV      1,2    ;SCALE TO SF11
ADDZL    1,1    ;
ADD      1,2    ;
MOVZR    2,2    ;DIV BY 2 FOR FILTERING
ADD      0,2    ;
STA      2,ZETA ;STORE FILTERED ZETA
LDA      1,TEST ;LOAD THRESHOLD BOUND
SUBZL    2,1,SZC ;ZETA-TEST
JMP      @TAB   ;ABOVE THRSOLD, JMP MAIN PGM
JMP      0,3    ;BELOW, RETURN
.BLK     20
.ZREL    ;TABLE STORAGE SUBROUTINE *****
TABLS:   TABL   ;IT STORES 1ST 264 VALUES
.NREL    ;SPECIFIED IN CALLING STMT
TABL:    STA    3,TEM ;STORE RTN ADDR
LDA      0,TABC ;LOAD TBL COUNTER
INC      0,0,SZR ;IS TBL FULL?
INC      0,0,SNR ;
JMP      4,3    ;YES, RETURN
STA      0,TABC ;STORE TBL COUNTER
LDA      2,TBLX ;LOAD X-TBL
ADD      0,2    ;TRUE ADDRESS
TAB1:    LDA    1,@0,3 ;LOAD 1ST X VALUE
STA      1,0,2  ;STORE IT
LDA      1,@1,3 ;LOAD 2ND X VALUE
STA      1,1,2  ;STORE IT
LDA      2,TBLY ;LOAD Y-TBL
ADD      0,2    ;TRUE TBL ADDRESS
LDA      1,@2,3 ;LOAD 1ST Y VALUE
STA      1,0,2  ;STORE IT
LDA      1,@3,3 ;LOAD 2ND Y VALUE
STA      1,1,2  ;STORE IT
TABC2:   JMP    4,3 ;RETURN
TB1X:    TBX+277
TB1Y:    TBY+277
.BLK     20
.ZREL    ;EXPONENTIAL SUBROUTINE *****
EXP:     EX     ;USES TABLE LOOKUP TO CALCULATE
.NREL    ;EXP(-X)
EX:      STA    3,TEM ;STORE RTN ADDR
LDA      2,@0,3 ;LOAD ARGUMENT
LDA      0,MSK4 ;LOAD ARGUMENT MASK
AND#     2,0,SZR ;IS ARG>8?
JMP      EX3    ;YES, JMP EX3
ADDZL    2,2    ;SHIFT LEFT BY 2
LDA      3,MSK  ;LOAD MASK
MOVS     3,1    ;SWAP BYTE INTO AC1
EX1:     ANDS    2,3 ;HOB IN AC3
AND      2,1    ;LOB IN AC1
LDA      2,TBL  ;LOAD TABLE ADDR

```



```

      ADD      2,3      ;ACTUAL ADDRESS
      LDA      2,1,3    ;LOAD ARGMNT+1
      LDA      3,0,3    ;LOAD ARGUMENT
      MOV      3,0      ;DUPLICATE VALUE
      SUB      2,0      ;SLOPE IN AC0
EX2:   MOVS     0,2      ;PREPARE SLOPE FOR MUL
      SUBO     0,0      ;CLR AC0
      MUL
      SUB      0,3      ;EXPT IN AC3
      JMP      .+2      ;
EX3:   SUBO     3,3      ;ARG>8, EXPT=0
      LDA      2,TEM     ;RELOAD RTN ADDR
      STA      3,@1,2    ;STORE EXPT
      JMP      12,2      ;RETURN
      .BLK     20

```

```

TBL:   TABLE
TABLE: 4000

```

```

3701
3604
3511
3417
3330
3242
3156
3073
3012
2732
2654
2600
2524
2452
2402
2332
2264
2217
2153
2110
2046
2006
1746
1707
1652
1615
1561
1526
1473
1442
1411
1361
1332
1304

```

1256	213	34	6	1		
1231	207	33	6	1		
1204	203	33	5	1		
1161	177	32	5	1		
1135	173	31	5	1		
1113	167	30	5	1		
1071	164	27	5	1		
1047	160	27	5	1		
1026	155	26	4	1		
1006	151	25	4	1		
766	146	25	4	1		
746	143	24	4	1		
727	140	23	4	1		
711	135	23	4	1		
673	132	22	4	1		
655	127	22	4	1		
640	125	21	3	1		
623	122	21	3	1		
607	117	20	3	1		
573	115	20	3	1		
557	113	17	3	1		
544	110	17	3	1		
531	106	16	3	1		
516	104	16	3		TBX:	.BLK 340
504	102	15	3		TBY:	.BLK 340
472	100	15	3			.END
460	76	15	3			
447	74	14	2			
436	72	14	2			
425	70	13	2			
415	67	13	2			
404	65	13	2			
374	63	12	2			
365	62	12	2			
355	60	12	2			
346	57	11	2			
337	55	11	2			
330	54	11	2			
321	53	11	2			
313	51	10	2			
305	50	10	2			
276	47	10	2			
271	46	10	2			
263	44	7	2			
255	43	7	1			
250	42	7	1			
243	41	7	1			
236	40	7	1			
231	37	6	1			
224	36	6	1			
220	35	6	1			

VITA

Zdzislaw Heronim Lewantowicz was born on 12 August 1945 in Suchowola-Bialystok, Poland. He entered the United States in November, 1958. He graduated from Cathedral (Massachusetts) High School in 1964. In 1965 he became a United States citizen. In 1968 he graduated from Lowell Technological Institute with a Bachelor of Science degree in Electrical Engineering and concurrently was commissioned in the United States Air Force through the Reserve Officer Training Corps. He earned pilots wings in 1969 after completion of Undergraduate Pilot Training at Laredo AFB, Texas. From 1970 to 1971 he served in the Vietnam conflict as a Forward Air Controller flying Ol-E aircraft. From 1971 to 1975 he served as an instructor pilot in T-37 aircraft, and as an air operations officer responsible for flying procedures at Laredo AFB, Texas, and Craig AFB, Alabama. In 1975 Captain Lewantowicz was assigned to the Air Force Institute of Technology in pursuit of a Master's Degree in Electrical Engineering, Guidance and Control.

Permanent address: 24 Ionia Street
Springfield, MA 01109

This thesis was typed by Mrs. Donna M. Hadley.

UNCLASSIFIED

SECURITY CLASSIFICATION OF THIS PAGE (When Data Entered)

REPORT DOCUMENTATION PAGE		READ INSTRUCTIONS BEFORE COMPLETING FORM
1. REPORT NUMBER GE/EE/76-29 ✓	2. GOVT ACCESSION NO.	3. RECIPIENT'S CATALOG NUMBER
4. TITLE (and Subtitle) LASER POINTING AND TRACKING USING AN ADAPTIVE EXTENDED KALMAN FILTER		5. TYPE OF REPORT & PERIOD COVERED
7. AUTHOR(s) Edzislav H. Lewantowicz		6. PERFORMING ORG. REPORT NUMBER
9. PERFORMING ORGANIZATION NAME AND ADDRESS Air Force Institute of Technology ✓ (AFIT-EN) Wright-Patterson AFB, Ohio 45433		8. CONTRACT OR GRANT NUMBER(s)
11. CONTROLLING OFFICE NAME AND ADDRESS Advanced Beam Control (AFWL/ALD) Air Force Weapons Laboratory Kirtland AFB, NM 87117		10. PROGRAM ELEMENT, PROJECT, TASK AREA & WORK UNIT NUMBERS Project 3173-1898-63605F
14. MONITORING AGENCY NAME & ADDRESS (if different from Controlling Office)		12. REPORT DATE December 1976
		13. NUMBER OF PAGES 136
		15. SECURITY CLASS. (of this report) UNCLASSIFIED
16. DISTRIBUTION STATEMENT (of this Report) Approved for public release; distribution unlimited		15a. DECLASSIFICATION/DOWNGRADING SCHEDULE
17. DISTRIBUTION STATEMENT (of the abstract entered in Block 20, if different from Report)		
18. SUPPLEMENTARY NOTES Approved for public release; IAW AFR 190-17 JERRAL F. GUISS, Captain, USAF Director of Information		
19. KEY WORDS (Continue on reverse side if necessary and identify by block number) Extended Kalman Filter Laser Pointing and Tracking Adaptive Laser Optics Techniques		
20. ABSTRACT (Continue on reverse side if necessary and identify by block number) An adaptive extended Kalman filter (EKF) is used in an Adaptive Laser Optics Techniques (ALOT) control loop to track the glint from a spherical target. A fourfold improvement in tracking bandwidth is obtained over a conventional conical scan ALOT tracking loop implemented with the same hardware. The increase in tracking bandwidth is manifested in the ratio between the (conical scan) dither frequency and the tracking bandwidth which is 2.5:1		

UNCLASSIFIED

SECURITY CLASSIFICATION OF THIS PAGE (When Data Entered)

UNCLASSIFIED

SECURITY CLASSIFICATION OF THIS PAGE(When Data Entered)

Block 20 (continued)

for the EKF and 10:1 for the conventional analog or digital glint tracking schemes. The EKF provides correct pointing error estimates over essentially the entire range of the pointing error, whereas in a conventional conical scan loop the demodulated error versus true pointing error function is highly non-linear due to the nonlinearity of the glint. This results in a demonstrated ability of the EKF to track a larger amplitude disturbance than the conventional conical scan loop. Adaptive schemes are employed to make the estimation algorithm insensitive to fluctuations in the mean level of reflected intensity and to variations in the strength of measurement noise.

UNCLASSIFIED

SECURITY CLASSIFICATION OF THIS PAGE(When Data Entered)